Non-equilibrium dynamics of one-dimensional isolated quantum systems

Ph.D. Thesis

Gergő Roósz

supervisor: Ferenc Iglói

Theoretical Physics Department, University of Szeged

Doctoral School of Physics

Wigner Research Center for Physics

Szeged, Hungary

2017

To Maria

Szerzői nyilatkozat

Kijelentem, hogy a doktori disszertációmban foglaltak a 2. és a 3. fejezetek kivételével, melyek az irodalomban fellelhető eredményeket tekintik át, saját munkám eredményei, és csak a hivatkozott forrásokat használtam fel. Tudomásul veszem azt, hogy disszertációmat a Szegedi Tudományegyetem könyvtárában, a kölcsönözhető könyvek között helyezik el.

Contents

Chapter 1

Introduction

Non-equilibrium relaxation in a closed quantum system following a change of some parameter(s) in the Hamiltonian is of recent interest, both experimentally and theoretically. Considering the speed of variation of the parameter, we generally discriminate between two limiting processes. For the *quench dynamics*, the parameter is modified instantaneously, which experimentally can be realized in ultra cold atomic gases [1–11] using the phenomenon of Feshbach resonance. In this process the evolution of different observables after the quench is of interest, as well as the possible existence and properties of the stationary state, in particular in integrable and non-integrable systems [12–57]. In the other limiting relaxation process, in the so called *nearly adiabatic dynamics* the parameter is varied very slowly, usually linearly in time with a rate $1/\tau$ across a phase-transition point. At the start of the process the system is in the ground state of the Hamiltonian. If the variation of the Hamiltonian would be much slower than the time scale of the smallest gap, the system would remain exponentially close to the instantaneous ground state. However when the system reaches the critical point, the smallest gap goes to zero, and the variation of the Hamiltonian cannot be slow enough to remain in the instantaneous ground state. The question, how far is the described system from the instantaneous ground state, is target of extensive investigations in the literature [50, 56, 58–74].

We mention that the parameter in the Hamiltonian of a closed system can be driven periodically or randomly in time, and the non-equilibrium dynamics of these driven systems draws attention both experimental [75] and theoretical [76] [77].

Many results for quantum quenches have been obtained for *homogeneous* systems [12, 16–33, 50, 51, 55]; for example, the relaxation of correlation functions in space and in time have generally an exponential form, which defines a quench-dependent correlation length and a relaxation time. Many basic features of the relaxation process can be successfully explained by a quasi-particle picture [38, 51, 56]: after a global quench quasi-particles are created homogeneously in the sample and move ballistically with momentum dependent velocities. The behavior of observables in the stationary state is generally different in integrable and in non-integrable systems. For non-integrable models, thermalization is expected [16–24, 50, 51] and the distribution of an observable is given by a thermal Gibbs ensemble; however, in some specific examples this issue has turned out to be more complex [25–27, 32]. By contrast, it was conjectured that stationary state averages for integrable

models are described by a generalized Gibbs ensemble [16], in which case each integral of motion is separately associated with an effective temperature.

Concerning quantum quenches in inhomogeneous systems, there have been only a few studies in specific cases; for example, entanglement entropy dynamics in random quantum chains [78–80] and in models of many-body localization [81,82]. In some of these cases the eigenstates are localized, which prevents the system from reaching a thermal stationary state.

A special type of inhomogeneity, interpolating between homogeneous and disordered systems, is a quasi-crystal [83,84] or an aperiodic tiling [85]. Quasi-crystals are known to have anomalous transport properties [86,87], which is due to the fact that in these systems the long-time motion of electrons is not ballistic, but an anomalous diffusion described by a power law. One may expect that the quasi-particles created during the quench have a similar dynamical behavior, which in turn affects the relaxation properties of quasi-crystals.

Quasi-crystals of ultra cold atomic gases have been experimentally realized in optical lattices by superimposing two periodic optical waves with different incommensurate wavelengths. An optical lattice produced in this way realizes a Harper's quasi-periodic potential [88,89], for which the eigenstates are known to be either extended or localized depending on the strength of the potential. Different phases of the Bose-Hubbard model with such a potential have been experimentally investigated [90,91]. There have also been theoretical studies concerning the relaxation process in the Harper potential [92,93].

The dissertation is organized as follows: In chapter 2 the investigated quantities are defined and the most important equilibrium properties of the investigated models are outlined. In chapter 3 some results about the after quench dynamics of spin chains from the literature are recapitulated. These results will be referred and extended in the later sections.

Our new results are presented in Chapters 4-8. Below we briefly summarize the main results from these Chapters.

In Chapter 4 the dynamics after a composite local quench is investigated. Composite here means that not only one site was modified during the quench, but the local magnetic fields on two neighboring sites and the coupling between them. The quench was done in a quantum Ising chain, and a coupling and the two neighboring local magnetic field are changed suddenly. We calculated the local magnetization on the quench site. A relation with a 2D classical spin system was found, and using this relation a closed formula was conjectured for the time evolution of the local magnetization. These closed formulas are the main results of the chapter. We validated the formulas with precise numerical calculations using free-fermion techniques.

In Chapter 5 we investigated the after quench dynamics of the Fibonacci quasi-crystal. The quantum Ising chain in its homogeneous version is perhaps the most studied model for non-equilibrium relaxation [13–15,34–44,57,94]. We focus on the Fibonacci lattice, for which many equilibrium properties of the quantum Ising model are known [95–101]. In this chapter we investigated the after-quench dynamics of the magnetization and entanglement

entropy with numerical free-fermion calculations. We found, that the entanglement entropy shows a power law increase after the quench, and the magnetization shows a stretched exponential increase. We also found a dynamical phase transition associated with the local magnetization, which is not present in the homogeneous system. The results were interpreted with quasi-classical reasoning.
In chapter 6 the quench dynamic of the Harper model was investigated. In this model there is a localization-delocalization transition, separating a localized phase and an extended phase. We investigated the dynamics of the entropy and the magnetization after different quenches ending in the extended phase, at the critical point or in the localized phase. We explored the functional form of the relaxation of the entanglement entropy and the magnetization in the aforementioned quenches. We found, that both quanties remain finite if the quench ends in the localized phase. If the quench ends in the extended phase the behavior is strongly similar to the behavior of the homogeneous systems: The entanglement entropy grows linearly, and the magnetization decrease exponentially. If the quench ended at the transition point, the entanglement entropy grows as a power-law, and the magnetization decreases with a starched exponential.
In chapter 7 we investigated a nearly adiabatic process in the Harper model by slowly varying one of the parameters of the Hamiltonian, and the system is driven over the transition point. We investigated how far is the system from the instantaneous ground state after crossing the localization-delocalization transition with finite speed. We present the results of our large-scale numerical simulations, and give a modified version of the so-called Kibble-Zurek scaling, which fits the numerical results well.
In chapter 8 we investigated the local magnetization after a global quench in a disordered Ising chain. We explored the functional form of the relaxation of the local magnetization with numerical free-fermion calculations. Two kinds of initial states were used in our calculations: one of these is ferromagnetic, in which all spins point in the X direction, the local magnetization is 1. The other initial state is paramagnetic, in which all spins show in the Z direction, and the local magnetization in the direction of the interaction (X-direction) is zero.

The main results are: If the system after the quench is off-critical, the magnetization remains finite. If the quench starts form the totally ferromagnetic phase, and ends in the critical point, the magnetization shows an ultra slow decrease. If the quench start from the totally paramagnetic state, and ends at the critical point, the magnetization increases, which is a unique property of the disordered Ising chain: In all quenches performed in homogeneous and quasi-periodic Ising chains the local magnetization always decreases. There has been intensive investigations about the after quench dynamics of the entanglement entropy in disordered spin chains [79–82]. The results about the magnetization are in good agreement with these previous studies. At the end of the dissertation there is an Appendix, in which detailed calculations are presented: the solution of the eigenvalue problem of different spin chains; the calculation of the magnetization and the entanglement entropy in spin chains; some facts about the "meaning" of the entanglement entropy. The dissertation is based on the following articles:

1. Ferenc Iglói, Gergő Roósz, Yu-Cheng Lin *Nonequilibrium quench dynamics in quantum quasicrystals* New J. Phys. **15**, 023036 (2013)

2. Ferenc Iglói, Gergő Roósz, Loic Turban *Evolution of the magnetization after a local quench in the critical transverse-field Ising chain* J. Stat. Mech. (2014) P03023

3. Gergő Roósz., Uma Divakaran, Heiko Rieger, Ferenc Iglói *Non-equilibrium quantum relaxation across a localization-delocalization transition* Phys. Rev. B **90**, 184202 (2014)

4. Gergő Roósz, Yu-Cheng Lin, Ferenc Iglói *Critical quench dynamics of random quantum spin chains: Ultra-slow relaxation from initial order and delayed ordering from initial disorder* New J. Phys. **19**, 023055 (2017)

Our related work about a randomly driven quantum Ising chain is: Gergő Roósz, Róbert Juhász, Ferenc Iglói *Nonequilibrium dynamics of the Ising chain in a fluctuating transverse field* Phys. Rev. B **93**, 134305 (2016)
In the thesis the following abbreviations are used:

TIC	Transverse-field Ising Chain
SDRG	Strong Disorder Renormalization Group
RSRG-X	Real-Space Renormalization Group for eXcited states
CFT	Conformal Field Theory

Chapter 2

Ground-state properties of quantum spin chains

In this Chapter we review the previously known ground-state properties of the models studied in this work. We also list the definitions of the investigated quantities. The details of calculation are presented in Appendix B.
The models investigated in this work are special cases of the inhomogeneous XY-model

$$H = \frac{1}{2}\sum_{l=1}^{L} h_l \sigma_l^z + \frac{1+\gamma}{2}\sum_{l=1}^{L} J_l \sigma_l^x \sigma_{l+1}^x + \frac{1-\gamma}{2}\sum_{l=1}^{L} J_l \sigma_l^y \sigma_{l+1}^y \ . \tag{2.1}$$

Here L is the number of spins, σ_l^z and σ_l^x are the Pauli matrices. Here $\hbar = 1$ and the parameters J_l and h_l are dimensionless numbers. With the Jordan-Wigner transformation [104] [105] the operator (2.1) can be written with fermion operators c_k and $c_k^\dagger$:

$$\begin{aligned} H = -\sum_{l=1}^{L} h_l (c_l^\dagger c_l - 1/2) - \frac{1+\gamma}{2}\sum_{l=1}^{L-1} J_l (c_l^\dagger - c_l)(c_{l+1}^\dagger + c_{l+1}) - \frac{1-\gamma}{2}\sum_{l=1}^{L-1} J_l (c_l^\dagger + c_l)(c_{l+1} - c_{l+1}^\dagger) \\ + J_L w \left[\frac{1+\gamma}{2}(c_L^\dagger - c_L)(c_1^\dagger + c_1) + \frac{1-\gamma}{2}(c_L^\dagger + c_L)(c_1^\dagger - c_1)\right] e^{-i\pi \sum_{j=1}^{L} c_j^\dagger c_j} \end{aligned} \tag{2.2}$$

Here $w = 0$ corresponds to the free boundary conditions, and $w = 1$ corresponds to the periodic boundary conditions. The $P = e^{-i\pi \sum_{j=1}^{L} c_j^\dagger c_j}$ parity operator commutes with the Hamiltonian 2.2. One can diagonalize the Hamiltonian in the eigensubspaces of P. P has two eigenvalues, $+1$ if the number of particles is even, and -1 if the number of particles is odd. In the even subspace $P = +1$, in the odd subspace $P = -1$. In the even and in the odd subspace the Hamiltonian is quadratic in the c_l, $c_l^\dagger$ operators. The ground state of Hamiltonian 2.2 is in the even subspace. With an appropriate Bogoliubov transformation [196] new fermions (η_k and $\eta_k^\dagger$) can be introduced

$$\eta_k = \sum_i^N \left(\frac{1}{2}(\Phi_k(i) + \Psi_k(i))c_i + \frac{1}{2}(\Phi_k(i) - \Psi_k(i))c_i^\dagger\right) \ , \tag{2.3}$$

and with these new fermionic operators the (2.1) Hamiltonian is diagonal:

$$H = \sum_{k=1}^{L} \epsilon_k \eta_k^\dagger \eta_k + \text{const.} \,. \tag{2.4}$$

The $\Phi_k(i)$ and $\Psi_k(i)$ quantities in equation (2.3) are real numbers. Their calculation, and the details of this standard diagonalization technique can be found in Appendix A. For later reference I define here the Majorana operators:

$$\check{a}_{2l-1} \quad = c_l + c_l^\dagger \tag{2.5}$$

$$\check{a}_{2l} \quad = i(c_l - c_l^\dagger) \,, \tag{2.6}$$

which are self adjoint operators, and often make calculations more simple. The Majorana operators satisfies the following simple anti-commutation rule: $\{\check{a}_l, \check{a}_k\} = 2\delta_{l,k}$. The time evolution of the Majorana operators after a sudden quench can be expressed in the form $\check{a}_m(t) = \sum_{n=1}^{2L} P_{m,n}(t)\check{a}_n$, where $P_{m,n}(t)$ are real coefficients. The calculation of the $P_{m,n}(t)$ coefficients are detailed in Appendix A.5. One gets the inhomogeneous XX model with transverse field with $\gamma = 0$:

$$\mathcal{H}_{XX} = -\frac{1}{2}\sum_{n=1}^{L}(\sigma_n^x\sigma_{n+1}^x + \sigma_n^y\sigma_{n+1}^y) - \frac{1}{2}\sum_{n=1}^{L} h_n\sigma_n^z \,, \tag{2.7}$$

here all of the couplings are 1, and the h_n transverse field is inhomogeneous. With $h_n = h\cos(2\pi n\frac{\sqrt{5}-1}{2})n$ one gets the Harper model, which is investigated in more detail in this work. One gets the transverse-field Ising chain from Hamiltonian (2.2) with $\gamma = 1$:

$$\mathcal{H}_{\text{Ising}} = -\frac{1}{2}\sum_{i=1}^{L-1} J_i\sigma_i^x\sigma_{i+1}^x - \frac{1}{2}\sum_{i=1}^{L} h_i\sigma_i^z + wJ_L\sigma_L^x\sigma_1^x \,. \tag{2.8}$$

In this work, three variants of the Ising chain will be investigated: One nearly homogeneous with a (generalized) local defect, a quasi-periodic, and a disordered where the magnetic fields and the couplings are (independent) random numbers.

One of the investigated quantities is the *local magnetization*. The Ising model shows ferromagnetic order in the x direction if the transverse field is small enough. The most straightforward choice to characterize the magnetic order would be the expectation value of σ_x. However this expectation value in the ground-state is always zero because of symmetry reasons. One possible solution is to add an infinitesimally small symmetry breaking field. One adds a longitudinal field b to the Ising Hamiltonian and investigates the magnetization in the ground state of the modified Hamiltonian $H_b = H_{\text{Ising}} + bV$ with $V = \sum_{i=1}^{N}\sigma_i^x$ It can be shown [167] , that the magnetization in the $b \to 0$ limit can be calculated as the off-diagonal matrix member of σ_l between the ground state of (2.8) denoted by $|\Psi_0\rangle$, and the excited state of (2.8) denoted by $|\Psi_1\rangle$.

$$m_l = \lim_{b\to 0}\langle\sigma_l^x\rangle = \langle\Psi_0|\sigma_l^x|\Psi_1\rangle \tag{2.9}$$

An other interesting quantity investigated in this work is the *entanglement entropy*. The formal definition is as follows. One divides the investigated system to two parts A and B. One consider the density matrix of the system, which is simply the projector made from the state vector of the system: $\rho = |\Psi\rangle\langle\Psi|$. The reduced density matrix of subsystem A is defined by tracing out for the degrees of freedom of the B system.

$$\rho_A = \mathrm{Tr}_B \rho \tag{2.10}$$

The reduced density matrix of the B subsystem is defined similarly $\rho_B = \mathrm{Tr}_A \rho$. The entanglement entropy is defined as the von Neuman entropy of ρ_A or ρ_B:

$$S = \mathrm{Tr}_A \rho_A \ln \rho_A = \mathrm{Tr}_B \rho_B \ln \rho_B \, . \tag{2.11}$$

The set of the non-zero eigenvalues of ρ_A and ρ_B are identical, this is the reason why the second equality holds in the previous equation. More details on the definition of the entanglement entropy, and the calculation method for spin chains are included in Appendix B.3. In this work A is always the first l spins of the chain, and B is the other $L - l$ spins. The definition allow any kind of partition. The choice of two intervals is the most simple and perhaps the most interesting.

2.1 Homogeneous transverse-field Ising chain

The homogeneous Ising chain is derived from (2.8) with setting all of the couplings to J and all of the magnetic fields to h. The model is exactly solvable, one first transform it to a fermion system with the Jordan-Wigner transformation (A.5) [104] than diagonalize it with a Bogoliubov transformation [105] [106]. The steps of this calculation are outlined in Appendix A.3. There is a quantum phase transition in the model, the transition point is $h = 1$. For $h < 1$ there is a long-range order in the x direction which is characterized by non-zero transverse magnetization m_l. The $h < 1$ phase is ferromagnetic, and the $h > 1$ phase is paramagnetic.

The paramagnetic and the ferromagnetic phases are mapped to each other by the duality transformation [107]. To see this, let us investigate the Ising model with periodic boundary conditions ($w = 1$ in equation (2.8)). One can define a new set of Pauli matrices:

$$\left.\begin{array}{rcl} \tau_i^x &=& \sigma_{i+1}^z \sigma_i^z \\ \tau_i^z &=& \Pi_{m<i} \sigma_m^x \\ \tau_i^y &=& -i \tau_i^z \tau_i^x \end{array}\right\} \, . \tag{2.12}$$

With these matrices the Hamilton operator takes the form:

$$\begin{aligned}\mathcal{H}_{\text{Ising}}^{\text{periodic}} &= -\frac{1}{2}\sum_{i=1}^{L}\sigma_i^x\sigma_{i+1}^x - \frac{h}{2}\sum_{i=1}^{L}\sigma_i^z = \\ &= -\frac{1}{2}\sum_{i=1}^{L}\tau_i^z - \frac{h}{2}\sum_{i=1}^{L}\tau_i^x\tau_{i+1}^x = \\ &= h\left[-\frac{1}{h}\frac{1}{2}\sum_{i=1}^{L}\tau_i^z - \frac{1}{2}\sum_{i=1}^{L}\tau_i^x\tau_{i+1}^x\right] . \end{aligned} \tag{2.13}$$

So the spectra of the Hamiltonians $\mathcal{H}_{\text{Ising}}^{\text{periodic}}(h)$ and $h\mathcal{H}_{\text{Ising}}^{\text{periodic}}(1/h)$ is the same. If h is in the ferromagnetic phase than $1/h$ is in the paramagnetic phase, the duality connect the two sides of the critical point.

The most important correlation functions have been calculated in [106]. The long-range limit of the XX correlation function ($C_r^x\langle\sigma_i^x\sigma_{i+r}^x\rangle$) shows the phase transition spectacularly. In the paramagnetic phase $\lim_{r\to\infty} C_r^x = 0$, there is no long range order. In the ferromagnetic phase the long range limit is nonzero:

$$\lim_{r\to\infty} C_r^x = (1-h^2)^{1/4} . \tag{2.14}$$

The m_l transverse magnetization behaves similarly to the C_r^x correlation function, non-zero in the ferromagnetic phase, goes to zero approaching the critical point ($m_l = (1-h^2)^\beta$), and zero in the paramagnetic phase. The magnetization exponent is $\beta = 1/8$.

Using the C_r^x correlation function one can obtain the correlation length of the system. One find [108] that the correlation function shows an asymptotic decrease $C_r^x \sim \exp(-r/\xi)$, where the inverse of the correlation length is:

$$\frac{1}{\xi} = \begin{cases} \sqrt{\frac{T}{\pi}(\frac{1}{h}-1)}e^{-2(1/h-1)/T} & h<1, T\to 0 \\ \frac{\pi}{4}\frac{T}{2} & h=1 \\ 1-1/h+\sqrt{\frac{T}{\pi}(\frac{1}{h}-1)}e^{-2(1/h-1)/T} & h>1, T\to 0 \end{cases} . \tag{2.15}$$

At the critical point, the XX correlation function decays as a power law: $C_r^x \sim 1/r^{1/4}$, which defines the $\eta = 1/4$ critical exponent [106]. In equation (2.15) T is the temperature. In the ground state (at zero temperature) one finds $\xi = 1/(1-1/h)$ for $h > 1$, so the critical exponent of the correlation length is $\nu = 1$. Approaching the critical point from the paramagnetic phase the smallest gap closes as $\Delta \sim (h-1)$ [107], so the dynamical exponent of the model is $z = 1$. The entanglement entropy between two blocks of spins remains finite in the $L \to \infty$ thermodynamic limit both in the ferromagnetic and paramagnetic phases. This behavior is a special case of the general "area-law": In a non-critical system the entanglement entropy is proportional to the area between the two subsystem [109]. In the critical point of the TIC, the entanglement entropy shows a totally different behavior, it grows logarithmically [110]:

$$S = c/6 \ln L . \tag{2.16}$$

where $c = 1/2$ is the central charge of the corresponding conformal field theory [168]. The logarithmic growth of the entanglement entropy is a typical property of one-dimensional critical systems. In a finite system the entanglement entropy shows a maximum at the critical point.

2.2 Finonacci Ising quantum quasi-crystal

The Finonacci Ising quasi-crystal is defined by the Hamiltonian:

$$\mathcal{H} = -\frac{1}{2}\left[\sum_i J_i \sigma_i^x \sigma_{i+1}^x + h \sum_i \sigma_i^z\right] , \tag{2.17}$$

(σ_i^x and σ_i^z are Pauli matrices at site i.) The couplings, J_i, are site dependent, and parameterized as:

$$J_i = J r^{f_i} , \tag{2.18}$$

Here $r > 0$ is the amplitude of the inhomogeneity, $r = 1$ corresponds to the homogeneous system, the smaller r correspond to the stronger inhomogeneity. The f_i numbers are integers taken from a quasi-periodic sequence, from the so-called Fibonacci sequence.

The interaction J in (2.18) is fixed with $J = r^{-\rho}$, where

$$\rho = \lim_{L\to\infty} \frac{\sum_{i=1}^{L} f_i}{L} = 1 - \frac{1}{\omega} , \tag{2.19}$$

is the fraction of units 1 in a very long (infinite) sequence.

The Fibonacci sequence is defined by the following algebraic expression :

$$f_i = 1 + \left[\frac{i}{\omega}\right] - \left[\frac{i+1}{\omega}\right] , \tag{2.20}$$

where $[x]$ denotes the integer part of x, and $\omega = (\sqrt{5}+1)/2$. The sequence can alternatively defined by a substitution rule

$$\begin{aligned} A &\rightarrow AB \\ B &\rightarrow A \end{aligned}$$

The lengths of the possible realizations of the Fibonacci chain are Fibonacci numbers (1,2,3,5 ...). The first few realizations are:

$$\begin{aligned} &A \\ &AB \\ &ABA \\ &ABAAB \end{aligned} \tag{2.21}$$

One can get the $(n+1)$ string by copying the $(n-1)$th string after the nth string. The phase transition of the homogeneous model survive in the quasi-periodic one, there is a ferromagnetic phase if h is smaller than a critical value, and there is a paramagnetic phase, if h is bigger than the critical h_c. The critical magnetic field can be calculated with Pfeuty's result [111]. Pfeuty investigated an inhomogeneous Ising chain (2.8) with inhomogeneous couplings *and* magnetic fields. The smallest excitation becomes zero (the system is critical) in an inhomogeneous Ising model if

$$\Pi_{i=1}^{L} h_i = \Pi_{i=1}^{L} J_i \ . \tag{2.22}$$

This relation holds for arbitrary choice of the couplings and magnetic fields, so for every type of inhomogeneity. In Hamiltonian (2.17) the parameters were selected such a way that the critical point is $h_c = 1$.

In the literature various types of quasi-periodic sequences have been defined with various substitution rules [101] [112]. The Fibonacci sequence was found to be an irrelevant perturbation in the transverse Ising model, which means, the critical properties (exponents) are common with the homogeneous model.

2.2.1 Other quasi-periodic sequences defined by substitution

In this section some examples of quasi-periodic sequences are listed, and their basis properties are obtained.

1. Fibonacci sequence defined above in detail.

2. Thue-Morse sequence. The substitution rule is

$$\begin{aligned} A &\rightarrow AB \\ B &\rightarrow BA \end{aligned} \tag{2.23}$$

   Starting with letter A the first few realizations are: A, AB, $ABBA$, $ABBABAAB$.

3. Period doubling sequence. The substitution rule is:

$$\begin{aligned} A &\rightarrow BB \\ B &\rightarrow BA \end{aligned} \tag{2.24}$$

   Starting with letter B the first few realizations are: B, BA, $BABB$, $BABBBABA$.

4. The Rudin-Shapiro-sequence is defined using an alphabet of four letters A,B,C,D.

The substitution rule is:

$$A \to AB$$
$$B \to AC$$
$$C \to DB$$
$$D \to DC$$

Starting with letter A the first few realizations are: A, AB, $ABAC$, $ABACABDC$. Usually when the Rudin-Shapiro-sequence is investigated only two interaction strength are used (J_0 and J_1), and each letter denotes two neighboring couplings:

$$A \to J_0 J_0$$
$$B \to J_0 J_1$$
$$C \to J_1 J_0$$
$$D \to J_1 J_1$$

For example the string $ABAC$ denotes the next set of couplings: J_0, J_0; J_0, J_1; J_0, J_0; J_1, J_0.

A quasi-periodic sequence usually described by the asymptotic density of different interactions, and the so-called wandering exponent (β), which characterizes the deviation of the couplings from the average. More formally the wandering exponent is defined by the following equation:

$$\sum_{i=1}^{L} J_i - L\overline{J} \sim L^{\beta} \ , \tag{2.25}$$

where $\overline{J}$ is the average coupling in the thermodynamic ($L \to \infty$) limit. The asymptotic density of the different letters, and the wandering exponent can be obtained investigating the substitution matrix. We present this method on the Fibonacci sequence, and list the results for the other sequences. Let us denote the string which substitutes A (B) with $s(A)$ ($s(B)$). For the Fibonacci chain $s(A) = AB$ and $s(B) = A$. The number of the B letters in $s(A)$ is denoted by $n_B^{s(A)}$. The substitution matrix is defined as:

$$M = \begin{pmatrix} n_A^{s(A)} & n_A^{s(B)} \\ n_B^{s(A)} & n_B^{s(B)} \end{pmatrix} \ . \tag{2.26}$$

For the Fibonacci chain:

$$M = \begin{pmatrix} 1 & 1 \\ 1 & 0 \end{pmatrix} \ . \tag{2.27}$$

And the number of the A and B letters in the mth realization is:

$$\begin{pmatrix} n_A^{(m)} \\ n_B^{(m)} \end{pmatrix} = \begin{pmatrix} n_A^{s(A)} & n_A^{s(B)} \\ n_B^{s(A)} & n_B^{s(B)} \end{pmatrix}^{(m-1)} \begin{pmatrix} n_A^{(1)} \\ n_B^{(1)} \end{pmatrix} \tag{2.28}$$

The asymptotic density of letters are given by the components of the eigenvector of M corresponding to it's maximal eigenvalue. The wandering exponent is $\beta = \frac{\ln|\lambda_1|}{\ln|\lambda_2|}$, where λ_1 is the largest eigenvalue of M, and λ_2 is the second largest eigenvalue of M. In the case of the Rudin-Shapiro chain M is a 4×4 matrix. The results for the different sequences are as follows:

1. In the Fibonacci sequence the density of A letters is $\rho_A = 1/\omega$, the density of the B letters is $\rho_B = 1/\omega^2$. The wandering exponent is $\beta = -1$.

2. For the Thue-Morse sequence $\rho_A = \rho_B = 1/2$ and $\beta = -\infty$.

3. For the period doubling sequence $\rho_A = 1/3$, $\rho_B = 2/3$ and $\beta = 0$.

4. For the Rudin-Shapiro sequence $\rho(J_0) = \rho(J_1) = 1/2$ and $\beta = 1/2$.

2.2.2 Harris-Luck criteria

The Harris-Luck criteria classifies the different quasi-periodic sequences according to their effect on the static critical behavior. The criteria can be obtained with the following phenomenological argument. Let us consider a spherical region of the quasi periodic model with radius R, and let's denote this region with Ω. (In one dimension Ω is an interval of length $2R$.) Let's denote the number of couplings in Ω by $B(\Omega)$, and the sum of the couplings by $\Sigma(\Omega) = \sum_{i,j\in\Omega} J_{i,j}$. The aforementioned two quantities are proportional to the volume $|\Omega|$ of the region Ω, which is proportional to R^D, where D is the spatial dimension of the system. The average coupling J_0 is defined as $J_0 = \lim_{R\to\infty} \Sigma(\Omega)/B(\Omega)$. The J_0 average coupling determines the h_c critical field in the thermodynamic limit.
For a big but finite Ω region the deviation from the average is characterized by:

$$\Sigma(\Omega) - J_0 B(\Omega) \sim R^{D\beta} \,, \tag{2.29}$$

where β is the wandering exponent. The correlation length of the system is ξ, $\xi \sim \delta^{-\nu}$, where δ is the distance from the critical point. The typical difference of the J couplings from J_0 is:

$$\frac{J - J_0}{J} \sim \frac{\Sigma(\Omega) - J_0 B(\Omega)}{B(\Omega)} \sim \frac{\xi^{D\beta}}{\xi^D} = \xi^{-D(1-\beta)} \,. \tag{2.30}$$

We introduce the local control parameter δ_i which is given by $\delta_i \sim J_i$. The typical deviation of the local control parameter is:

$$\Delta\delta_i \sim \xi^{-D\nu(1-\beta)} \,. \tag{2.31}$$

The perturbation is irrelevant if $\Delta\delta_i \ll \delta$ in the thermodynamic limit, which gives the following criteria for the irrelevance:

$$D\nu(\beta - 1) + 1 < 0 \,. \tag{2.32}$$

The above condition is called the Harris-Luck criteria. The criteria states, that in the transverse Ising chain where $D = 1$ and $\nu = 1$ the Fibonacci and the Thue-Morse sequence are irrelevant perturbations, the period doubling sequence is a marginal perturbation, and the Rudin-Shapiro is a relevant perturbation.

2.3 Harper model

The Harper-model [88], also called Aubry-André model [89], is a quasi-periodic version of the XX-model. It's Hamilton operator is:

$$\mathcal{H} = -\frac{1}{4}\sum_{n=1}^{L}(\sigma_n^x\sigma_{n+1}^x + \sigma_n^y\sigma_{n+1}^y) - \sum_{n=1}^{L} h_n\sigma_n^z \ . \tag{2.33}$$

Here $h_n = h\cos(2\pi\beta n)$ with $\beta = \frac{\sqrt{5}-1}{2} = 1/\omega$ is the inverse of the golden mean, h is the amplitude of the quasi-periodic modulation. The ω parameter is irrational, this makes the system quasi-periodic. There is a localization-delocalization transition in the model [102], the transition point is $h = 1$. For $|h| < 1$ the eigenstates are extended over the whole system, for $|h| > 1$ the eigenstates are exponentially localized [89]. With the Jordan-Wigner transformation, a set of fermionic operators (c_l, $c_l^\dagger$) can be introduced (see Appendix A), and the Hamiltonian takes the following form (which is a special case of equation 2.2):

$$\mathcal{H} = -\frac{1}{2}\sum_{n=1}^{L}(c_n^\dagger c_{n+1} + c_{n+1}^\dagger c_n) - h\sum_{n=1}^{L}\cos(2\pi\beta n)c_n^\dagger c_n \ , \tag{2.34}$$

which was also the original form of the model introduced by Harper [88].

2.3.1 Aubry-André duality

Following Aubry and André [89] a new set of fermion operators ($c_{\overline{k}}$, $c_{\overline{k}}^\dagger$, $k = 1 \dots L$) are introduced:

$$c_{\overline{k}} = \frac{1}{\sqrt{L}}\sum_n \exp(i2\pi\overline{k}\beta n)c_n \tag{2.35}$$

which are eigenstates of the momentum operator with eigenvalue: $k = \overline{k}F_{n-1}\mathrm{mod}F_n$, where F_n is the n-th Fibonacci number and $L = F_n$. In terms of these the Hamiltonian is given by:

$$\mathcal{H} = -\frac{h}{2}\left[\sum_{\overline{k}=1}^{L}(c_{\overline{k}}^\dagger c_{\overline{k}+1} + c_{\overline{k}+1}^\dagger c_{\overline{k}}) - \frac{2}{h}\sum_{\overline{k}=1}^{L}\cos(2\pi\beta\overline{k})c_{\overline{k}}^\dagger c_{\overline{k}}\right] \ . \tag{2.36}$$

Note that Eq.(2.36) is in the same form as that in Eq.(2.34), thus the Hamiltonian satisfies the duality relation:

$$\mathcal{H}(h) \sim h\mathcal{H}(1/h) \ . \tag{2.37}$$

Here $\sim$ denotes, that the two Hamiltonians are similar: their spectrum is the same.

Through Eq.(2.37) the small h regime of the Hamiltonian, in which the eigenstates are extended in real space are connected with the large h regime, in which the eigenstates have extended properties in Fourier space, thus these are in real space localized. The localization transition takes place at the self-duality point, thus the critical amplitude of the field is $h_c = 1$. For $h > 1$ the localized states have a finite correlation length, ξ, which is given as [89]:

$$\xi = \frac{1}{\ln(h)}, \quad h > 1 \,, \tag{2.38}$$

for all eigenstates of $\mathcal{H}$. We will use the $h \to \pm\infty$ limits in Chapter 7. For large $|h|$ the $\phi_{q,n}$ quantities are given as:

$$\phi_{q,n} = \delta_{n,n_q}, \quad \epsilon_q = -h\cos(2\pi\beta n_q), \quad |h| \gg 1 \,. \tag{2.39}$$

2.4 Disordered quantum Ising chain

The disordered Ising chain is defined by the Hamiltonian:

$$\mathcal{H} = -\frac{1}{2}\left[\sum_{i=1}^{L} J_i \sigma_i^x \sigma_{i+1}^x + \sum_{i=1}^{L} h_i \sigma_i^z\right] \,. \tag{2.40}$$

Here J_i and h_i are positive independent random numbers, selected from the distributions $\pi(J_i)$ and $\rho(h_i)$ respectively. It was found, that the critical behavior is universal, independent form the concrete shape of the distribution in the thermodynamic limit [115].

In the numerical simulations (presented in Chapter 8) We used uniform distribution over $[0, 1]$ for $\pi(J_i)$, and uniform distribution over $[0, h]$ for $\rho(h_i)$. The results recapitulated in this section are true for general selection of $\pi(J_i)$ and $\rho(h_i)$.

Pfeuty's result about the criticality of the Ising chain [111] also holds for one realization of the disordered chain, so a concrete realization is critical if $\Pi_{i=1}^{L}(h_i) = \Pi_{i=1}^{L} J_i$ (see equation (2.22)), or equivalently $\sum_{i=1}^{L} \ln(h_i) = \sum_{i=1}^{L} \ln J_i$. The distribution of the disordered chains is called critical if the average of the logarithm of the local magnetic fields (h_i) and the average of the logarithm of the couplings (J_i) are equal:

$$\overline{\ln h} = \overline{\ln J} \,. \tag{2.41}$$

Here the over line denotes the average over the probability distribution. Note, that with our choice of parameters the system is critical with $h = 1$. If $\overline{\ln h} > \overline{\ln J}$ the system is paramagnetic if $\overline{\ln(h)} < \overline{\ln(J)}$ the system is ferromagnetic. The distance of the critical point is usually measured with the parameter, introduced by Fisher [115]:

$$\delta = \frac{\overline{\ln(h)} - \overline{\ln(J)}}{\mathrm{var}(h) + \mathrm{var}(J)} \,, \tag{2.42}$$

where $\mathrm{var}(J)$ is the varience of the couplings, and $\mathrm{var}(h)$ is the variance of the magnetic fields. The disordered Ising chain shows equilibrium properties which are rather different

from the properties of the homogeneous or quasi-periodic models.

Investigating the local magnetization one finds, in the critical point the typical realizations gives negligible contribution to the average. The average is dominated by so-called rare events, which has vanishing probability but gives $O(1)$ contribution to the average [115] [116].

An other remarkable property of the disordered Ising chain is the existence of the so-called Griffiths phase [116]. This phase is region in the neighborhood of the critical point. It is the region where in the ferromagnetic phase some rare samples can be paramagnetic, and in the paramagnetic phase some rare samples can be ferromagnetic. I summarize here the properties of the surface magnetization, and the low-lying excitations. The surface magnetization is a good example for a rare-event dominated average, and the properties of the low-lying excitations will be used in Chapter 8. The surface magnetization $m_s = m_1$ is related to the local transverse fields and couplings with a relatively simple formula [117] [118] :

$$m_s = \left[1 + \sum_{l=1}^{L-1} \Pi_{j=1}^{l} \left(\frac{h_j}{J_j}\right)^2\right]^{-1/2} , \tag{2.43}$$

where h_i and J_i are arbitrary positive real numbers. In the critical point, the typical value of the magnetization is determined by the largest term of the sum in equation (2.43). The typical value of the largest term is $\sim \exp(\text{const}L^{1/2})$ so the typical value of the surface magnetization is:

$$m_s^{\text{typ}}(L) \sim \exp(-\text{const.}L^{1/2}) . \tag{2.44}$$

The average surface magnetization shows a rather different behavior [14]. There are rare realizations where the random variables $\epsilon_j = \ln \frac{h_j}{J_j}$ behaves like a surviving walk. This realizations has $O(1)$ contribution to the average of the magnetization, and dominate the average. The average magnetization is:

$$[m_s]_{av}(L) \sim L^{-x_m^{(s)}} \quad x_m^{(s)} = 1/2 . \tag{2.45}$$

In the ferromagnetic phase close to the critical point the surface magnetization is: $[m_s]_{av}(\delta) \sim |\delta|^{\beta_s}$ with $\beta_s = 1$. The typical and the average correlations can be described with different correlation lengths. From the finite size dependence of the surface magnetization one obtains: $\xi \sim |\delta|^{-\nu}$ with $\nu = 2$. The typical correlations decay faster: $\xi_{\text{typ}} \sim |\delta|^{-\nu_{\text{typ}}}$ with $\nu_{\text{typ}} = 1$.

In the remaining of this section we summarize the basic properties of the low-lying excitations of the disordered transverse Ising model. The lowest excitation energy is [98]:

$$\epsilon_1(L) \sim m_s \overline{m_s} \Pi_{i=1}^{L-1} \frac{h_i}{J_i} , \tag{2.46}$$

where m_s and $\overline{m_s}$ are the boundary magnetizations on the two ends of the chain.

In the critical point the order of magnitude of the lowest excitation is given by the boundary magnetization, so

$$\epsilon(\delta = 0, L) \sim \exp\left[-\text{const}L^{1/2}\right] . \tag{2.47}$$

The typical time scale is given by the inverse of the lowest excitation $t_r \sim \epsilon^{-1}$, and the length scale in the neighborhood of the critical point is given by the system size ($\xi \sim L$), so the length and time scale is connected as:

$$\ln \tau \sim \xi^{\Psi} \ , \tag{2.48}$$

where $\Psi = 1/2$ [115] [117] [103]. In the homogeneous and quasi periodic quantum Ising chains a power law scaling connect the time and the length scale $t_r \sim \xi^z$ with a finite z dynamical exponent. The (2.48) equation is a sign of an ultra-slow dynamics, where the dynamical exponent is formally infinite.
In the paramagnetic Griffiths phase, where $\delta > 0$, and $\max\{J\} > \min\{h\}$ there are rare regions of size l_{rare} where the local couplings are stronger than the local magnetic fields, and the system is locally ferromagnetic. Note that the boundaries of the Griffiths phase depends on the probability distribution of h_i and J_i. For example with the box distributions used in Chapter 8 and already mentioned after the definition of the model, the Griffiths phase extends over the whole off-critical (ferromagnetic and paramagnetic) region. The energy gap in the aforementioned locally ferromagnetic rare samples is exponentially small in l_{rare}: $\epsilon \sim \exp[-\text{const} l_{\text{rare}}]$, so the relation between the length and the time scale is:

$$t_r \sim \xi^z \ , \tag{2.49}$$

with a finite dynamical exponent z. This scaling relation is typical for the Griffiths phase [119]. The dynamical exponent in the Griffiths phase is continuous function of the δ parameter. The precise value of z is given by the positive root of the equation:

$$\left[\left(\frac{J}{h}\right)^z\right] = 1 \ . \tag{2.50}$$

In the ferromagnetic phase the lowest excitation is exponentially small. The dynamical exponent is usually obtained from the second gap, and found to be the positive root of

$$\left[\left(\frac{h}{J}\right)^z\right] = 1 \ . \tag{2.51}$$

However, the exponentially small first gap is also interesting from the viewpoint of the dynamics, as the reader will see it in chapter 8.

The eigenstates of the off-critical disordered Ising model are localized [115]. In the critical system there is a finite localization length for every excitations with $\epsilon > 0$, but the localization length is divergent for $\epsilon \to 0$ [120] [115]. The equilibrium properties of the random chain can be best understood with the strong disorder renormalization group (SDRG), which was applied by Fisher [115] to the critical point of the model and later was generalized to the Griffiths phase [116]. The SDRG is a real-space renormalization group method where the decimation step is the elimination of the strongest of the couplings and magnetic fields. It is possible to follow the transformation of the distribution of the magnetic fields and couplings under the renormalization flow. From these distributions

one can conclude exact results about the thermodynamic behavior.

Chapter 3

Quench dynamics of homogeneous systems

The quench dynamic means, that the quantum system is in its ground state initially, and an external parameter is changed instantaneously. With the new value of the external parameter the initial ground state is not an eigenstate of the new Hamiltonian, and a non-trivial time evolution starts. More formally let's denote the Hamiltonian of the system with $H(h)$, where h is the external parameter. For $t < 0$ $h = h_0$ and the system is prepared in the ground state of $H(h_0)$. Let's denote this initial state with $|\Psi_0^{(0)}\rangle$. At $t = 0$ the value of the external parameter is changed instantaneously to $h \neq h_0$, and remain h for $t > 0$. The wave vector of the system is

$$|\Psi(t)\rangle = e^{-iH(h)t}|\Psi_0^{(0)}\rangle \ . \tag{3.1}$$

for $t > 0$. The $|\Psi_0^{(0)}\rangle$ original state of the system is usually not eigenstate of the after-quench Hamiltonian $H(h)$, and a non-trivial dynamics starts after the quench.

Usually we use the Heisenberg picture. The operator of physical observable A evolves in the Heisenberg picture as

$$A^H(t) = e^{iH(h)t}Ae^{-iH(h)t} \ . \tag{3.2}$$

The expectation value of the A observable is calculated as $\langle A\rangle = \langle\Psi_0^{(0)}|A^H(t)|\Psi_0^{(0)}\rangle$. A two point correlation function can be calculated as $C_{A,B}(t_1,t_2) = \langle\Psi_0^{(0)}|A^H(t_1)B^H(t_2)|\Psi_0^{(0)}\rangle = \langle\Psi_0^{(0)}|\exp(iH(h)t_1)A\exp(-iH(h)(t_1-t_2))B\exp(-iH(h)t_2)|\Psi_0^{(0)}\rangle$. The time evolution of the most simple operators are written down in detail in Appendix A.

3.1 Numerical results on global quenches

3.1.1 Magnetization

In [37] the authors investigated the quantum Ising model. Here we recapitulate the main numerical results about the dynamics of the magnetization (order parameter). For very long times ($t \gg L$) the magnetization reaches an asymptotic value in a finite system.(In figure 3.1 this regime is not show. The oscillations which can be seen in figure 3.1 decay,

and become negligible for very long times.) The magnetization is measured on the l th site in a system of total length of L spins. We assume $L/2 > l$ so the nearest boundary is at the first spin. For times of the same order of magnitude of the system length, different regimes can distinguished.

1. For short times ($t \ll L$) the relaxation of the magnetization is exponential:

$$m_l(t) \approx A(t)\exp(-t/\tau) \quad \text{for } t < t_l \ . \tag{3.3}$$

   This regime can be seen in figure 3.1 in the left-bottom panel before the first minimum. The $A(t)$ prefactor is $\mathcal{O}(1)$. It is found to be oscillating if the quench ends in the disordered phase $A(t) \sim \cos(at+b)$, and positive ($A(t) \sim \cos(at+b)+c > 0$) if the quench ends in the ferromagnetic phase. This first regime ends after t_l time. It was found that $t_l = l/v_{max}$, where v_{max} is the maximum group velocity [1] in the system. In other words v_{max} is the time needed by the fastest possible signals to reach the lth spin from the boundary. If the bulk of an infinite system is investigated,($L \to \infty$ and $l \to \infty$ with $l/L =$ constant) only this first regime exist.

2. Quasi-stationary regime. This regime can be seen in the left upper panel of figure 3.1, when the magnetization is measured far from the center of the chain. (The length of the chain was $L = 256$ so the center is $l = 128$. If the measured spin is far from the center, the quasi-stationary regime is long (see the curve corresponding to $l = 16$), if the spin is closer to the center the quasi-stationary regime becomes shorter (see the curve corresponding to $l = 64$), if the measured spin is in the middle of the chain ($l = 128$) the quasi-stationary regime vanishes.)
   In this regime the decrease of the magnetization is much slower than in the previous one. This regime starts when the fastest quasi-particles starting from the closer boundary reach the measured spin (t_l), and ends when the quasi-particles starting from the other end of the chain (Lth) spin reach the measured spin (time $(L-l)/v_{max}$). This regime holds for $t_l < t < T - t_l$ where $T = l/v_{max}$.
   If one investigates a half infinite system, so the $L \to \infty$ limit with fixed l, the magnetization remains forever in this stationary regime.

3. Reconstruction regime.
   After time $T - t_l$ the magnetization starts to increase

$$m_l(t) \sim \exp(t/\tau') \ . \tag{3.4}$$

   This regime ends at time T, when the fastest signals has run over the whole chain.

4. After time T approximately periodic behavior starts with period T. This periodicity is the result of repeating reflection of signals at the end of the chain.

[1] The group velocity is given by $v_k = \frac{\partial \epsilon(k)}{\partial k}$

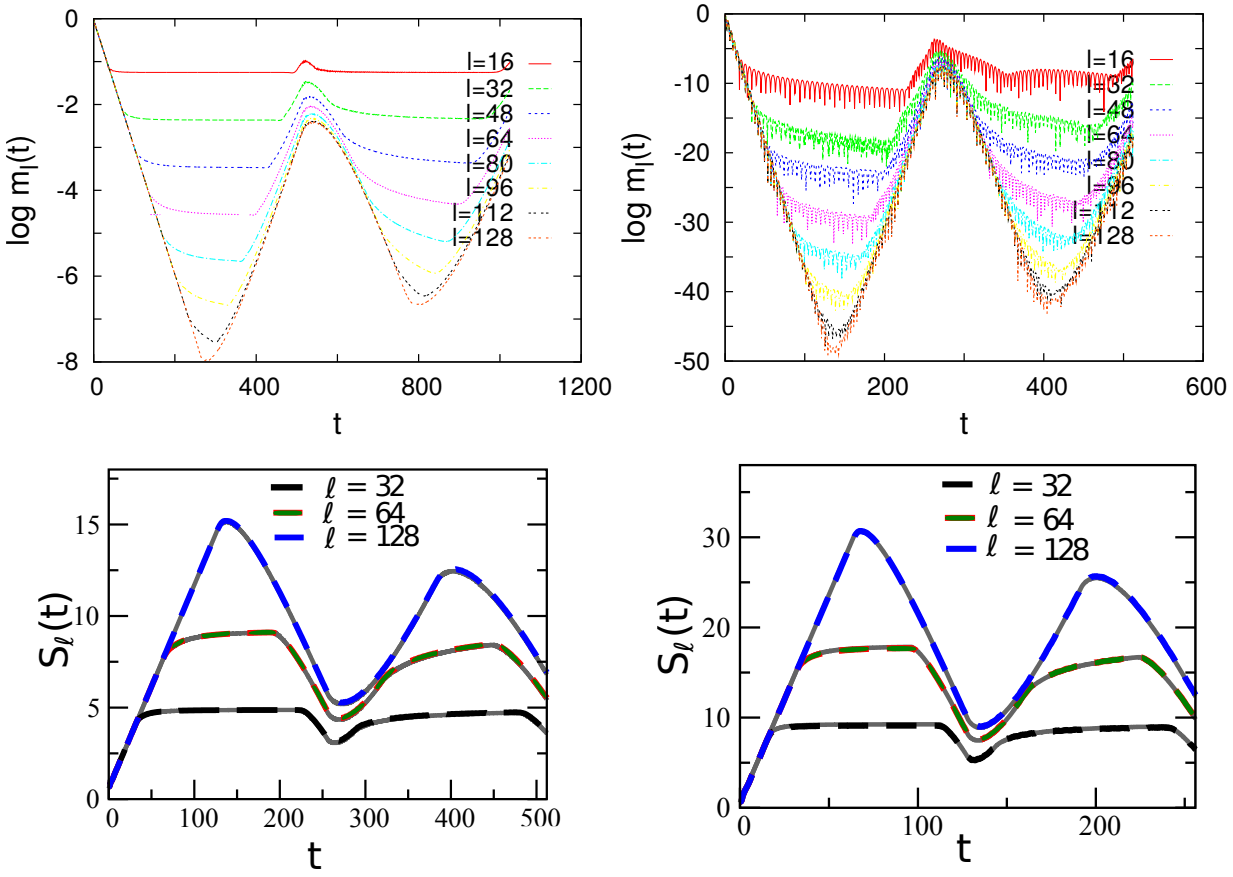

Figure 3.1. Upper row: Magnetization dynamics after a quench from $h_0 = 0$ to $h = 0.5$ (left) and from $h = 0.5$ to $h = 1.5$ (right). Lower row: Entanglement entropy dynamics after a quench from $h_0 = 0$ to $h = 0.5$ (left) and from $h_0 = 0.5$ to $h = 1.5$ (right). The gray curve is the result of the semiclassical calculation which is detailed in section 3.2.3 This figure is based on figure 1. of [79].

3.1.2 Entanglement entropy

Numerical investigations about the dynamics of the entanglement entropy were done in [56] and [122]. In this subsection the main numerical results about the after quench dynamics are recapitulated. The entanglement between the block of the first l spins, and the other $L - l$ spins was calculated. The typical dynamics of entropy is shown in figure 3.1.

The dynamics can divided to different regimes (shown in figure 3.1, lower panel), similarly to the magnetization:

1. For $t < l/v_{max}$ the entanglement entropy increase. The functional form is found to be:

$$S = \alpha(h, h_0)t \ , \tag{3.5}$$

the $\alpha(h, h_0)$ prefactor depends on the pre- and afterquench magnetic fields.

2. There is an intermediate region

$$l/v_{max} < t < (L - l)/v_{max} \ , \tag{3.6}$$

where the entanglement entropy remain nearly constant. In the $L \to \infty$ limit with

finite l this constant value is the asymptotic value ($t \to \infty$) of the entanglement entropy.

3. For
$$(L-l)/v_{max} < t < T = L/v_{max} \tag{3.7}$$
the entropy decreases.

4. After $t > T$ an approximately periodic oscillation begins with period T.

3.2 Quasi-classical description

The quasi-classical description was first applied by Sachdev and Young [123] for finite temperatures in equilibrium. Later this type of description was modified to describe zero temperature non-equilibrium dynamics [37] of the local magnetization and the correlation functions and also has been used to interpret the dynamical entanglement entropy [122] [56]. In this subsection we follow articles [37] and [122] and describe the dynamics of the magnetization and the entanglement entropy with the use of quasi-particles.

The quasi-classical transition works best if the quench ends in the ferromagnetic phase ($h < 1$), and additionally h is small, not too close to the critical point.

With zero transverse magnetic field the ground state is twofold degenerate $|\Psi_0\rangle = a|+++\cdots+\rangle + b|---\ldots\rangle$ where $|+\rangle$ and $|-\rangle$ are eigenstates of $|\sigma_x\rangle$. The lowest excitation is $(L-1)$ times degenerate: $|n\rangle = |++\cdots++--\cdots--\rangle$, here n is the position of the domain wall (kink).

A small transverse magnetic field $h > 0$ destroys the degeneracy of the lowest lying excitations. First order perturbation gives that the low lying excitations are Fourier transformations of the $|n\rangle$ domain wall states.

$$|\Phi(p)\rangle = \sum a_n |n\rangle \tag{3.8}$$

where $a_n = \sqrt{2/L}\sin(pn)$, $\epsilon_h(p) = 1 - h\cos(p)$ and p has $L-1$ discrete values in the $[0, \pi]$ interval.

The low lying excitations are Fourier transformations of domain walls, so a wave packet formed from them represents a moving domain wall. It is known that the group velocity of a wave packet which is localized in momentum space around momentum p is

$$v_p = \frac{\partial \epsilon_p}{\partial p} = \frac{h \sin p}{\epsilon_p} \ . \tag{3.9}$$

In the quasi-classical picture the quasi-particles are created at the moment of the quench homogeneously in the chain with momentum dependent probabilities. After they have been created, they move ballisticaly (with constant speed) and are reflected from the ends of the chain. After their creation the quasi-particles are considered to move deterministically. The Ising model (with arbitrary couplings and magnetic field) can be transformed to free fermions, the details can be found in Appendix A. In particular the after-quench

Hamiltonian with magnetic filed h can be written with fermion operators η_k and $\eta_k^\dagger$ in the following diagonal form:

$$H = \sum_k \epsilon(k)\eta_k^\dagger \eta_k; \tag{3.10}$$

where k is the momentum, which is a quasi-continuous variable in a large system, and $\epsilon_h(k) = \sqrt{(h-\cos p)^2 + \sin^2 p}$ the excitation energies. The η operators are connected to the c operators by tha following Bogoliubov transformation:

$$\eta_q = u_q c_q + i v_q c_{-q}^\dagger \tag{3.11}$$

$$\eta_{-q}^\dagger = i v_q c_q + u_q c_{-q}^\dagger \,, \tag{3.12}$$

where $u_h(p) = \sqrt{(\varepsilon_h(p) + h - \cos p)/(2\varepsilon_h(p))}$ and $v_h(p) = \sqrt{(\varepsilon_h(p) - (h-\cos p))/(2\varepsilon_h(p))}$ The ground state of the after quench Hamiltonian is the vacuum of the η fermions, denoted by $|0\rangle$, The ground state before the quench (denoted by Ψ_0) can be expressed with the ground state after the quench ($|0\rangle$)

$$|\Psi_0\rangle = \Pi_p \left[U_n + i V_n \eta_p^\dagger \eta_{-p}^\dagger\right] |0\rangle \,, \tag{3.13}$$

where $V_p = u_{h_0}(p)v_h(p) - v_{h_0}(p)u_h(p)$ and $U_p = u_{h_0}(p)u_h(p) + v_{h_0}(p)v_h(p)$, and defined in detail in Appendix A.3. From (3.13) one can see, that the quasi-particles are created in pairs with opposite momenta. (This is also required to fulfill the conservation of the momenta.) The probability of the creation of a quasi-particle pair on a given site with momenta p and $-p$ is:

$$f_p = \langle \Psi_0 | \eta_p^\dagger \eta_p | \Psi_0 \rangle = V_p^2 \,, \tag{3.14}$$

$$f_p = \frac{1}{2}\left[1 - \frac{h_0 h - (h_0 + h)\cos p + 1}{\epsilon_{h_0}(p)\epsilon_h(p)}\right] \,. \tag{3.15}$$

The motion of the quasi-particle pairs is periodic with period time $2T_p = 2\frac{L}{v_p}$. The position of the initially right moving quasi-particle is denoted by $x_1(t)$, the position of the initially left moving quasi-particle is denoted by $x_2(t)$. If a quasi-particle pair start from x_0 the left moving particle reach the boundary at $t_a = x_0/v_p$, the right moving quasi-particle reach the left boundary at time $t_b = (L - x_0)/v_p$. For $t < T_p$ the positions of the quasi-particles are:

$$x_1(t) = \begin{cases} x_0 + v_p t & \text{for} \quad t \le t_b \\ 2L - x_0 - v_p t & \text{for} \quad t_b < t \le T_p \,, \end{cases} \tag{3.16}$$

$$x_2(t) = \begin{cases} x_0 - v_p t & \text{for} \quad t \le t_a \\ v_p t - x_0 & \text{for} \quad t_a < t \le T_p \,. \end{cases} \tag{3.17}$$

The quasi-particles meet at $t = T_p$ in $L - x_0$. Between T_p and $2T_p$ another two reflections happen, and at $t = 2T_p$ the quasi-particles meet again, at the position of their creation, x_0 and with the same direction of velocities as at the time of their creation. The quasi-particles move periodically with $2T_p$ period.

When a quasi-particle passes a spin the spin is flipped in the X direction. The two elements of the quasi-particle pair are correlated with each other, but the quasi-particles

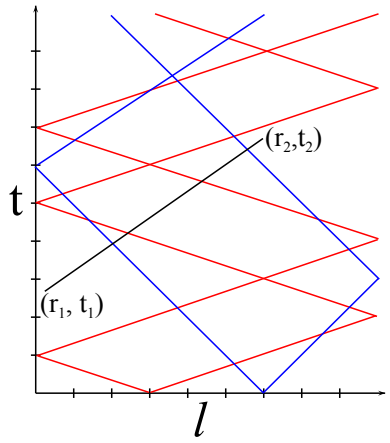

Figure 3.2. Quasi-particle trajectories after a global quench.

from different pairs (starting from different positions) are uncorrelated.

3.2.1 Correlation functions

The correlation functions are defined as:

$$C(r_1,t_1;r_2,t_2) = \langle\Psi_0|\sigma^x_{r_1}(t_1)\sigma^x_{r_2}(t_2)|\Psi_0\rangle \ . \tag{3.18}$$

The behavior of this correlations are interesting on its own right, however in this work I include them, because they are used during the calculation of the local magnetization. The motion of the quasi-particles after the quench is deterministic, but the creation process is stochastic. To calculate the expectation value of correlation functions, one has to average over the possible initial configurations of the quasi-particles.

With a given quasi-particle initial configuration $C(r_1,t_1;r_2,t_2)$ is $+1$ if the trajectories intersect the $(r_1,t_1;r_2,t_2)$ line even times, and -1 if the trajectories intersect the $(r_1,t_1;r_2,t_2)$ line odd times.

The probability, that the quasi-particles started from the same site intersect the line $(r_1,t_1;r_2,t_2)$ an odd number of times is denoted by $Q(r_1,t_1,r_2,t_2)$.

The probability that for a given set of n sites the kinks passed odd times the $(r_1,t_1;r_2,t_2)$ line is:

$$\frac{C(r_1,t_1;r_2,t_2)}{C_{eq}(r_1,r_2)} = \sum_{n=0}^{L}(-1)^n Q^n (1-Q)^{L-n}\frac{L!}{n!(L-n)!} = (1-2Q)^L \approx e^{-2Q(r_1,t_1;r_2,t_2)L} \ . \tag{3.19}$$

To calculate $Q(r_1,t_1;r_2t_2)$ one has to average over the quasi-particle pairs with different momenta between 0 and π:

$$Q(r_1,t_1;r_2,t_2) = \frac{1}{2\pi}\int_0^\pi dp f_p(h_0,h) q_p(r_1,t_1;r_2,t_2) \ . \tag{3.20}$$

In the previous equation $q_p(r_1,t_1;r_2,t_2)$ denotes the probability that the two trajectories of a quasi-particle pair ($x_1(t)$ and $x_2(t)$) together intersect the line $(r_1,t_1;r_2,t_2)$ odd

number of times. The q_p probability can be calculated as the sum of the probabilities $q_p(x_0|r_1,t_1;r_2,t_2)$:

$$q_p = \frac{1}{L}\int_0^L dx_0 q_p(x_0|r_1,t_1;r_2,t_2)\ , \tag{3.21}$$

where $q_p(x_0|r_1,t_1;r_2,t_2)$ denotes the probability that the quasi-particle pair which originally started from x_0 with momenta p intersects the line $(r_1,t_1;r_2,t_2)$ together odd number of times.

3.2.2 Local magnetization

The local magnetization can be expressed as the correlation function of the lth spin at time t, and the lth spin at $t=0$ with the condition that the spin is fixed initially ($\sigma_l^x=+1$).

$$m_l(t) = m_l^{eq} C|_{\sigma_l^x(t=0)=+1}(l,0;l,t) \tag{3.22}$$

The aforementioned quantities ($q(t,l)$, $q_p(t,l)$) take special, more simple form:

$$q(t,l) = Q|_{\sigma_l^x(t=0)=+1}(l,0;l,t) \tag{3.23}$$

$$q(t,l) = \frac{1}{2\pi}\int_0^\pi dp f_p(h_0,h) q_p(t,l) \tag{3.24}$$

$$q_p(t,l) = \frac{1}{L}\int_0^L dx_0 q_p(x_0|t,l)\ . \tag{3.25}$$

To calculate the local magnetization one has to evaluate $q_p(t,l)$.
for early times, when the reflections at the ends did not play a role, $q_p(t,l)$ is simply proportional with the length of the region from where the quasi-particles could reach the l th site. The first reflected quasi-particles reach the lth spin at $t_1 = l/v_p$, so for $t<t_1$ $q_p(t,l) = 2v_pt/L$.

After the quasi-particles reflected from the left boundary (neighborhood of the first spin) arrives, the $q_p(t,l)$ probability remains constant. This constant period remain until the reflections from the right end did not arrive, so for $t_1 = l/v_p < t < t_2 = (L-l)/v_p$ the $q_p(t,l)$ probability is constant $p_q(t,l) = 2l/L$.

When the quasi-particles reflected from the right end arrives at the investigated site l, the $q_p(t,l)$ probability becomes to decrease, and it decreases until $t = T_p = L/v_p$. At time T_p the $q_p(t,l)$ probability becomes zero again.

$$q_p(t,l) = \begin{cases} 2v_pt/L & \text{for} \quad t \le t_1 \\ 2l/L & \text{for} \quad t_1 \le t \le t_2 \\ 2-2v_pt/L & \text{for} \quad t_2 \le t \le T_p \end{cases} \tag{3.26}$$

Since after T_p time the quasi-particles reach their original position, q_p is periodic with period T_p:

$$q_p(t+nT_p,l) = q(t,l) \quad (n=1,2\dots)\ . \tag{3.27}$$

The q function is not periodic, because the quasi-particle pairs with different momenta

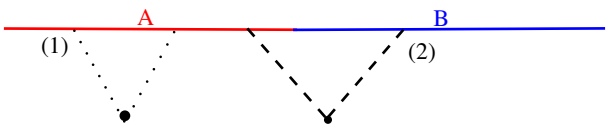

Figure 3.3. The quasi-particle pair denoted by (1) gives no contribution to the entanglement entropy. The other quasi-particle pair denoted by (2) gives non-zero contribution to the entanglement entropy.

has different speed and different period time. In an half-infinite system, so in the limit of $L \to \infty$ with $l = \text{const.}$ the t_2 time becomes formally infinite, and

$$q_p(t,l) = \begin{cases} 2v_p t/L & \text{for} \quad t < t_1 \\ 2l/L & \text{for} \quad t > t_1 \ . \end{cases} \tag{3.28}$$

The magnetization is in the $L \to \infty$ limit:

$$m_l(t) = m_l^{eq} \exp(-t\frac{2}{\pi}\int_0^\pi dp v_p f_p(h_0,h)\Theta(l-v_p t))\exp(-l\frac{2}{\pi}\int_0^\pi dp f_p(h_0,h)\Theta(v_p t-l)) \tag{3.29}$$

The relaxation time of the magnetization is:

$$\tau_{\text{mag}}^{-1}(h_0,h) = \frac{2}{\pi}\int_0^\pi dp v_p f_p(h_0,h) \ . \tag{3.30}$$

3.2.3 Entanglement entropy

In this section the quasi-classical description of the after quench entanglement entropy, and some analytical results about the entropy are summarized. From (3.13) it can be seen that the quasi-particles from one pair are entangled, and quasi-particles from different pairs are not entangled.

A quasi-particle pair gives non-zero contribution to the entanglement entropy between blocks A and B if one member of the pair is in A and the other member is in B.

The contribution of one quasi-particle pair is

$$s_p = -(1-f_p)\ln(1-f_p) - f_p \ln f_p \ . \tag{3.31}$$

Summing up the contributions of all quasi-particle pairs one obtains the precise value of the entanglement entropy, see figure 3.1 The summing up of the entropies of quasi particles (equation 3.31) is straightforward in the $L \to \infty$ and $l \gg 1$ limit.

$$S_l(t) = \begin{cases} t\frac{1}{2\pi}\int dp v_p s_p & \text{if} \quad t < l/v_{max} \\ l\frac{1}{2\pi}\int dp s_p & \text{if} \quad t \gg l/v_{max} \ , \end{cases} \tag{3.32}$$

which corresponds to the exact results of [57]. In this limit ($L \to \infty$ and $l \gg 1$), there is only an increasing regime, and a plateau regime. There are no oscillations, because the quasi particles are reflected only from one end. The oscillations in finite systems (figure 3.1) are results of the interference of the quasi particles reflected from the opposite ends of

the system.

3.3 Spectra and the dynamical properties

Usually the spectra of the Hamiltonian (after the quench) determines the mean features of the dynamics. This will be illustrated by examples. The spectra of the operators can be divided to three classes [113]:

1. Absolutely continuous spectra. The spectra of the most homogeneous systems are absolutely continuous. For example the spectra of the homogeneous Ising model or the homogeneous XX model is absolutely continuous. However, there are inhomogeneous models with absolutely continuous spectra, for example the spectra of the Harper model is absolutely continuous in its extended phase.
   The models with absolutely continuous spectra usually have eigenstates extended over the whole system. [2]

2. The second type is the so-called singular continuous spectra. Such spectra shows a fractal like behavior.
   This type of spectra is observed in certain quasi-periodic systems: in the critical point of the harper model [102] or in the Fibonacci quasi-crystal [113].

3. The third kind is the pure point spectra, which is typical for disordered systems (disordered Ising chain [115], Anderson model with diagonal and off diagonal disorder [120]).
   There are quasi-periodic systems with pure point spectra, an example is defined by a substitutionary rule in [121] and the Harper model in its localized phase is also has pure point spectra.
   Usually there is a finite localization length if the spectrum is pure point spectrum. The energy-dependent localization length shows the spatial extension of the eigenstates with the given energy. It can happen, that the localization length is finite almost in the whole spectra, but becomes divergent at a special energy value. This happens in the critical point of the disordered Ising chain [115] and in the off-diagonal Anderson model [120]. [3]

There are a vast of literature about the dynamics of systems with various types of spectrum. The results of the numerical and exact investigations can be summarized as follows:

1. In the case of absolutely continuous spectra the dynamics is usually ballistic. Ballistic here means that the "signals" travel with constant velocity in the chain.

[2] It is naturally possible to create a Hermitian operator with absolutely continuous spectra and localized eigenstates. For example one can consider the spectra of the homogeneous XX model, and a complete basis of localized eigenvectors. Then one define the operator as the eigenbasis is the aforementioned localized complete set, and the spectra is the spectra of the XX model. However in simple physically inspired models the absolutely continuous spectra is exist together with the extended eigenstates.

[3] The spectra of the one particle excitations of the disordered Ising chain and the set of the positive eigenenergies of the off-diagonal Anderson model are identical.

2. If the spectra is singular continuous the dynamics is slower,the wave packets spread as a power law. This was observed in the critical point of the Harper model [102] and in the Fibonacci quasi-crystal.

3. If there is pure point spectrum, localization or extremely slow dynamic was found. Here localization means that the wave packet reaches a finite width in an infinite system, as in the localized phase of the Harper model. Ultra slow growth of the entanglement entropy after a quench was found in the disordered Ising chain and for other disordered models.

A qualitative explanation of the above results was developed by Thouless and Piéchon in their articles [128]. They investigated the typical variation of the energy levels (ΔE) of a one-dimensional system when the boundary conditions are changed. The ΔE energy scale defines a time scale $t^* \sim 1/\Delta E$. A wave packet needs t^* time to spread trough the entire chain of length L. One gets the diffusion exponent of the wave packet with the $x^2(t^*) \sim (t^*)^2 \sim L^2$ relationship. In a model with absolutely continuous spectrum the typical variation of energy levels is $\Delta E \sim 1/L$, which implies $\sigma = 1$. In a model with pure point spectrum, $\Delta E \sim 1/L$ and $\sigma \sim \ln L/L \approx 0$. If the spectra is singular-continuous, the relation between the variation of energy levels and the system size is more complicated,$\Delta E \sim L^{-1/\alpha}$, with various exponents α. Detailed investigations shows, that the qth moment of a wave-packet starting form the i_0th site behaves as $x^{(q)}(i_0, t) \sim t^{\sigma(i_0,q)}$, where the exponent $\sigma(i_0, q)$ depends on the initial position i_0.

3.4 Experiments

In the past two decades the experimental study of non-equilibrium quantum dynamics become possible in systems of trapped ultra-cold atoms [12]. The gas of neutral atoms (mostly alkali atoms) is cooled with subsequent methods. In a typical experiment the gas is first cooled by laser cooling [129] and then trapped in a magnetic or magneto-optical trap, and the trapped gas is cooled further by microwave evaporate cooling [130]. These systems were the first realizations of a Bose-Einstein condensate of weakly interacting particles, and the pioneers of this experiments Eric A. Cornell, Wolfgang Ketterle and Carl E. Wieman has been awarded with the 2001 Nobel Prize in Physics for constructing these experiments. The usual way of studying a trapped condensate is the time-of-flight measurement: The trap is turned off instantaneously, and the atoms of the condensate extends ballistically. The extended atomic cloud is photographed later. Since the condensate is located in a small volume, the velocity distribution can be obtained by time-of-flight measurement [131]. Cooling and trapping fermions is also possible. however technically even more challenging, since the thermalization during the evaporating cooling is slower than in the bosonic case due to the exclusion principle [132].
The systems built from trapped cold atoms are well isolated from the environment and can be considered as closed systems during the duration of experiments. The time scale of the dynamics of these cold-atom systems is much longer than the usual time scales in

solid sates. The reason of the longer time scale, is the dilute nature of this systems. The typical time scale is a few ms which makes possible to experimentally follow the dynamics. The interaction strength (usually characterized by the s-wave scattering length) between the trapped atoms is tunable with an external magnetic filed due to the Fresbach resonance [133].

With the use of the so-called optical lattices [134] experimental realization of lattice models became possible. An optical lattice is formed by the interference of contra propagating laser beams, which create an effective optical potential. Atoms can be trapped at the minima of the optical potential. (The minima of the optical potential are actually maxima of the light intensity.)

One of the most natural models emerging in optical lattices is the Bose-Hubbard model and the Fermi-Hubbard model [135]. Even the monitoring of a single atom became possible in Hubbard-like models [136]. Among investigating naturally emerging models in optical lattices it is possible to simulate several solid-state-physics inspired models [137]. Ising and XY models were engineered on triangular lattice [138]. The metal-insulator transition was observed in the experimental realization of the Harper-model [139]. Disordered systems were also realized in optical latices [137].

The quench dynamics of isolated systems were investigated in many experiments. Kinoshita investigated [3] [4] the quench dynamics and the steady state of an effectively one-dimensional system. It was found, that the system does not reach a thermal steady state in the obtainable time regime, the system was close to the integrable Lieb-Lüttinger model. The nearly integrability may be the reason of the lack of the thermalization. Marc Cheneau and his colleges investigated the spreading of correlations in a one dimensional Bose-Hubbard model [10]. They demonstrated experimentally the light-cone-like spreading of the correlations, which is characteristic in homogeneous systems, and has been used in Section 3.2.

Nearly-adiabatic dynamics was also investigated in systems of ultra-cold atoms. Weiler *et al.* investigated a Bose gas, which was cooled below the BEC transition point [140]. They demonstrated spontaneous forming of defects (vortices) during the process. Sadler *et al.* [6] investigated a spinor Bose gas (^{87}Rb). This system shows both magnetism and superfluidity. They have driven this system over a quantum phase transition, and investigated the density of "generated defects". Here defects refer to any difference from the ground state of the instantaneous Hamiltonian.

A periodically driven interacting Harper model was studied recently [75]. The periodic driving induce a delocalized regime in the phase diagram of the system.

These experiments with cold atoms draw attention on their own right. On the other hand, these experiments lead to better understanding of solid state physics. Furthermore these systems may serve as a hardware of quantum computing [139].

Chapter 4

Local quenches

4.1 Introduction

The non-equilibrium process after a sudden change of a parameter "quench" at $T = 0$ is of recent interest, and there were much attention paid to the [13–51, 55–57] global quenches, where the parameters are varied homogeneously in space.

The *local quench* is another interesting question, when parameters are modified locally at a given site. Experimental realization of local quenches is X-ray [141] absorption in metals. The theoretically most investigated systems in this field are the critical one-dimensional systems.

For those systems, exact analytical results have been derived using conformal field theory (CFT) [142, 143].

In CFT one investigates the continuum limit of the model, where the system evolves in a continuous two dimensional space-time (x, t). In this description the local quench means the sudden change of a parameter at a given spatial (x) position, for example the strength of the coupling at $x = 0$, changes from κ_1 before the quench $(t < 0)$ to κ_2, after the quench $(t > 0)$. The expectation value of operators are calculated with path-integral methods. These conformal methods usually work for appropriate boundary conditions: $\kappa = 0$ (uncoupled half chains) or $\kappa = \infty$ (fixed local spin) and $\kappa = 1$, i.e., uniformly coupled chain. Among other quantities the after quench entanglement entropy has been studied by CFT ([122,144–147]), after joining two initially independent systems (changing from $\kappa_1 = 0$ to $\kappa_2 = 1$), the entropy grows logarithmically [142], and the prefactor of the logarithm is universal $\mathcal{S}(t) = (c/3) \ln t + \text{const}$, it is one third of the central charge of the CFT. In finite systems the entropy cannot grow without limit, in a system of length L the entropy starts to grow for short times, but for long times it shows a periodic variation in terms of t/L [143].

Various correlation functions and also the magnetization have been investigated with CFT: the time (measured from the time of the quench) and spatial (distance measured from the site of the local quench) dependence is usually characterized by power laws [142], and the exponents are combinations of bulk and surface static scaling dimensions. The CFT predictions have been tested against numerical calculations in concrete models [94], and good agreement has been found.

There were studies about local quenches in non-conformally invariant systems. For quenches ending in the ordered phase of the transverse Ising chain, a semiclassical description was applied [38], which has been verified by numerical simulations [94]. The strong disorder renormalization group method was modified to describe the dynamics of disordered systems [103] such as TIC (transverse Ising chain), and the entanglement entropy [79, 82] and the full counting statistics was [80] investigated with this modified renormalization group. In critical disordered systems, both quantities has an ultra slow $\mathcal{S}(t) \sim \ln \ln t$ time dependence, which was tested against numerical calculations.

In this section we study the time evolution of the local magnetization at the critical point of the TIC, after a generalized local quench: The value of the local coupling and also the value of the local fields are changed at the time of the quench $t = 0$. The static critical behavior near a local defect in the TIC is non-universal, the scaling dimension of the local magnetization continuously varies with the defect strength $x_i = x_i(\kappa_i)$ [118,148–152]. Later this question has been studied with various methods, S-matrix theory [153], , conformal methods [154–159] and conformal field theory [160–162].

The ground state [122], [163–165] and the dynamical [122, 166] entanglement entropy across a defect also shows a similar behavior: the so-called effective central charge is a prefactor of the entropy, and a continuous function of the defect parameters. It is expected, that the non-equilibrium relaxation of the magnetization is also non-universal.

4.2 Model

I consider a critical TIC of length L with free boundary conditions and a defect at $L/2$. The Hamiltonian of the system is

$$\mathcal{H}_i = -\frac{1}{2}\left[\sum_{n=1}^{L-1}\sigma_n^x\sigma_{n+1}^x + (J_i-1)\sigma_{L/2}^x\sigma_{L/2+1}^x + \sum_{n=1}^{L}\sigma_n^z + (h_{i1}-1)\sigma_{L/2}^z + (h_{i2}-1)\sigma_{L/2+1}^z\right] . \quad (4.1)$$

The index $i = 1, 2$ refers to the values of the transverse fields h_{i1}, h_{i2} and the coupling J_i, before and after the quench at $t = 0$. In this chapter the after quench time dependence of the local magnetization is in the focus of the interest. I follow the evolution of the local magnetization at the defect, $m_d(t) = m_{n=L/2}(t)$. To investigate this generalized local quench a two dimensional classical model is introduced in section 4.3. The imaginary time version of the above described quench is in close relation with this classical model. The imaginary time version of the quench is defined on the n-τ plane, where n is the number of the spins, and τ is the imaginary time. The quench process investigated in the $n - \tau$ plane corresponds to a two-dimensional ($2d$) classical critical Ising model with a composite ladder defect at the center (see figure 4.1 for an illustration; the x axes corresponds to τ and n corresponds to y).

With the help of the two-dimensional classical model, exact results can be obtained for the imaginary time version. This results are summarized in section 4.3.

The real time behavior is obtained by analytical continuation the imaginary time behavior in section 4.3. To do this, we use previous exact results from the literature about special

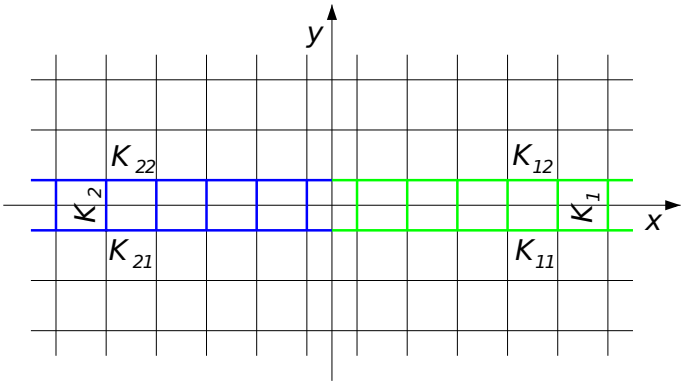

Figure 4.1. Composite line defect in the critical two-dimensional square lattice Ising model. The composite defect is made of two half-lines of perturbed couplings on a ladder.

cases of the local quench.
The results are validated by large scale numerical simulations which are written down in section 4.4.

4.3 Composite defect exponents

In this section the critical classical Ising model on the square lattice is investigated with a line defect as shown in figure 4.1. The composite defect results from the junction of two semiinfinite line defects, indexed 1 and 2, with different horizontal (K_{ij}) and vertical (K_i) perturbed couplings ($i, j = 1, 2$). Since the scaling dimension of the bulk energy density, $x_e = 1$, is the same as the dimension of the line defect, the perturbation is marginal and varying local magnetic exponents are expected as for the infinite line defect [148, 149].

In the off-critical system the local behavior of the magnetization, at a distance from the defect smaller than the bulk correlation length ξ, is governed by three different exponents. In the central region the local magnetization exponent x_{12} is influenced by the two parts of the composite defect. Outside this region, at a distance larger than ξ from the junction, the local magnetization exponents, x_1 and x_2, are the same as for infinite line defects.

One can calculate the composite defect exponent x_{12} using conformal methods and finite-size scaling [154–159].

In a first step, the infinite critical system of figure 4.1, with a single composite line defect along the x-axis, is transformed into a cylinder with two equidistant line defects, 1 and 2, parallel to the cylinder axis, through the conformal transformation $w = (L/2\pi) \ln z$ where $z = x + iy$ and $w = u + iv$. The system after the transformation (shown in figure 4.2(a)), is infinite along the u-axis and periodic with size L, even, in the transverse direction. The gap-exponent relation [168] can be used in the cylinder geometry to calculate the composite defect exponents.

Although the column-to-column transfer matrix can in principle be diagonalized for arbitrary couplings, the calculations are more simple in the strongly anisotropic (Hamiltonian) limit [107, 169] where the couplings in the longitudinal direction (K_u in the bulk and K_{ij} on the line defects) are strong while the couplings in the transverse direction (K_v

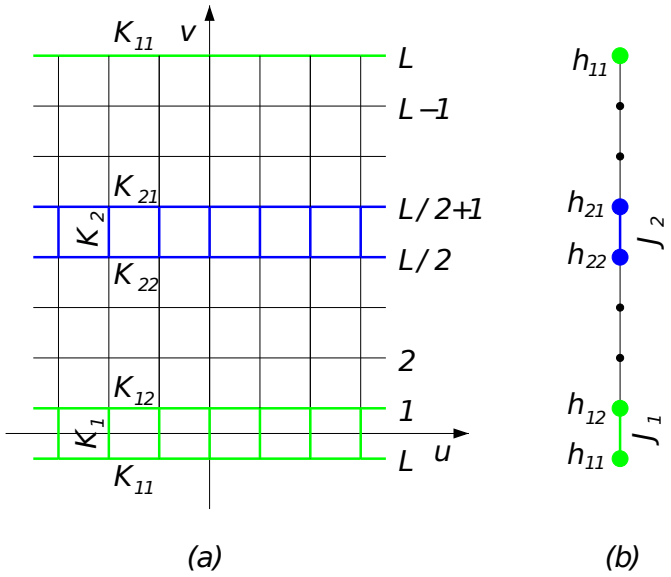

Figure 4.2. (a) Under the conformal transformation $w = (L/2\pi)\ln z$ the full plane with a composite line defect becomes an infinite cylinder with circumference L and two infinite equidistant line defects, parallel to the cylinder axis. (b) In the extreme anisotropic limit, the column-to-column transfer operator can be expressed as the exponential of the Hamiltonian of a TIC, up to a rescaling factor.

in the bulk and K_i on the line defects) are weak. For a critical bulk in the extreme anisotropic limit, corresponding to a continuous imaginary time along the u-axis, the ratio $K_{vc}/K^*_{uc} \to 1$ whereas on the line defects $K_i/K^*_{uc} \to J_i$ and $K^*_{ij}/K^*_{uc} \to h_{ij}$. Here K^*_{uc} is defined by the implicit equation $\tanh K^*_{uv} = \exp(-2K_{uv})$.

Then the transfer operator is $\mathcal{T} = \exp(-2K^*_{uc}\mathcal{H})$ where $\mathcal{H}$ is the Hamiltonian of a TIC [106] (see figure 4.2(b))

$$\mathcal{H} = -\frac{1}{2}\left[\sum_{n=1}^{L}\sigma^x_n\sigma^x_{n+1} + (J_1-1)\,\sigma^x_L\sigma^x_1 + (J_2-1)\,\sigma^x_{L/2}\sigma^x_{L/2+1}\right.$$
$$\left. + \sum_{n=1}^{L}\sigma^z_n + (h_{11}-1)\,\sigma^z_L + (h_{12}-1)\,\sigma^z_1 + (h_{22}-1)\,\sigma^z_{L/2} + (h_{21}-1)\,\sigma^z_{L/2+1}\right]. \quad (4.2)$$

With the Jordan-Wigner transformation the Pauli spin operators σ^x_n and σ^z_n, are expressed in terms of fermion operators. [104] See details in Appendix A.4. The Hamiltonian becomes quadratic in terms of fermion operators, but involves an operator $\mathcal{P} = (-1)^Q$, associated with the bond between the last (Lth) and the first spin.. The $\mathcal{P}$ operator commutes with $\mathcal{H}$, and its eigenvalues are $+1$ and -1 corresponding to $Q = 0$ and $Q = 1$. The number of fermions is even (odd) if $Q = 0$ ($Q = 1$). In each subspace $\mathcal{H}(Q)$ is diagonalized by a Bogoliubov transformation [106, 170] and takes the form $\mathcal{H} = \sum_k \epsilon_k \left(\eta^\dagger_k\eta_k - \frac{1}{2}\right)$ in terms of the new fermion operators η_k and $\eta^\dagger_k$. One gets the square of the excitation energies as the Q-dependent eigenvalues of the $L \times L$ matrix equation $(\mathbf{M} - \epsilon^2_k)\,\mathbf{\Phi}_k = 0$ with line n $(1 < n < L)$ given by:

$$h(n-1)J(n-1)\Phi_k(n-1) + [h^2(n) + J^2(n-1) - \epsilon^2_k]\Phi_k(n) + h(n)J(n)\Phi_k(n+1) = 0. \quad (4.3)$$

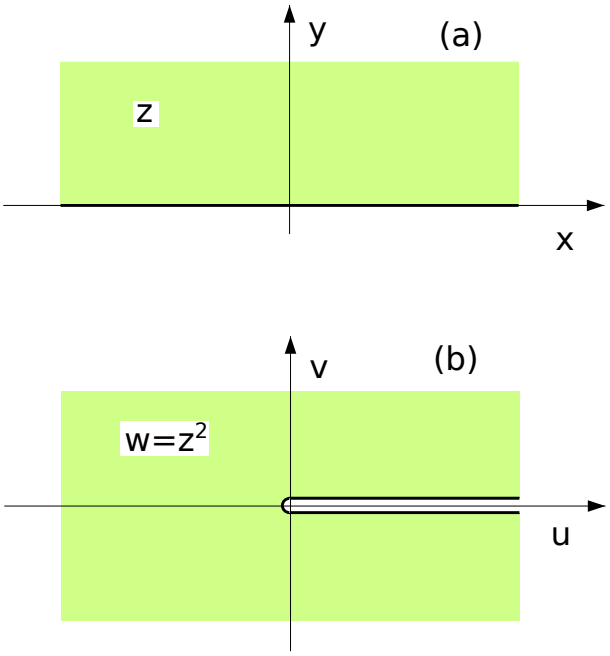

Figure 4.3. The conformal transformation $w = z^2$ maps the upper half-plane onto the full plane with a cut along the positive real axis.

In lines 1 and L one has to replace J_1 by $(-1)^{Q+1}J_1$. $h(n)$ is the transverse field at site n and $J(n)$ the coupling between sites n and $n+1$ as shown in figure 4.2(b).

With $\epsilon_k^2 = 4\sin^2(k/2)$ and using the Ansatz

$$\begin{aligned} \Phi_k(1) = -A\,, \quad \Phi_k(n) = (-1)^n \left(B\, e^{ikn} + C\, e^{-ikn}\right) \quad (n = 2, L/2)\,, \\ \Phi_k(L/2{+}1) = (-1)^{L/2+1} D, \quad \Phi_k(n) = (-1)^n \left(E\, e^{ikn} + F\, e^{-ikn}\right) \quad (n = L/2{+}1, L), \end{aligned} \tag{4.4}$$

equation (4.2) becomes a linear system of six equations for the amplitudes A to F. The characteristic equation gives the allowed values of k in each Q sector.

In the limit of large systems (continuum limit, $1/L \to 0$), with $\epsilon_k = k = \alpha/L$, one can expand the characteristic equation in powers of $1/L$. To leading order, $\mathrm{O}\,(L^{-2})$, is found to be

$$\begin{aligned} \cos\alpha &= \frac{\left[\kappa_1 - (-1)^Q\,\kappa_2\right]^2 - \left[1 + (-1)^Q\,\kappa_1\kappa_2\right]^2}{\left[\kappa_1 - (-1)^Q\,\kappa_2\right]^2 + \left[1 + (-1)^Q\,\kappa_1\kappa_2\right]^2}\,, \\ \kappa_i &= \frac{J_i}{h_{i1}\,h_{i2}} \qquad (i = 1, 2)\,, \end{aligned} \tag{4.5}$$

where κ_i is an effective bond interaction. This can be rewritten as

$$\cot\left(\frac{\alpha}{2}\right) = \pm\frac{\kappa_1 - (-1)^Q\,\kappa_2}{1 + (-1)^Q\,\kappa_1\kappa_2} = -\tan\left(\frac{\alpha}{2} - \frac{\pi}{2}\right)\,. \tag{4.6}$$

By introducing the angle $\theta_i = \arctan(1/\kappa_i)$ $(i = 1, 2)$ one gets the relation

$$\begin{aligned} \tan\left(\frac{\alpha}{2} - \frac{\pi}{2}\right) &= \pm\frac{\tan\theta_1 - (-1)^Q \tan\theta_2}{1 + (-1)^Q \tan\theta_1 \tan\theta_2} \\ &= \pm\tan\left[\theta_1 - (-1)^Q \theta_2\right] . \end{aligned} \tag{4.7}$$

Thus the fermionic excitation energies take the form [157, 159]

$$\epsilon_r^{\pm}(Q) = \frac{2\pi}{L}\left(1/2 \pm \Delta_Q + r\right) , \qquad Q = 0, 1 , \tag{4.8}$$

where r is an integer and

$$\Delta_0 = \left|\frac{\theta_1 - \theta_2}{\pi}\right| , \quad \Delta_1 = 1 - \frac{\theta_1 + \theta_2}{\pi} . \tag{4.9}$$

One gets the magnetization exponent from the gap-exponent relation [168]

$$x_{12} = \frac{L}{2\pi}(E_\sigma - E_0) , \tag{4.10}$$

where $E_0 = E_0(0)$ is the ground-state energy of $\mathcal{H}$ in equation (4.2 which belongs to the even sector of the fermionic Hamiltonian whereas E_σ, which is the first excited state of $\mathcal{H}$, belongs to the odd sector. These two states belong to different sectors, so the gap involves the difference ΔE between the ground-state energies in the two sectors and is given by

$$E_\sigma - E_0 = \Delta E + \epsilon_0(1) = E_0(1) - E_0(0) + \epsilon_0(1) , \tag{4.11}$$

with [157]

$$\Delta E = \frac{2\pi}{L}\left[\frac{1}{2}\left(\Delta_1^2 - \Delta_0^2\right)\right] , \quad \epsilon_0(1) = 1/2 - \Delta_1 . \tag{4.12}$$

A simple expression for the local magnetization exponent is obtained by collecting the above results:

$$x_{12} = \frac{2}{\pi^2}\arctan\left(\frac{1}{\kappa_1}\right)\arctan\left(\frac{1}{\kappa_2}\right) = \sqrt{x_1 x_2} . \tag{4.13}$$

This result can be proven for the "composite defect" shown in figure 4.3(b) where $\kappa_1 = 0$ (cut on the positive u-axis) and $\kappa_2 = 1$ (no perturbation around the negative u-axis). Then x_1 is the free surface exponent $x_{ms} = 1/2$, x_2 the bulk exponent $x_m = 1/8$ and from equation (4.13) one gets $x_{12} = 1/4$. Now the conformal transformation $w = z^{\omega/\pi}$ is applied to the critical upper half-plane of figure 4.3(a). The result of the conformal transformation is a corner with opening angle ω and corner exponents are related to the surface exponents via $x_c = \pi x_{ms}/\omega$ [171, 172]. If $\omega = 2\pi$, the transformed system is the full plane with a cut (see figure 4.3(b)) so that $x_{12} = x_{ms}/2 = 1/4$.

The gap giving the local energy density exponent is $E_\epsilon - E_0$, where E_ϵ is the lowest eigenstate of $\mathcal{H}$ with two fermions. Both states contains even fermions so that, according

to equation (4.8), the local energy exponent, given by

$$\frac{L}{2\pi}(E_\epsilon - E_0) = \frac{L}{2\pi}\left[\epsilon_0^-(0) + \epsilon_0^+(0)\right] = 1\,, \tag{4.14}$$

keeps its unperturbed value. It is necessary to keep a truly marginal behavior for the local magnetization when the defect strength is modified. Otherwise the criterion of marginality would no longer be satisfied.

4.2 Scaling behavior in imaginary time

In this short section the result obtained for the imaginary time scaling $t = i\tau$ of critical systems are summarized and stated in a form, that the real-time continuation become straightforward.

The parameters of the defect are different for $\tau < 0$ and for $\tau > 0$. The magnetization has the following finite-size scaling behavior along the defect line:

$$m_d(\tau, L) = L^{-x_i}\,\widetilde{m}_d^i(\tau/L), \quad i = 1(2), \quad \tau < 0\ (>0)\,. \tag{4.15}$$

According to exact calculations, which can be found in the next subsection, the local scaling exponent x_i is a function of the following combination of the defect parameters

$$\kappa_i = \frac{J_i}{h_{i1}h_{i2}}\,. \tag{4.16}$$

and it is given by

$$x_i = \frac{2}{\pi^2}\arctan^2\left(\frac{1}{\kappa_i}\right)\,. \tag{4.17}$$

The scaling function $\widetilde{m}_d^i(z) = \text{const}$ for $|z| \gg 1$, i.e., for $|\tau| \gg L$ and for $|z| \ll 1$ it behaves as a power law $\widetilde{m}_d^i(z) \sim |z|^{\omega_i}$. The value of the exponent ω_i depends on the scaling behavior of the local magnetization in the region $\tau \ll L$, where the two different semiinfinite defect lines are connected. In the junction point the local critical behavior is influenced by both defects and the scaling of the magnetization in the asymptotic limit is:

$$m_d(\tau \ll L, L) \sim L^{-x_{12}}\,, \tag{4.18}$$

where x_{12} is the composite defect (generalized corner) exponent.

Since both scaling equations (4.15) and (4.18) are true for the system, the ω_i exponent has to be $x_{12} - x_i$. Using the previous result one gets for the magnetization profile in the $0 < \tau \ll L$ limit:

$$m_d(\tau) \sim \tau^{x_{12}-x_2}\,, \quad 0 < \tau \ll L\,. \tag{4.19}$$

At the end of this section some special cases are treated. The scaling behavior of the magnetization is the same on both sides of the defect, which is not trivial due to the (possible) asymmetry. An other interesting property of the magnetization is obtained if fixed-spin initial condition is realized either with $h_{1j} = 0$ ($j = 1$ and/or 2) or with $J_1 = \infty$,

leading to $\kappa_1 = \infty$. With this initial condition, according to equation (4.17), $x_1 = x_{12} = 0$, so that equation (4.19) simplifies to

$$m_d^{(+)}(\tau) \sim \tau^{-x_2} \quad 0 < \tau \ll L\,. \tag{4.20}$$

The protocol where two half-chains, initially disconnected, are connected by a bulk coupling for $\tau > 0$ is a special case of the general local quench investigated here, and due to it's simplicity it is worth to investigate this special case. The scaling dimensions of the magnetization are denoted by x_m and x_{ms}, in the bulk and at a free surface, respectively. Initially $\kappa_1 = 0$ and $x_1 = x_{ms} = 1/2$ whereas $\kappa_2 = 1$ and $x_2 = x_m = 1/8$ for $\tau > 0$. In this special case the scaling of the magnetization is

$$m_d^{(fb)}(\tau) \sim \tau^{1/8}\,, \quad 0 < \tau \ll L\,. \tag{4.21}$$

Here the (fb) superscript refers to the free boundary (surface).

4.3 Scaling behavior in real time

For the scaling behavior of the magnetization in real time, some results have been obtained in special cases, when the final state is the homogeneous bulk one ($\kappa_2 = 1$), and the initial state is also special, the spin at the defect is fixed ($\kappa_1 = \infty$) or the chains are disconnected (free) ($\kappa_1 = 0$). There is CFT-result [142] for the fixed spin initial condition.

$$m_d^{(+)}(t) \sim t^{-2x_m} \quad 0 < t \ll L\,. \tag{4.22}$$

This result have been tested by numerical simulations on the TIC [94]. The time dependence of the local magnetization is periodic in a finite system of length L. In an open chain the result of [94] are described by the following sinusoidal form:

$$m_d^{(+)}(t, L) \sim \left[L \sin\left(\pi \frac{t}{L}\right)\right]^{-2x_m}, \quad 0 < t < L\,, \tag{4.23}$$

which transforms to equation (4.22) for $t \ll L$. For the case, when the two half chains are disconnected, the results of [94] can be summarized as:

$$m_d^{(fb)}(t, L) \sim L^{-1/2} \left[L \sin\left(\pi \frac{t}{L}\right)\right]^{1/4}, \quad 0 < t < L\,. \tag{4.24}$$

In the limit of short times the previous formula takes the following shape:

$$m_d^{(fb)}(t) \sim m_0(L)\, t^{1/4}, \quad 0 \leq t \ll L\,, \tag{4.25}$$

where $m_0(L) \sim L^{-x_{ms}}$ is the equilibrium value of the defect magnetization in the initial state.

The time exponent in equation (4.25) is $1/4 = 2(x_{ms}/2 - x_m)$ where the $x_2 = x_m$ and

$x_{12} = x_{ms}/2$ exponents of the protocol ($\kappa_1 = 0$ to $\kappa_2 = 1$) are in evidence.

For fixed spin initial state (equation (4.22)) the same form applies with $x_{12} = 0$.

If t^2 is substituted for τ the scaling equations in imaginary time (equations (4.20) and (4.21)) and real time (equations (4.22) and (4.25)) become equivalent.

Thus one can wrote for the general behavior of the real time magnetization (in the asymptotic limit of large systems $L \gg 1$) :

$$m_d(t) \sim m_0(L)\, t^{2(x_{12}-x_2)}, \quad 0 < t \ll L\,, \tag{4.26}$$

with $m_0(L) \sim L^{-x_1}$. In a finite-size system periodic behavior is expected in the form:

$$m_d(t,L) \sim L^{-x_1} \left[L \sin\left(\pi \frac{t}{L}\right) \right]^{2(x_{12}-x_2)}, \; 0 < t < L\,. \tag{4.27}$$

The above two equations are the main results of this chapter. At this point these formulas are conjectures and will be tested by large-scale numerical simulations in the next sections.

4.4 Numerical investigations

4.4.1 Technical details

In the numerical calculations the techniques presented in the Appendix A and in chapter B.1 are used. The TIC is expressed in terms of free fermions, (Appendix A) and the magnetization is calculated as a Pfaffian (described in section B.1). From technical point of view the process requires the numerical diagonalization of $2L \times 2L$ matrices with the real time t entering as a parameter in the calculation.

In the calculations the maximum of the system sizes was $L = 4096$, in the general case the largest system size was $L = 512$.

From the equation (4.27) one can obtain the finite size values of the defect exponents.

I calculated the defect magnetization in a system of size L at times $t = L/2$ and $t = 3L/4$ and in a system of size $L/2$ at time $t = L/4$.

I investigated the ratios [1]

$$\begin{aligned} r(L) &= m_d(t = L/2, L)/m_d(t = L/4, L/2)\,, \\ r'(L) &= m_d(t = L/2, L)/m_d(t = 3L/4, L)\,. \end{aligned} \tag{4.28}$$

With these ratios one gets the nest combinations of exponents

$$\frac{\ln r(L)}{\ln 2} = \alpha(L) \to -x_1 + 2(x_{12} - x_2)\,, \tag{4.29}$$

[1] The value of the defect magnetization in equation (4.27) should be equal at $t = L/4$ and $t = 3L/4$ due to the sine in equation (4.27). However in a finite system, at $L/4$ there are oscillations around the leading behavior which are often not negligible, see next section.

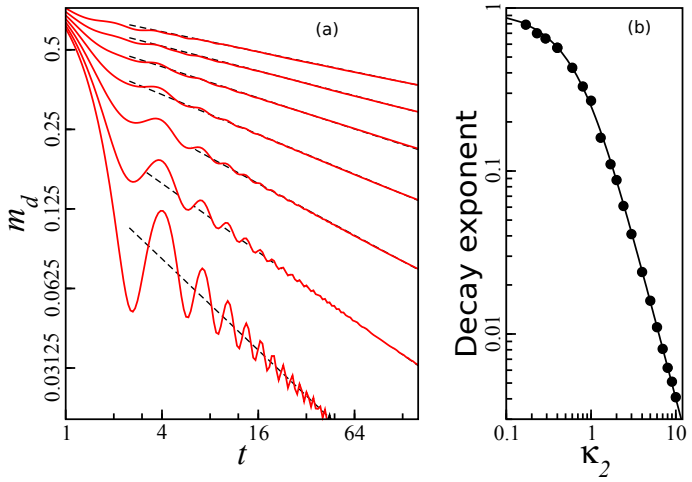

Figure 4.4. (a) Double logarithmic plot of the time evolution of the defect magnetization in a finite system of length $L = 1024$ after a quench from an ordered defect initial state. The values of κ_2 in the final state vary between 1.6 and 0.4, in steps of 0.2, from top to bottom. The dashed lines show the prediction of equation (4.26). The amplitude of the initial oscillations is increasing with decreasing κ_2. (The oscillations decay with time.) (b) The decay exponents in a system of length $L = 512$ are shown by circles for different values of κ_2 in a double logarithmic scale. The error of the estimate is smaller than the size of the symbols. The theoretical prediction $2x_2(\kappa_2)$ is shown by the line.

and

$$\frac{2\ln r'(L)}{\ln 2} = \alpha'(L) \to 2(x_{12} - x_2)\,. \tag{4.30}$$

The equation (4.29) does not depend on the exact functional form of time evolution in finite systems (does not depend on the sine in (4.27) it is the consequence of the asymptotic behavior (4.26)). The functional form of the relaxation in finite systems (the sine in equation (4.27)) can be checked using (4.30), this equation is true only if the functional form in (4.27) is correct. I tested (4.29) and (4.30) in chains up to $L = 4096$.

4.4.2 Ordered defect in the initial state

The initially ordered defect site is reached with $\kappa_1 = \infty$. In this case the exponents $x_1 = 0$ and $x_{12} = 0$ are zero. Since the other two exponents are zero, only x_2 remains in the scaling relation of the magnetization (4.26).

I used in the numerical calculations $h_{11} = h_{12} = 0$ and $J_1 = 1$ which corresponds to an ordered defect in the initial state ($\kappa_1 = \infty$). The final state of the quench is parametrized by $h_{21} = h_{22} = 1$ and $J_2 = \kappa_2$. The time dependence of the magnetization is shown in figure 4.4(a), for various κ_2 values.

If the quench ends with homogeneous chain, $\kappa_2 = 1$ (middle curve in figure 4.4(a)), the relaxation of the magnetization behaves as the conformal result: $m_d^{(+)}(t) \sim t^{-1/4}$, see equation (4.22). This has been checked before in [94]. If the coupling at the defect is larger than the bulk value, $\kappa_2 > 1$, the decay becomes slower and slower. The exponent of the decay ($2x_2$) is in good agreement with the prediction of equation (4.26). If the after quench defect coupling is weaker than the bulk coupling, $\kappa_2 < 1$ there is a decaying oscillatory modulation on the prediction of equation equation (4.26). The amplitude of

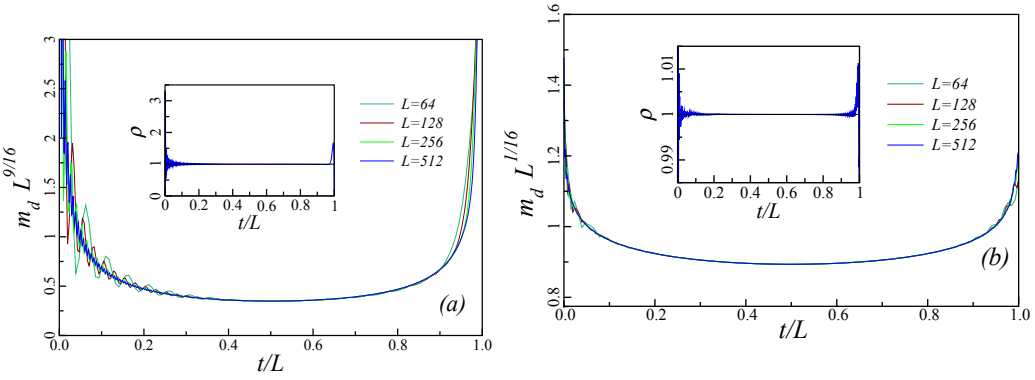

Figure 4.5. Scaling plot of the defect magnetization. The system sizes range from 64 to 512. The quench starts from an initially ordered defect (a) to $\kappa_2 = \sqrt{2} - 1$ and (b) to $\kappa_2 = \sqrt{2} + 1$. In the two insets, ρ is the ratio of the numerical result for $L = 512$ to the analytical prediction in equation (4.27). The effect of the oscillations can be seen in the insets when t/L is close to 0 or 1.

	$\kappa_2 = \sqrt{2}+1$		$\kappa_2 = 1$		$\kappa_2 = \sqrt{2}-1$	
L	$\alpha(L)$	$\alpha'(L)$	$\alpha(L)$	$\alpha'(L)$	$\alpha(L)$	$\alpha'(L)$
128	-0.06208	-0.06243	-0.25305	-0.25758	-0.55512	-0.65624
256	-0.06235	-0.06293	-0.25224	-0.25308	-0.57922	-0.62445
512	-0.06266	-0.06267	-0.25118	-0.25072	-0.60196	-0.54546
1024	-0.06258	-0.06247	-0.25008	-0.25056	-0.54929	-0.57194
2048	-0.06248	-0.06254	-0.25015	-0.25027	-0.56824	-0.56046
4096	-0.06251	-0.06250	-0.25006	-0.25013	-0.56219	-0.56107
Conjecture	-0.0625	-0.0625	-0.25	-0.25	-0.5625	-0.5625

Table 4.1. Finite-size estimates of the relaxation exponent at the defect as defined in equations (4.29) and (4.30) after a quench from an ordered defect to different values of κ_2. In the last line the conjectured exact results are given.

the oscillations increase with decreasing κ_2. For short time, and small enough κ_2 the local magnetization may change sign. In this oscillating regime it would be difficult to directly obtain the decay exponents from a log-log plot. To obtain the exponents, we have measured the series of minimum $[m_{min}(t_i)]$ and maximum values $[m_{max}(t_i)]$ of the oscillations.

The average of the neighboring maximum and minimum $m_{av}(t_i) = [m_{max}(t_i)+m_{min}(t_i)]/2$ is expected to represent an effective (non-oscillating) decay. I used this series to obtain the decay exponents. [1]

The estimated decay exponent is shown in figure 4.4(b) as a function of κ_2. The estimated exponent values are in good agreement with the prediction of equations (4.26) and (4.17).

The time dependence of the oscillation amplitudes, $\Delta m(t_i) = m_{max}(t_i) - m_{min}(t_i)$ was also studied. The decay follows a power law, $\Delta m(t) \sim t^{-a}$, where $a = 1.6(2)$. The a exponent has weak κ_2 dependence, at least for small values of κ_2. To investigate the origin of these oscillations let us consider the quench to two uncoupled half chains, i.e., to $\kappa_2 = 0$. With these parameters the quench is equivalent with the decay of the surface magnetization

[1] Alternatively one may have to consider so long systems, where the oscillations decay in $t \ll L$ times. For small κ_2 this requires too long systems.

starting from a fixed surface spin. With the notation of [14] (equation (4.8)) one gets for the magnetization at the defect: $m_d^{(+)}(t) = P_{1,1}(t)$. (Here $P_{1,1}(t)$ is a coefficient in the time evolution of the Majorana operators. See details in Appendix A.) This value can be calculated in the critical point exactly [14]. In the thermodynamic limit the result is

$$m_d^{(+)}(t) = \frac{J_1(2t)}{t} \simeq \frac{t^{-3/2}}{\sqrt{\pi}} \cos\left(2t - \frac{3}{4}\pi\right), \quad \kappa_2 = 0 \ , \tag{4.31}$$

the second equation holds for $t \to \infty$. Here $J_1(x)$ is the Bessel function of the first kind. In the second part of the equation the asymptotic behavior of the Bessel function (at large t) was used. The surface magnetization for $\kappa_2 = 0$ shows a purely oscillating behavior, the amplitude of the oscillations decays with an exponent $a = 3/2$.

The $a = 3/2$ value for the limiting case $\kappa_2 = 0$, is in correspondence with the numerical estimates calculated for small κ_2 values. The numerical investigations for $\kappa_2 > 0$ and the exact calculations for the limiting case $\kappa_2 = 0$ suggest, that the time dependence can be described as a sum of two terms.

Namely, there is a power law decay, corresponding to equation (4.26) and it is the dominant term for positive κ_2 values. There is an oscillating correction to (4.26), which is usually much smaller than the mean term, but become relevant if $\kappa_2 \ll 1$. Thus the following form is expected:

$$m_d^{(+)}(t) \simeq A(\kappa_2) t^{-2x_2(\kappa_2)} + B(\kappa_2) t^{-a} \cos(2t + \phi) \ . \tag{4.32}$$

Here $a \approx 1.5$ and the prefactors, $A(\kappa_2)$ and $B(\kappa_2)$ are even functions of κ_2 due to symmetry. For small κ_2 we have $A(\kappa_2) \sim \kappa_2^2$ and $B(\kappa_2) \simeq 1/\sqrt{\pi} - b\kappa_2^2$. Let's investigate the finite-size behavior of the defect magnetization. According to (4.27) the defect magnetization is periodic function of the time, with period L. [2]. This behavior can be explained in the framework of the semiclassical approach. In the semiclassical description one considers quasi-particles, which move ballistically in the chain, and reflected at the free ends. Figure 4.5(a) shows the scaled magnetization $L^{2x_2} m_d^{(+)}$ as a function of t/L for $\kappa_2 = \sqrt{2} - 1$. Figure 4.5(a) shows the same quantity for $\kappa_2 = \sqrt{2} + 1$.

If the after quench defect coupling (κ_2) is small, there are strong oscillations for short times ($t/L \ll 1$), in agreement with equation (4.32). There is a good data collapse, in agreement with 4.27 if t/L and κ is not too small.

This is shown in the insets of figure (4.5) in which the ratio ρ of the numerical results for $L = 512$ and the analytical conjecture in (4.27) is shown as a function of t/L. For the latter the prefactor is fixed in order to have a ratio $\rho = 1$ at $t = L/2$.

With the equations (4.29) and (4.30) finite-size estimates for the defect exponent x_2 has been obtained. The finite-size exponents listed in table 4.1 converge quite fast to the expected values, this verifies equation (4.26), and means that the sine in equation (4.27) is probably exact.

For the smallest value of κ_2, $\sqrt{2} - 1$, there are strong oscillations, so the data are

[2] For $t > L$ the absolute value of the sine has to be taken in equation (4.27).

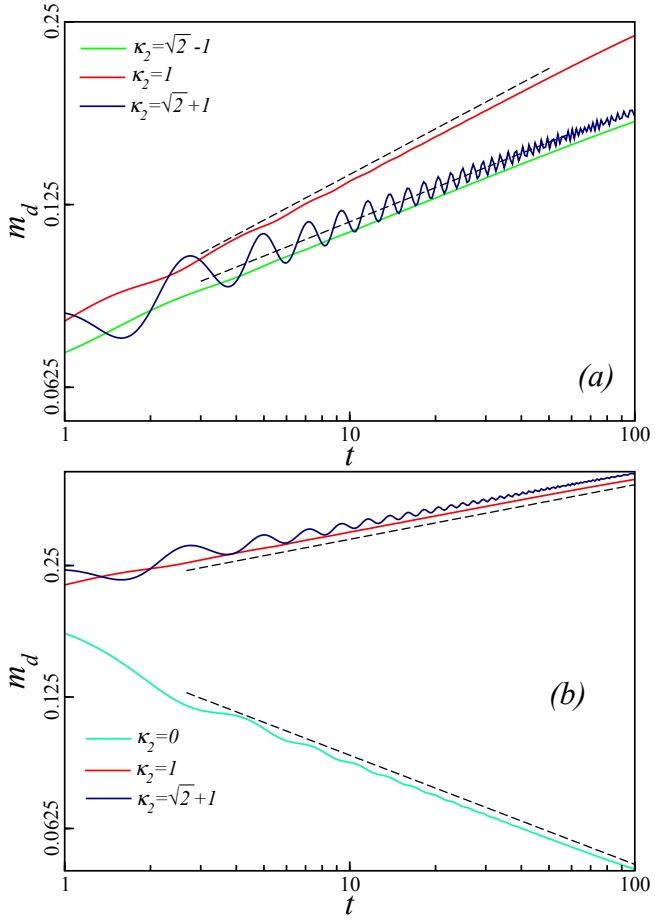

Figure 4.6. Time dependence of the defect magnetization on a log-log plot. The length of the chain is $L = 512$. The strength of the defect changes from (a) $\kappa_1 = 0$ and (b) $\kappa_1 = \sqrt{2} - 1$ to different values of κ_2 during the local quench. The analytical result in equation (4.26) is indicated by the dashed lines. Note that in both figures there are two quenches with the same decay exponent.

non-monotonic in L.

4.4.3 Non-ordered defect in the initial state

For initially non-ordered defects the parameters $h_{11} = h_{12} = 1$ and $J_1 = \kappa_1$ were used in the initial state and the quench is performed to the final state with parameters $h_{21} = h_{22} = 1$ and $J_2 = \kappa_2$.

I have chosen the values of κ_1 and κ_2 from the set $\{0, \tan(\pi/8) = \sqrt{2}-1, 1, 1/\tan(\pi/8) = \sqrt{2}+1\}$.

Whit this choice defect exponents are rational numbers $\{1/2, 9/32, 1/8, 1/32\}$, and the same is true for the composite defect exponents.

The time dependence of the defect magnetization can be seen in log–log plots for different values of the initial and final defect couplings with $\kappa_1 = 0$ and $\sqrt{2} - 1$ in figure 4.6, $\kappa_1 = 1$ and $\sqrt{2} + 1$ in figure 4.7. The values of κ_2 are the remaining ones in the set given above.

The curves have a linear scaling behavior and the slope is in good agreement with the analytical expression in (4.26). The short-time behavior is more or less oscillating, depending on the relative strength of the defect, before and after the quench.

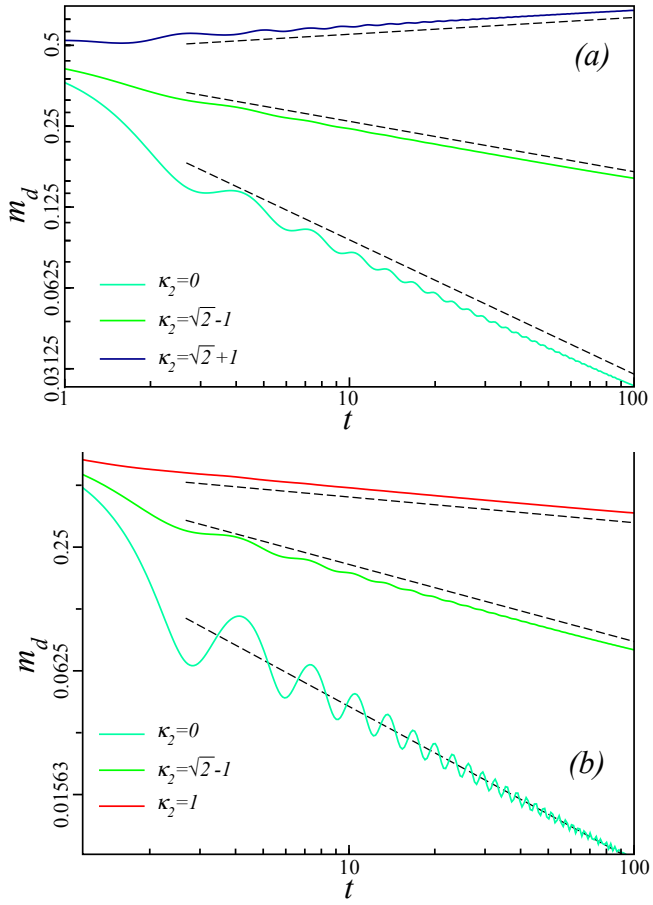

Figure 4.7. As in figure 4.6, for (a) $\kappa_1 = 1$ and (b) $\kappa_1 = \sqrt{2} + 1$.

In order to check the scaling prediction and the functional form given in equation (4.27) we studied the finite-size behavior of the defect magnetization. The scaled defect magnetization $m_d(t, L)L^{x_1-2(x_{12}-x_2)}$ can be seen in figure 4.8 for $\kappa_1 = 0$ and for two values of κ_2. For the smaller value of the coupling $\kappa_2 = \sqrt{2} - 1$ the data collapse is excellent (figure 4.8(a)). For $\kappa_2 = \sqrt{2} + 1$ (figure 4.8(b)) the collapse is not so perfect due to oscillations. The amplitude of these oscillations decrease with the system size. The overall trend confirms the conjectured result in equation (4.27). The insets shows the ratio ρ of the numerical results for $L = 512$ to the analytical conjecture in (4.27). The amplitude of the latter is chosen so that $\rho = 1$ at $t = L/2$. These figures also validate the conjectured result of equation (4.27).

With the relations (4.29) and (4.30) quantitative estimates of the defect exponents have been calculated for finite sizes up to $L = 4096$.

The obtained estimates of the exponents for $\kappa_1 = \sqrt{2} - 1$ and different values of κ_2 are shown in table 4.2.

For each combination of κ_1 and κ_2 the effective exponents converge to the conjectured values.

At the largest size the finite-size estimate for $\alpha(L)$ agrees with the conjectured value up to four or five digits except when κ_2 is small. For small κ_2 the defect magnetization shows strong oscillations (see equation (4.32)).

There is very good, although somewhat less accurate correspondence between the estimates for the exponent $\alpha'(L)$ and the conjectured values. This shows that the conjecture

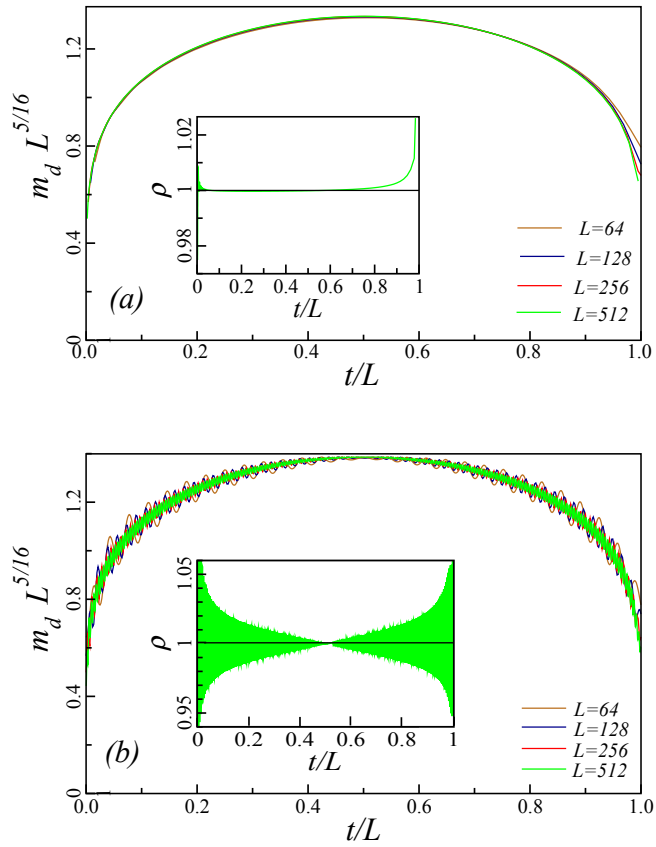

Figure 4.8. Scaling plot of the defect magnetization. The local quench goes from the initial state with $\kappa_1 = 0$ to a final state with (a) $\kappa_2 = \sqrt{2} - 1$ and (b) $\kappa_2 = \sqrt{2} + 1$. The ratio ρ of the numerical result for $L = 512$ to the analytical conjecture in equation (4.27) is plotted in the inset.

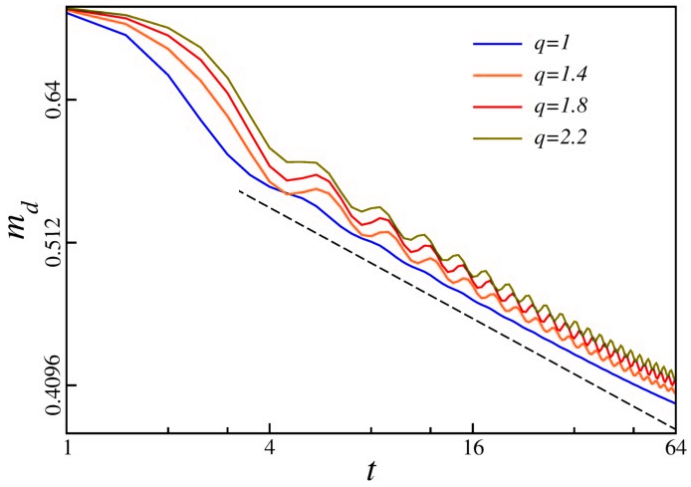

Figure 4.9. Log–log plot of the time dependence of the defect magnetization in a chain of length $L = 256$ with a more complex defect structure after the quench. In the initial state $J_1 = 1 + \sqrt{2}$, $h_{11} = h_{12} = 1$ thus $\kappa_1 = 1 + \sqrt{2}$ and $x_1 = 1/32$. In the final state $J_2 = 1$, $h_{21} = \sqrt{q}$, $h_{22} = 1/\sqrt{q}$ thus $\kappa_2(q) = 1$, $x_2 = 1/8$ and $x_{12} = 1/16$. The slopes for the different values of q are in good agreement with the expected one, $2(x_{12} - x_2) = -1/8$ (dashed line).

about the finite-size scaling form in equation (4.27) is most probably exact. The deviations between the conjectured analytical formula and the numerical results came form oscilla-

	$\kappa_2 = 0$		$\kappa_2 = 1$		$\kappa_2 = \sqrt{2}+1$	
L	$\alpha(L)$	$\alpha'(L)$	$\alpha(L)$	$\alpha'(L)$	$\alpha(L)$	$\alpha'(L)$
128	-0.52609	-0.23745	-0.15460	-0.12094	-0.15554	0.13977
256	-0.52870	-0.24379	-0.15547	-0.12299	-0.15528	0.12397
512	-0.52970	-0.24679	-0.15586	-0.12399	-0.15584	0.12133
1024	-0.53061	-0.24839	-0.15606	-0.12449	-0.15607	0.12086
2048	-0.53093	-0.24923	-0.15616	-0.12474	-0.15617	0.12476
4096	-0.53109	-0.24962	-0.15620	-0.12487	-0.15620	0.12446
Conjecture	-0.53125	-0.25	-0.15625	-0.125	-0.15625	0.125

Table 4.2. Finite-size estimates of the relaxation exponent at the defect as defined in equations (4.29) and (4.30) after a quench from $\kappa_1 = \sqrt{2}-1$ to different values of κ_2. The conjectured exact results are given in the last line.

tions which are results of the discrete lattice spacing. The conformal results are connected to the continuous limit of the model, therefore the conformal results are not expected to describe the aforementioned oscillations.

4.5 Discussion

In this chapter the evolution of the local magnetization was studied in the transverse field Ising chain (TIC) after a quench, when parameters at a defect are suddenly modified. At short time, the defect magnetization follows a power-law behavior. This behavior is closely related to the local static critical behavior at a composite line defect in the $2d$ classical Ising model, which corresponds to the imaginary time version of our problem.

The composite defect exponents have been exactly calculated making use of conformal invariance [171, 172]. The local magnetic exponents are continuously varying with the parameters of the composite defect (i.e., their values before and after the quench in real time) because the perturbation is marginal .

In finite chains the defect magnetization is found to be a periodic function of time and its asymptotic functional form has been conjectured based on the results of [94] an my numerical data.

I have checked numerically (see figure 4.9 for an illustration) that details of the local defect structure (asymmetry in the transverse fields, etc.) are indeed irrelevant and that only the values of κ_1 and κ_2 matter in this respect. The defect exponents x_1 and x_2, as well as the composite defect exponent x_{12}, are functions of the defect parameters κ_1 and κ_2, as given in equation (4.16). I compared the analytical expressions for $t \ll L$, as well as for $t/L = \mathcal{O}(1)$ with the results of large-scale numerical calculations and an excellent agreement has been found.

This chapter is based on the following article:

F. Iglói, G. Roósz, L. Turban *Evolution of the magnetization after a local quench in the critical transverse-field Ising chain* J. Stat. Mech. (2014) P03023

In this article my contributions are the numerical simulations.

Chapter 5

Quench dynamics of the Ising quantum quasi-crystal

5.1 The model

We investigate the quantum Finonacci Ising quasi-crystal, which has been defined in Section 2.2

$$\mathcal{H} = -\frac{1}{2}\left[\sum_{i=1}^{L-1} J_i \sigma_i^x \sigma_{i+1}^x + h\sum_{i=1}^{L} \sigma_i^z\right] . \tag{5.1}$$

The length of the system L is a Fibonacci number, $L = F_n$. ($F_1 = 1$, $F_2 = 1$, $F_{n+1} = F_n + F_{n-1}$)

The couplings, J_i, are site dependent, and parameterized as $J_i = Jr^{f_i}$. Here $0 < r \leq 1$ is the amplitude of the inhomogeneity, $r = 1$ correspond to the homogeneous system, the smaller r correspond to the stronger inhomogeneity. The f_i numbers are integers taken from the Fibonacci sequence defined in section 2.2 $f_i = 1 + \left[\frac{i}{\omega}\right] - \left[\frac{i+1}{\omega}\right]$, where $[x]$ denotes the integer part of x, and $\omega = (\sqrt{5}+1)/2$. The interaction J in (2.18) is chosen to be $J = r^{-\rho}$, where ρ is the fraction of units 1 in a very long (infinite) sequence, calculated in section 2.2. With this choice of J the critical point of the system remains $h = h_c = 1$.

5.2 Entanglement entropy

For a chain of total length F_n with periodic boundary conditions, the entanglement entropy S_ℓ between a block of length $\ell = F_{n-2}$ and its environment which has a length of F_{n-1} has been calculated. We investigated various values of $0 < r < 1$ for the inhomogeneity amplitude. The numerical calculations have been started from the fully ordered state with $h_0 = 0$ to a state with $h > 0$ both in the ordered and in the disordered phases, as well as at the critical point. The numerical results for $\mathcal{S}_\ell(t) - \mathcal{S}_\ell(0)$ are shown in figure 5.1. For all cases mentioned, $S_\ell(t)$ exhibits two time-regimes: in the late-time regime, the entropy is oscillating around an L dependent value, for short times, it increases with time according to a power-law:

$$\mathcal{S}(t) \sim t^\sigma , \tag{5.2}$$

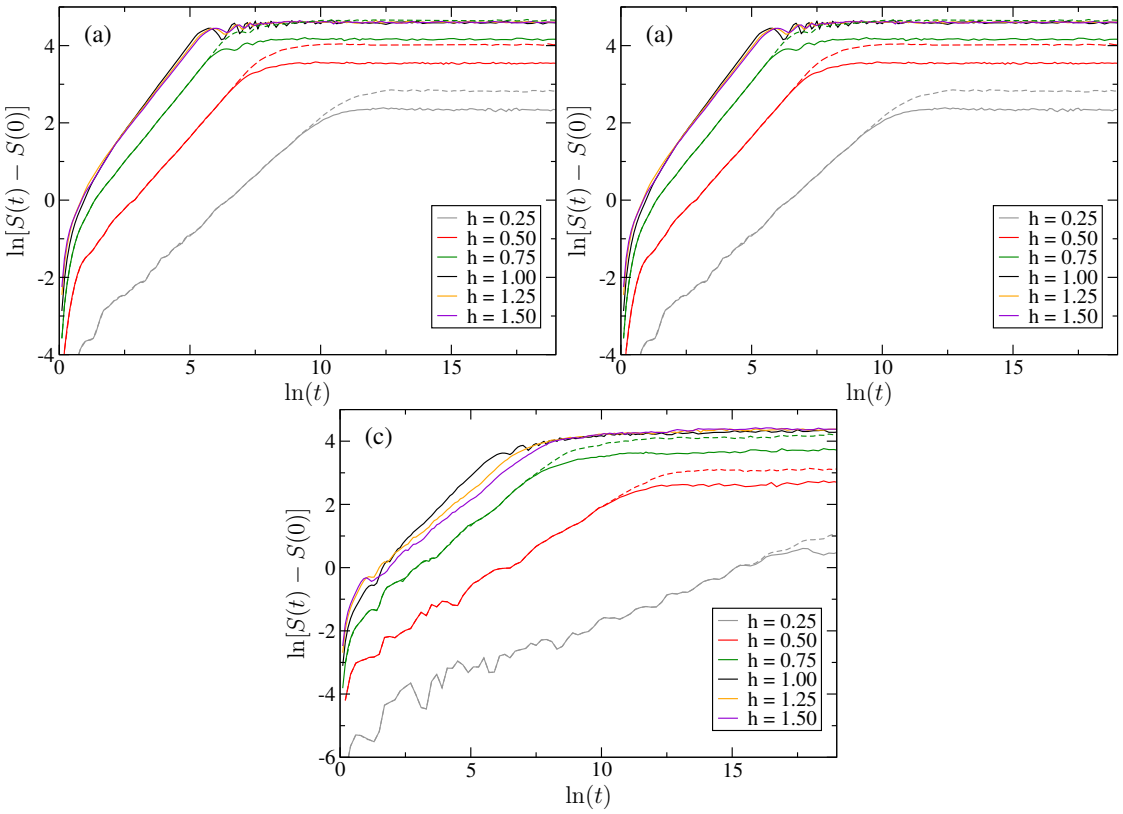

Figure 5.1. Dynamical entropy after a quench from $h_0 = 0$ to various values of h at the aperiodicity parameters (a) $r = 0.75$, (b) $r = 0.5$ and (c) $r = 0.25$. The solid lines are the results for $L = F_{16} = 987$, and the dashed lines (only at $h = 0.25$, $h = 0.5$ and $h = 0.75$) correspond to the data for $L = F_{17} = 1597$. The "noise" (irregular variation) present on the curves in the small t regime is due to such low-energy excitations, which are related to local properties of the quasi-periodic chain and are independent of the chain lengths.

with some exponent $\sigma < 1$, this sort time regime is the linear part in figure 5.1, where the logarithm of the entropy is shown as the function of the logarithm of the time. The numerical results show, that σ depends on the after quench magnetic field h, and does not depend significantly on the initial magnetic field h_0. The (fitted) values of σ for $r = 0.25$, 0.5 and 0.75 are shown in figure 5.6. For the investigated cases, σ reaches it's maximum when the quench ends in the critical point ($h = 1$). The σ exponent depends on the inhomogeneity: The greater inhomogeneity (smaller r) results in slower dynamics (smaller σ).

A characteristic fingerprint of the quasi-periodicity has been seen here: the power law time dependence of the entanglement entropy. In the disordered systems the time evolution is much slower (there is localization, or extra slow evolution in $\log \log t$ form). In the homogeneous systems the entanglement entropy usually grows linearly in time, which is faster than the power law of the quasi-periodic systems. The power-law growth of the entanglement entropy can understood in the frame of the semiclassical theory, if one suppose that the quasi-particles moves with an anomalous diffusion. The width of a wave grows with $x \sim t^D$ where the diffusion exponent is $0 < D < 1$. The semiclassical interpretation will be discussed in section 5.4.

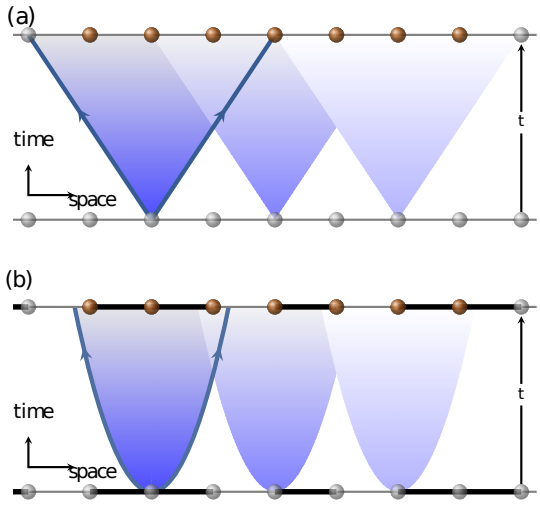

Figure 5.2. Schematic illustration of the light cones of quasi-particles for a homogeneous quantum Ising chain (a) and for a chain with an aperiodic modulation of the couplings (the thin/thick lines between sites represent weak/strong couplings according to a Fibonacci sequence) (b). The quasi-particle excitations emitted at time $t = 0$ move ballistically in the homogeneous lattice, while their motion is anomalous diffusive with $x \sim t^D$ $(D < 1)$ in the quasi-periodic lattice. Pairs of quasi-particles moving to the left or right from a given point are entangled; they will contribute to the entanglement entropy between a region A (the region with orange sites) and the rest of the chain, region B, if they arrive simultaneously in A and B.

5.3 Local magnetization

We calculated the local magnetization $m_l(t)$ in open chains of length $L = F_n$. The magnetization was calculated at site $l = F_{n-1}$[1], we refer this value as bulk magnetization, and denote it with $m_\mathrm{b}(t)$. The surface magnetization $m_1(t)$ was also studied, and some exact results were obtained.

We are interested in the asymptotic behavior of the surface magnetization for long time after the quench. When the quench ends in the ordered phase, $h < 1$, the lowest excitation energy is $\epsilon_1 \approx 0$ (*i.e.* $\cos(\epsilon_1 t) = 1$). As a consequence $P_{1,2k-1}(t)$ in (A.43) has a time independent part. The non-oscillating part of the surface magnetization is defined as: $\overline{m_1} = \lim_{t\to\infty} \frac{1}{t} \int_0^t m_1(t')\mathrm{d}t'$. The stationary value is:

$$\overline{m_1} = \Phi_1(1) \sum_{j=1}^{L} \Phi_1(j)\Phi_1^{(0)}(j) \; . \tag{5.3}$$

Here $\Phi_1^{(0)}(j)$ is one of the coefficients used in the diagonalization of the pre-quench Hamiltonian, $\Phi_k^{(0)}(j)$ was mentioned in equation (2.3) and defined in detail in Appendix A. The $\Phi_k(j)$ coefficients corresponds to the diagonalization of the after-quench Hamiltonian. The ground state surface magnetization is $m_1(h, t = 0) = \Phi_1(1)$ [117, 118], it is finite for $h < 1$ and zero in the paramagnetic phase. The $\Phi_1^{(0)}(1)$ factor shows a similar behavior: it is

[1]With this special choice, one can minimize the finite size effects: The selected spin has similar neighborhood in the chains of different lengths.

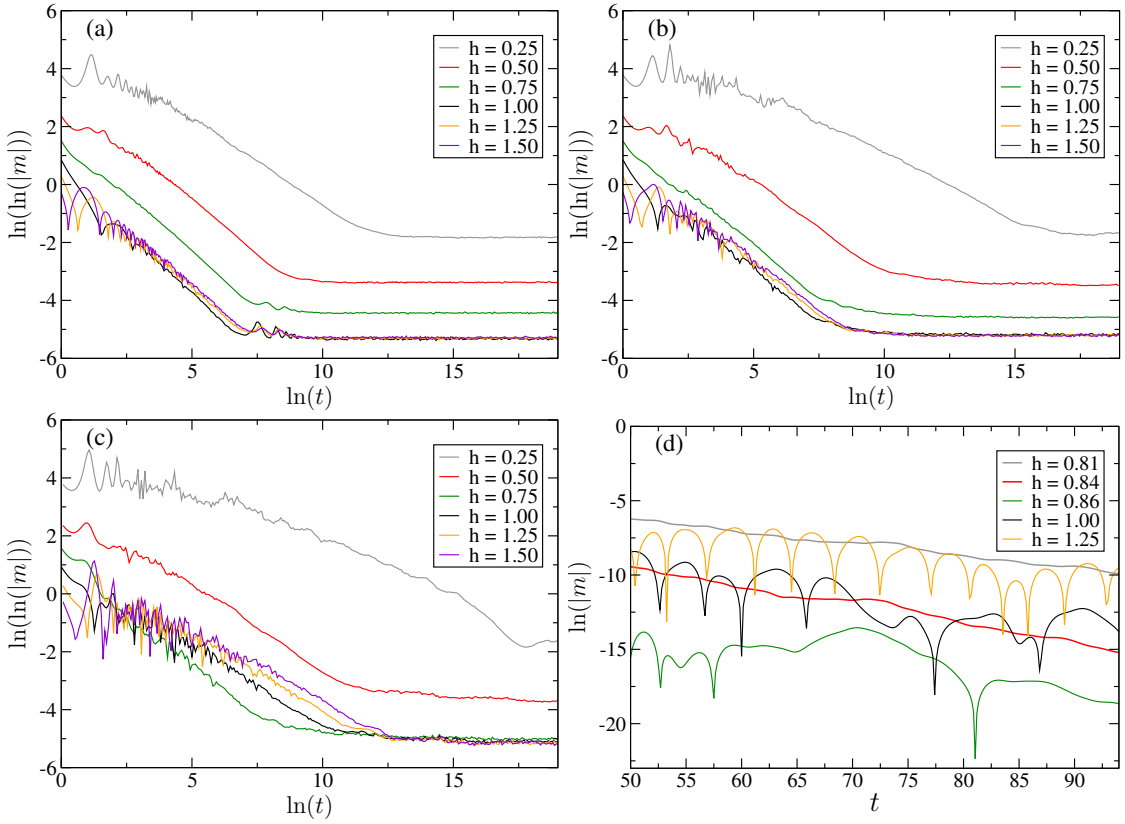

Figure 5.3. Double logarithm of the bulk magnetization as a function of the logarithm of the time. During the quench the transverse field is changed from $h_0 = 0$ to different values of h at the aperiodicity parameter $r = 0.75$ (panel (a)), $r = 0.5$ (panel (b)), $r = 0.25$ (panel (c)). The length of the chain is $L = F_{17} = 1597$ and the magnetization is considered at site $l = F_{16} = 987$. In panel (d) $\ln|m_{\rm b}(t)|$ is shown as a function of t in the window $50 < t < 100$ for different values of h at $r = 0.5$. The oscillations in $\ln|m_{\rm b}(t)|$ (*i.e.* in the prefactor $A(t)$) occur when h is larger than a certain value h^* (here $h^* \approx 0.85$), and the oscillations disappear for $h < h^*$; the dynamical phase transition described in the main text occurs at h^*.

non-zero for $h_0 < 1$, and zero for $h_0 > 1$. Consequently, the stationary surface magnetization is non-zero if $h_0 < 1$ and $h < 0$. If the quench starts from $h_0 = 0$, $\Phi_1^{(0)}(j) = \delta_{1,j}$ and $\overline{m_1} = \Phi_1^2(1)$ so one obtains[2]:

$$\overline{m_1}(h) = [m_1(h, t = 0)]^2 \ , \tag{5.4}$$

The above expression gives an exact connection between the asymptotic value of the surface magnetization and the ground state value of the surface magnetization. The (5.4) equation gives a direct connection between the critical exponent $\beta_{\rm s}^{\rm ne}$ of the non-equilibrium surface magnetization and the critical exponent $\beta_{\rm s}$ of the equilibrium surface magnetization $\beta_{\rm s}^{\rm ne} = 2\beta_{\rm s}$. According to (5.4) and [173], for the Fibonacci chain close to the critical point $h \to h_c = 1$, one has $\overline{m_1}(h) \sim 1 - h^2 = (h_c - h)(h_c + h) \sim h_c - h$, thus $\beta_s^{\rm ne} = 1$.

The time dependence of the bulk magnetization have been numerically calculated for quenches starting from $h_0 = 0$, and ending at various h values. For inhomogeneity values $r = 0.25, 0.5, 0.75$, the double logarithm of $|m_{\rm b}(t)|$ are shown in figure 5.3(a-c) as func-

[2]The (5.4) equation holds for transverse field Ising chains with any type of inhomogeneity.

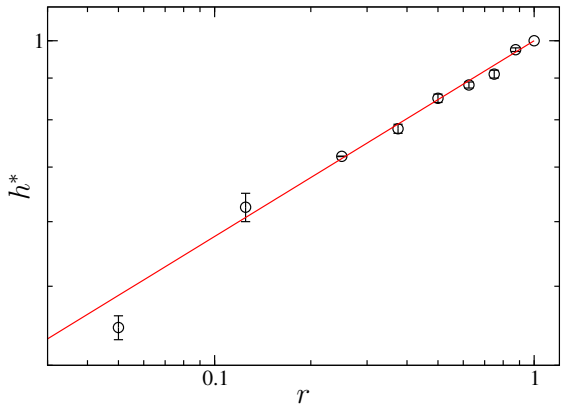

Figure 5.4. Position of the dynamical critical point for different values of the aperiodicity parameter in a double-logarithmic plot. The straight line has a slope $\alpha = 0.24$.

tions of $\ln t$. Investigating the figures 5.2(a-c) one obtains a linear dependence between $\ln|\ln|m_{\rm b}(t)||$ and $\ln t$, which means, that the local magnetization decreases as a stretched exponential function of time:

$$m_{\rm b}(t) \sim A(t)\exp\left(-Ct^{\mu}\right) \ . \tag{5.5}$$

The bulk magnetization decays exponentially in the homogeneous system, so for zero inhomogeneity ($r = 1$) $\mu = 1$.
There is a dynamical phase transition in the homogeneous case: If the quench ends in the ferromagnetic phase ($h < 1$), the magnetization remains positive for all times, however, if the quench ends in the paramagnetic phase ($h > 1$), the magnetization oscillate. One would expect, that there is a similar phase transition in the Finonacci Ising chain, and indeed, the $A(t)$ prefactor shows a dynamical phase transition, however the transition point depends on the strength of the inhomogeneity, on r. For small enough after quench magnetic fields, the magnetization remains positive, if the magnetic field is larger than a value $h(r)$, the magnetization decreases with oscillations. In the oscillating phase one can define a characteristic time, $t_{\rm per}(h,r)$, as the average period of $A(t)$. This time scale ($t_{\rm per}(h,r)$) diverges if $h \to h(r)^{+}$. This behavior is shown in figure 5.2, panel (d) in this figure $\ln|m_{\rm b}(t)|$ is plotted as a function of t. The curves for $h = 0.86, 1.0$ and 1.25 oscillate, but the oscillations vanish for $h = 0.81$ and for $h = 0.84$. The transition point is identified as $h^* = 0.850(5)$. In the quasi-periodic Finonacci Ising chain the dynamical phase transition point is different from the static phase transition point. (The latter is 1.) The dynamical phase transition point, $h(r)$, is smaller than the static phase transition point: $h(r) < 1$. The measured values of $h(r)$ can be approximated with a power law of r:

$$h^*(r) \sim r^{\alpha} \tag{5.6}$$

where the fitted value of α is $\alpha = 0.24(3)$ (see figure 5.4). This power law can be understood by investigating the local neighborhood of the measured spin. One doesn't expect oscillations if the chain is locally ferromagnetic. In the case of a weakly coupled spin with one

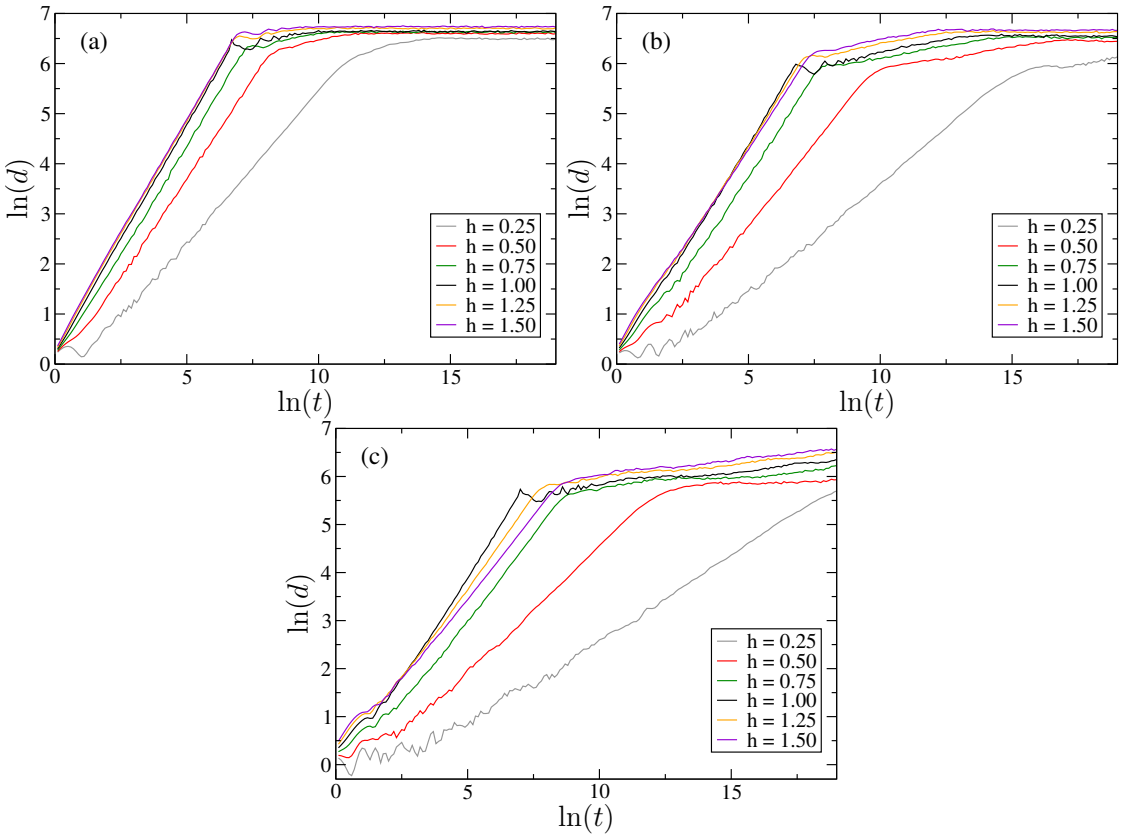

Figure 5.5. Double-logarithmic plot of time-dependent width of the wave-packet at different values of h for $r = 0.75$ (panel (a)), $r = 0.5$ (panel (b)), $r = 0.25$ (panel (c)).

strong (J_s) and one weak (J_w) bond, the chain is locally ferromagnetic if $\ln h < \ln J_s + \ln J_w$. It gives for the dynamical transition point $h^* = r^{2/\omega - 1}$. The fitted $\alpha = 0.24(3)$ exponent coincides with $2/\omega - 1 \approx 0.236$.

The exponent μ describing the decay of the local magnetization dependents both on h and r, but it does not vary significantly with h_0, at least for $h_0 < h$. Our results for the critical exponents $\mu = \mu(h, r)$ are shown in figure 5.6 for $r = 0.75$, 0.5 and 0.25 as functions of h. The exponent μ is maximal at the dynamical phase transition point $h^*(r)$.

5.4 Interpretation by wave packet dynamics

The behavior of the entanglement entropy and the local magnetization after quantum quenches has been successfully described with a semiclassical approach in previous studies. The semiclassical theory will be modified in this chapter to describe the dynamics of quasi-crystals. To do so, the quasi-particles will be described as wave packets, using the method of [87, 174].

We construct a wave packet connecting sites k and l at time t in the form (see the

"Propagator" section):

$$\mathcal{G}(l,k,t) = \langle 0|c_k(t)c_l^\dagger(0)|0\rangle = \frac{1}{2}\sum_q \Big\{ \cos(\epsilon_q t)\big[\Phi_q(l)\Phi_q(k) + \Psi_q(l)\Psi_q(k)\big] - \imath \sin(\epsilon_q t)\big[\Phi_q(l)\Psi_q(k) + \Phi_q(k)\Psi_q(l)\big]\Big\}, \tag{5.7}$$

which is localized at $t = 0$ since $\mathcal{G}(l,k,0) = \delta_{l,k}$.

The width of the wave packet starting from site k after time t is defined as:

$$d(k,t) = \left[\sum_l (k-l)^2 |\mathcal{G}(l,k,t)|^2\right]^{\frac{1}{2}} . \tag{5.8}$$

Since the spectrum of the Finonacci Ising chain is singular continuous, there are multiple energy scales $\Delta\epsilon \sim L^{-1/\alpha}$ with multiple exponents (α). The wave packet in an aperiodic chain is expected to follow an anomalous diffusion $d(k,t) \sim t^{D(k)}$. The diffusion exponent $D(k)$ may depend on the initial position k. The $D(k)$ exponent will extracted from numerical data. A global quench create quasi-particles at every lattice site, so we can measure the average of $d(k,t)$:

$$d(t) = \overline{d(k,t)} \sim t^D . \tag{5.9}$$

In the numerical calculations chains of length $L = F_{17} = 1597$ with periodic boundary condition were used. The homogeneous ($r = 1$) case was checked, and ballistic spreading ($D = 1$) was found, as it was expected. In the quasi-periodic chains anomalous diffusion was found ($D < 1$), which is seen in Figure 5.5. In Figure 5.5 the initially-position-averaged wave packet widths are plotted, as functions of time, in a double logarithmic plot. The diffusion exponent D is extracted from the fit to the linear part of the figures.

The variation of the exponents D, σ (entanglement entropy) and μ (local magnetization) with h at a fixed r is shown in Figure 5.6, In figure 5.6 it can bee seen, that the exponents are close to each other in the non-oscillatory phase ($h < h^*(r)$), and there are significant difference between them in the oscillatory phase ($h > h^*(r)$).

In the homogeneous transverse Ising chain, the dynamic of the entanglement entropy and the magnetization can be described with ballistically moving quasi-particles. In the non-oscillatory phase, one can qualitatively describe the dynamic of the entanglement entropy and the magnetization by considering quasi-particles which move with anomalous diffusion rather than constant speed.

5.5 Discussion

In this chapter we have studied the non-equilibrium dynamics of quasi-periodic quantum Ising chains after a global quench. In a quench process, the complete spectrum of the Hamiltonian is relevant for the time evolution of various observables. For the quasi-periodic quantum Ising chain the spectrum is in a very special form, which is given by a Cantor set of zero Lebesgue measure, i.e. purely singular continuous. We have calculated numer-

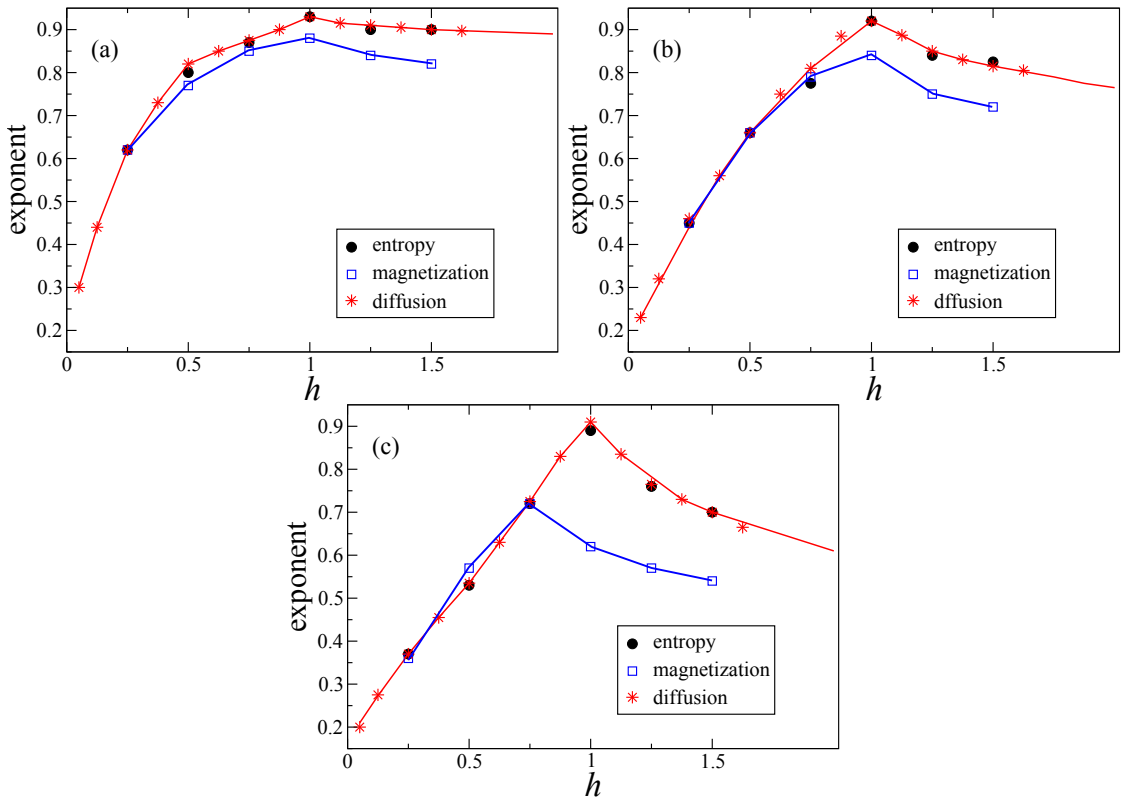

Figure 5.6. Scaling exponents calculated from the time-dependence of the width of the wave-packet, from the entanglement entropy and from the magnetization at different values of h for $r = 0.75$ (panel (a)), $r = 0.5$ (panel (b)), $r = 0.25$ (panel (c)). The full lines connecting the diffusion and magnetization exponents are guides to the eye.

ically two quantities: the dynamical entanglement entropy and the relaxation of the local magnetization. The entanglement entropy is found to increase in time as a power-law (see equation (5.2)), whereas the bulk magnetization decays in a stretched exponential way (see equation (5.5)). Both behaviors can be explained in a quasi-particle picture, in which the quasi-particles move by anomalous diffusion in the quasi-periodic lattice. The diffusion exponent has been calculated by a wave packet approach, and good agreement has been found with the exponents that we obtained for the entropy and for the magnetization. We note that the anomalous dynamics found in the global quench process is similar to the transport properties of quasi-crystals.

Relaxation of the bulk magnetization is found to present a non-equilibrium dynamical phase transition. The non-oscillating phase, in which the magnetization is always positive, and the oscillating phase, in which the sign of the magnetization varies periodically in time, is separated by a dynamical phase transition point, at which the time-scale of oscillations diverges. This singularity point, due to collective dynamical effects, is different from the equilibrium critical point.

A similar non-equilibrium dynamical behavior is expected to hold for other quasi-periodic or aperiodic quantum models as long as the spectrum of the Hamiltonian is also purely singular continuous; there is a large class of such models, for example the Thue-Morse quantum Ising chain. If, however the spectrum of the Hamiltonian of the model is in a different type, such as the Harper potential which has extended or localized states, the non-equilibrium dynamics is expected to be different than the case we consider in this chapter.

This chapter is based on the following article:

F. Iglói, G. Roósz, Y.-C. Lin *Nonequilibrium quench dynamics in quantum quasicrystals* New J. Phys. 15, 023036 (2013)

In this work the numerical calcuations about the entanglemet entropy were done by Prof. Dr. Yu-Cheng Lin. The other numerical works and the anyalisys were done by me. The "Interpretation by wave-packet dynamics" part is common work of the authors.

Chapter 6

Quench dynamics of the Harper model

In the previous chapters, the results about quench dynamics of the homogeneous transverse Ising model were shortly summarized, and we presented our own results abut the Finonacci Ising quasi-crystal.
The spectrum of the homogeneous transverse Ising model is absolute continuous, and the dynamics can be described using ballistically moving quasi-particles. The spectrum of the Finonacci Ising quasi-crystal is singular-continuous and the dynamics can be (qualitatively) described by diffusing quasi-particles.
In this chapter the Harper model will be investigated. The spectrum of this model can be absolutely continuous, singular continuous or pure point spectra, depending on the amplitude of the magnetic field [102], thus one expects a rich behavior of quench dynamics.

6.1 Quasi periodic XX-chain

The Harper model was defined in section 2.3, and the basic properties of the model was also summarized in that section. In this section only notations will be introduced. The Hamilton operator of the Harper model is:

$$\mathcal{H} = -\frac{1}{4}\sum_{n=1}^{L}(\sigma_n^x\sigma_{n+1}^x + \sigma_n^y\sigma_{n+1}^y) - \sum_{n=1}^{L} h_n\sigma_n^z \ . \tag{6.1}$$

Here $\sigma_n^{x,y,z}$ Pauli-matrices at site n. Periodic boundary conditions are applied, thus $\sigma_{L+1}^x \equiv \sigma_1^x$ and $\sigma_{L+1}^y \equiv \sigma_1^y$, and h_n is a quasi-periodic field:

$$h_n = h\cos(2\pi\beta n) \ , \tag{6.2}$$

where $\beta = \frac{\sqrt{5}-1}{2}$ the inverse of the golden mean. The size of the system is a Fibonacci number F_n. The Hamiltonian can written in terms of fermion creation and annihilation

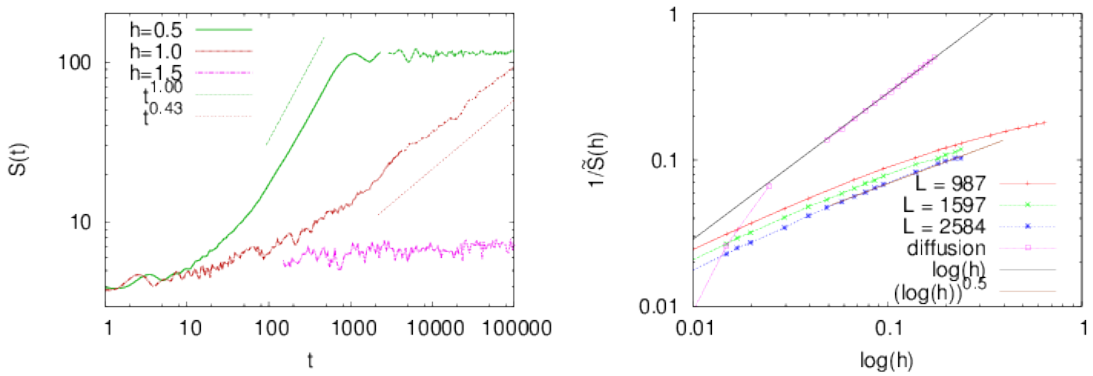

Figure 6.1. Dynamical entanglement entropy after a quench from $h_0 = 0$ to different values of h (left panel). Saturation values of the entanglement entropy and the limiting value of the width of the wave packet (diffusion) in the localized phase show a power-law divergence close to the transition point (right panel).

operators [105]:

$$\mathcal{H} = -\frac{1}{2}\sum_{n=1}^{L}(c_n^\dagger c_{n+1} + c_{n+1}^\dagger c_n) - h\sum_{n=1}^{L}\cos(2\pi\beta n)c_n^\dagger c_n \ , \tag{6.3}$$

thus equation (6.3) is a tight-binding model of spinless fermions in a quasi-periodic on-site potential.

This Hamiltonian was first investigated by Harper, who came to this problem with $h = 1$ studying the motion of electrons in a square lattice subject to perpendicular magnetic field [88]. A new set of fermion operators (η_q and $\eta_q^\dagger$) are introduced in order to diagonalize the model.

$$\eta_q = \sum_{n=1}^{L}\phi_{q,n}c_n \ , \tag{6.4}$$

with $\sum_{q=1}^{L}\phi_{q,n}\phi_{q,n'} = \delta_{n,n'}$

$$\mathcal{H} = \sum_q \epsilon_q\left(\eta_q^\dagger\eta_q - 1/2\right) \ . \tag{6.5}$$

Here the components of vectors ($\phi_{q,n}$) and the energy modes (ϵ_q) are given by the almost Mathieu equation [175]:

$$\frac{1}{2}\phi_{q,n-1} + h_n\phi_{q,n} + \frac{1}{2}\phi_{q,n+1} = -\epsilon_q\phi_{q,n} \ . \tag{6.6}$$

6.2 Entanglement entropy

I calculated the entanglement entropy, $\mathcal{S}_\ell$ between a block of length, $\ell = F_{n-2}$ and the rest of the chain (F_{n-1} spins) using periodic boundary conditions. There are two regimes in the variation of the entanglement entropy (as for homogeneous chains or Finonacci Ising chain): For short times the entanglement entropy grows, for long times it oscillates around its asymptotic value. If the quench ends in the extended phase, the entropy grows linearly with time $\mathcal{S}_\ell(t) \approx \alpha(h)t$ in the short-time regime, and its asymptotic value is proportional

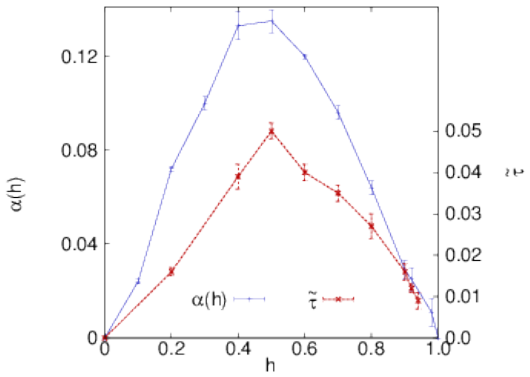

Figure 6.2. Prefactor of the linear part of the dynamical entanglement entropy (left axis) and the relaxation time (right axis) after a quench from $h_0 = 0$ to different values of h.

to the length of the block $\tilde{\mathcal{S}}_\ell \sim \ell$. This behavior is similar to the behavior in homogeneous systems. Fitted values of the prefactor α can be seen in figure 6.2. The α prefactor has its maximum around $h = 0.5$, from $h = 0$ to $h = 0.5$ it's increasing, from $h = 0.5$ to $h = 1.0$ it is decreasing, and it is zero at $h = 1.0$, signaling that the quenches ending at $h = 1.0$ show a different behavior.

If the quench ends in the transition point, the entanglement entropy grows with a power function:

$$S(t) \sim t^\sigma \ , \tag{6.7}$$

with an exponent $\sigma = 0.43(5)$, which is a fitted value see the left panel of 6.1.

If the quench ends in the localized phase ($h > 1$), the entanglement entropy saturates quickly, and its asymptotic value is independent of the length of the block ℓ. I have observed, that close to the critical point $\tilde{\mathcal{S}}(h)$ diverges:

$$\tilde{\mathcal{S}}(h) \sim |\ln(h)|^{-\sigma'} \ , \tag{6.8}$$

with an exponent: $\sigma' = 0.50(4)$, see in the right panel of Figure 6.1.

The σ' and σ exponents are not independent, the relation between them can be found with a phenomenological scaling. If the lengths are rescaled by a factor $b > 1$ the entanglement entropy scaled as:

$$\tilde{\mathcal{S}}(\ln h, t) = b^s \tilde{\mathcal{S}}(b/\ln h, t/b^z) \ , \tag{6.9}$$

for $h \geq 1$, where the form of the correlation length equation (2.38) was used, and the dynamical exponent is $z = 1$. Taking the scale factor $b = t^{1/z}$ one gets

$$\tilde{\mathcal{S}}(\ln h, t) = t^{s/z} \hat{\mathcal{S}}(t^{1/z} \ln h) \ . \tag{6.10}$$

The limiting value of the scaling function in the critical point $h = 1$ is $\lim_{u\to\infty} \hat{\mathcal{S}}(u) = \text{cst}$, thus $\sigma = s/z = s$. Taking $b = 1/\ln(h)$ one can show that $\sigma' = s$, thus $\sigma = \sigma'$ in agreement with the values extracted from numerical data.

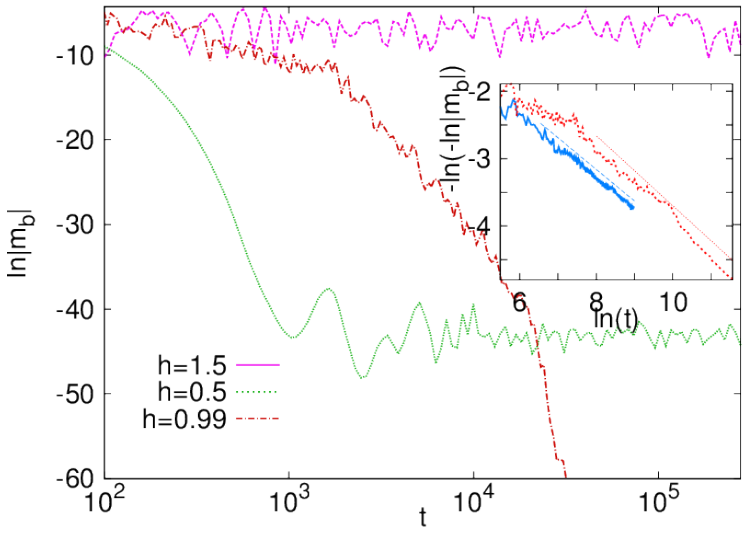

Figure 6.3. Bulk magnetization after a quench from $h_0 = 0$ to different values of h. In the inset quench to the critical region is shown in agreement with the stretched-exponential form in equation (6.11) (the straight lines have a slope $\mu = 0.47$).

6.3 Local magnetization

I calculated the local magnetization $m_l(t)$ in a chain of length $L = F_n$ at the $l = F_{n-2}$th spin. This value will be referred to bulk magnetization and will be denoted by $m_b(t)$. Numerical results about the time dependence of the bulk magnetization after a quench from $h_0 = 0$ to various values of h can be seen in figure 6.3. If the quench ends in the extended phase, $(0 < h < 1)$ the magnetization follows an exponential decay: $m_b(t) \sim \exp(-t/\tilde{\tau})$, similarly to the homogeneous system. Fitted values for the characteristic time $(\tilde{\tau}(h))$ are shown in figure 6.2 (right axis): The characteristic time shows a similar behavior as the prefactor of the linear part of the entanglement entropy.

For a critical quench $(h = 1)$, the behavior of the magnetization is a stretched exponential:

$$m_b(t) \sim A(t)\exp(-Ct^{\mu}) \; . \tag{6.11}$$

Here $A(t)$ is an oscillatory function, $\mu = 0.47(5)$. This is shown in the inset of figure 6.3. If the quench ends in the localized phase, the magnetization quickly reaches an asymptotic value, and oscillates around it.

6.4 Semiclassical interpretation

In this section a semiclassical interpretation [37, 38, 51, 56] will be developed, similarly as in the case of the Finonacci Ising chain.

$$\mathcal{G}(n, n', t) = \langle 0|c_n(t)c^{\dagger}_{n'}(0)|0\rangle = \sum_q \cos(\epsilon_q t)\phi_{q,n}\phi_{q,n'} \; , \tag{6.12}$$

in terms of the eigenvectors and eigenvalues of equation (6.6) calculated with the magnetic filed h, i.e. after the quench. For $t = 0$ $\mathcal{G}(n, n', 0) = \delta_{n,n'}$. The width of the wave-packet

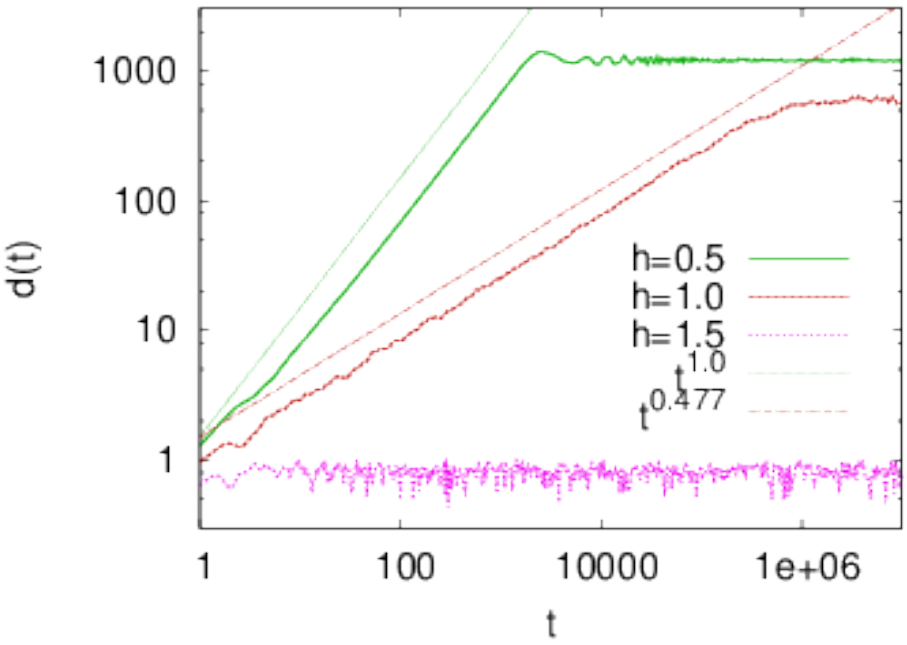

Figure 6.4. Time-dependent width of the wave packet at different amplitudes of the transverse field.

started from site n after time t is given by (similarly to equation (5.8)):

$$d(n,t) = \left[\sum_{n'}(n-n')^2|\mathcal{G}(n,n',t)|^2\right]^{1/2}, \tag{6.13}$$

which is then averaged over the starting positions, thus $d(t) = \overline{d(n,t)}$.

The $d(t)$ width has been calculated for various after quench transverse field, these results can be seen in figure 6.4. In the extended phase, in agreement with previous results [102] the wave packet width $d(t)$ grows linearly, which can be interpreted as the quasi-particles moving ballistically, i.e. with constant velocity. From this it follows, as in the homogeneous chains [38], that the entanglement entropy grows linearly, and the magnetization decreases exponentially.

If the quench ends in the localized phase ($h > 1$), the wave packet width $d(t)$ remains finite $d(t) \to \tilde{d}$. We found, that this finite asymptotic value ($\tilde{d}$) is proportional to the equilibrium localization length $\tilde{d} \sim \xi$, see in the right panel of figure 6.1.

If the quench ends at the critical point $h = 1$, the width of the wave packet grows with a power function of the time: $d(t) \sim t^D$, where D is $D = 0.477(10)$ in correspondence with the results of [102]. The anomalous diffusion of the quasi-particles lead to the power-law increase of the dynamical entanglement entropy eq. (6.7), and the stretched exponential behavior of the bulk magnetization equation (6.11). The semiclassical picture predict, that the diffusion exponent of the wave packet D, the exponent of the entanglement entropy σ, and the exponent of the magnetization μ should be equal, and indeed these tree are equal within the errors of the numerical data.

6.5 Discussion

In this chapter we studied the quench dynamics of the Harper model.

If the quench ends in the localized phase, the entanglement entropy grows proportional to the time, the magnetization decreases exponentially, and the diffusion exponent of the wave packet is close to one. The dynamics is similar to the after quench dynamics of the homogeneous systems: The reason is that the spectrum of the Harper model is absolutely continuous in the extended phase.
If the quench ended in the localized phase, the width of the wave packet remains finite for long times, similarly the entanglement entropy and the magnetization also reaches a finite limiting value. The asymptotic value of the wave packet width is proportional with the localization length $\tilde{d} \sim \xi = \frac{1}{\ln h}$. For the asymptotic value of the entanglement entropy the $\tilde{S} \sim |\ln(h)|^{-\sigma'}$ relation was found with $\sigma' = 0.5(4)$.
If the quench ended at the critical point, power-law growth of the wave packet was found $d(t) \sim t^{0.477}$ in agreement with the results of [102]. The entanglement entropy grows with a power function of the time $S(t) \sim t^{\sigma}$ with exponent $\sigma \approx 0.43(5)$. The local magnetization decrease with a stretched exponential function: $m_b(t) \sim \exp(-Ct^{\mu})$ with $\mu \approx 0.47(5)$.

This chapter is based on the following article:
G. Roósz., U. Divakaran, H. Rieger, F. Iglói *Non-equilibrium quantum relaxation across a localization-delocalization transition* Phys. Rev. B 90, 184202 (2014)

The numerical simulations presented in this chapter, and the quasi-classical reasoning were done by me. The scaling about the entanglement is common work with Prof. Dr. Heiko Rieger and Prof. Dr. Ferenc Igloi.

Chapter 7

Nearly adiabatic dynamics of the Harper model

Here the term "nearly adiabatic" means that a parameter of the system is varied very slowly. If the external parameter is varied infinitely slowly, the eigenstates of the initial Hamiltonian evolve to the eigenstates of the final Hamiltonian.
If the system crosses during the above mentioned process a second order phase transition, the dynamics slows down (the relaxation time diverges), and the system cannot follow the variation of the outer parameter, regardless of how slow the variation is. In consequence defects are generated. The standard "paradigm" to describe the generation of the defects is the so called Kibble-Zurek scaling.

7.1 Kibble-Zurek scaling

The Kibble-Zurek scaling gives a prediction about the density of the defects, using the critical exponents of the (crossed) transition point. The scaling is first used by Tom W. B. Kibble who studied the structure of the early universe [58]. Later it was applied to solid state physics by Wojciech H. Zurek [59]. Let us denote the correlation length as ξ and the correlation time as ξ_t, which are related as $\xi_t \sim \xi^z$, where z is the dynamical exponent. Let us suppose, there is a well defined moment, when the time evolution becomes non-adiabatic. Time evolution become non-adiabatic when the variation of the instantaneous relaxation time is faster than the typical speed of relaxation:

$$(\text{change of } \xi_t \text{ during } \xi_t \text{ time}) \sim \xi_t \, . \tag{7.1}$$

Which is equivalent with:

$$\xi_t \dot{\xi}_t \sim \xi_t \Rightarrow \dot{\xi}_t \approx 1 \tag{7.2}$$

Let's denote the external parameter with δ. The critical point is $\delta = 0$. The outer parameter is varied linearly in time: $\delta(t) = (t - t_{\text{crit.}})/\tau$. Here τ is a time scale, which characterizes the speed of the process. The nearly adiabatic (very slow) limit is: $\tau \gg 1$. The $t_{\text{crit.}}$ time is the time when the system crosses the critical point. Of course, it is basically possible to choose $t_{\text{crit.}}$ to be the zero of the time scale, however in the later part

of this chapter another choice will be appropriate.

Using the critical scaling of the correlation length ξ and relaxation time ξ_t one gets:

$$\xi_t \sim \xi^z \sim \delta(t)^{-\nu z} \sim (|t - t_{\text{crit.}}|/\tau)^{-\nu z} \tag{7.3}$$

Using the above relationship equation (7.1) takes the form:

$$1 \approx \dot{\xi}_t|_{t=\tilde{t}} \sim \frac{|\tilde{t} - t_{\text{crit.}}|^{-(\nu z+1)}}{\tau^{-\nu z}} \ . \tag{7.4}$$

Here $\tilde{t}$ is the time when the system loses the adiabatic behavior. The $|\tilde{t} - t_{\text{crit.}}|$ time difference is usually referenced in the literature as Kibble-Zurek time. One can calculate the instantaneous localization length at time $t = \tilde{t}$:

$$|\tilde{t} - t_{\text{crit.}}| \sim \tau^{\frac{\nu z}{\nu z+1}} \Longrightarrow \tilde{\xi} \sim |\tilde{t} - t_{\text{crit.}}|^{1/z} \sim \tau^{\frac{\nu}{\nu z+1}} \ . \tag{7.5}$$

In the Kibble-Zurek scaling the instantaneous localization length at time $t = \tilde{t}$ is considered to be the average distance of two defects, and the excitation probability $P(\tau)$ is supposed to be proportional to the density of the defects:

$$P(\tau) \sim (\text{density of deffects}) \sim \frac{1}{\tilde{\xi}^d} \sim \tau^{-\frac{d\nu}{1+\nu z}} \ .$$

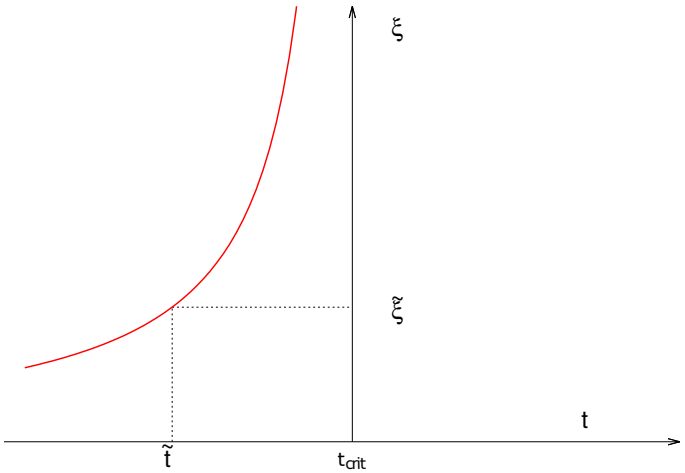

Figure 7.1. The red curve represent the diverging relaxation time. One supposes, that there is a given moment, when the time evolution becomes non-adiabatic. The time difference between the aforementioned moment and the crossing of the critical point is the so called Kibble-Zurek time.

Later (after we defined the excitation probability in our calculation) we return to the Kibble-Zurek scaling, and investigate in details what is the Kibble-Zurek prediction for the Harper model.

7.2 Density of defects in the adiabatic dynamics

The transverse field is varied linearly (and slowly) $h = h(t) = t/\tau$, and the defects created during this process. I investigate the density of the created defects, as a function of the τ time. The time evolution starts at $t = -\infty$, when the absolute value of the magnetic field is very large, $h \to -\infty$, so the initial state is a classical product state. In the initial state the direction of the magnetic field gives the direction of the spins: $\sigma_n^z = 1$ ($c_n^\dagger c_n = 1$) for $\cos(2\pi\beta n) > 0$ and $\sigma_n^z = -1$ ($c_n^\dagger c_n = 0$) for $\cos(2\pi\beta n) < 0$.

I used chains of even lengths, so in the initial state half of the spins directed in $-z$ direction and half of the spins directed in $+z$ direction, in fermionic language, the initial state is half-filled. The time evolution of the system is driven by the time dependent Schrödinger equation $\mathrm{d}\Psi/\mathrm{d}t = -i\mathcal{H}(t)\Psi(t)$, with the initial condition $\Psi(-\infty) = \Psi_0(-\infty)$. The ground state of the $H(t)$ Hamiltonian operator at time t is $\Psi_0(t)$: This ground state usually differs from the $\Psi(t)$ state which latter one is the result of a non-equilibrium time evolution. We will investigate how far the two states $\Psi(t)$ and $\Psi_0(t)$ are from each other, and what is the connection between the difference, and the "speed" of the variation of the magnetic field τ. To investigate such questions one has to quantify the difference of the two states. To do this, we will define the total excitation probability P, with the use of the fermionic representation.
The Heisenberg equation of motion of the $c_{n,H}(t)$ are linear (see in Appendix A.4 and [61]), because the Hamiltonian in equation(6.3) is quadratic. The evolution of vectors $\tilde{\phi}_{q,n}(t)$ satisfy the differential equation:

$$i\frac{\mathrm{d}\tilde{\phi}_{q,n}}{\mathrm{d}t} = \frac{1}{2}\tilde{\phi}_{q,n-1} + h_n\tilde{\phi}_{q,n} + \frac{1}{2}\tilde{\phi}_{q,n+1} \ , \tag{7.6}$$

with the initial condition: $\tilde{\phi}_{q,n}(-\infty) = \phi_{q,n}(-\infty)$, where the latter are given in equation (2.39).

The vector $\tilde{\phi}_{q,n}(t)$ at t time is generally different from the vector $\phi_{q,n}(t)$ which corresponds to the ground state of the $H(t)$ instantaneous Hamilton operator. .

In the initial state at $t = -\infty$ half of the fermionic states are occupied, these are denoted by Q^-. The other half of fermionic states, denoted by Q^+, are empty. If the time evolution would be perfectly adiabatic, all empty states would remain empty. We define the excitation probability as:

$$P_t = \frac{2}{L}\sum_{q\in Q^+}\sum_{q'\in Q^-} p_{q,q'} \ , \tag{7.7}$$

where $p_{q,q'}$ is called partial excitation probability and defined as:

$$p_{q,q'} = \left|\sum_n \tilde{\phi}_{q,n}(t)\phi_{q',n}(t)\right|^2 \ . \tag{7.8}$$

The excitation probability measures how many empty states become excited due to the finite speed of the variation of the magnetic field. P_t is normalized: $0 \le P_t \le 1$. If the

dynamics would be perfectly adiabatic, the P_t excitation probability would remain zero. For a process with finite speed τ, one waits that the slover process (larger τ) implies the smaller excitation probability P_t.

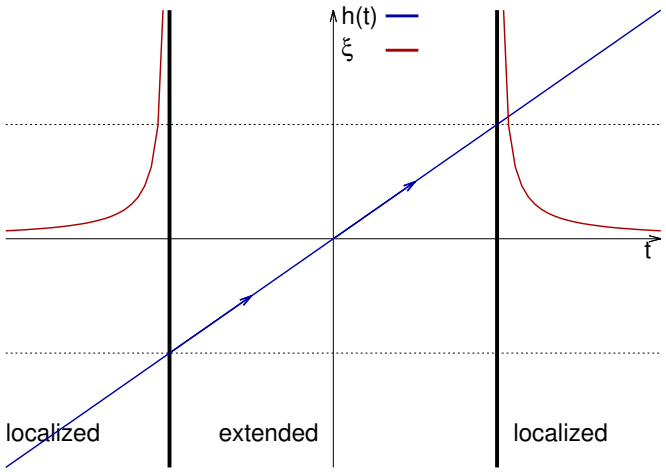

Figure 7.2. Magnetic field $h(t)$, and the instantaneous correlation length $\xi(t)$ as a function of the time during the quench. In the numerical calculations two type of quench protocols were used: each of the start at $t = -\infty$, the endpoints are $t = 0$ and $t = +\infty$.

We investigated two kinds of final states: *i*) the quench ends at $t = 0$, in the middle of the extended phase and *ii*) $t = \infty$, when the quench cross the full extended phase, and goes to the localized phase on the other site. (With positive h.) In the first case the localization-delocalization transition is crossed once (at $h = -1$), in the second case, the localization-delocalization transition is crossed twice: first at $h = -1$, and at $h = +1$.

7.3 Numerical results and scaling theory

I investigated the adiabatic dynamics by numerical calculations. The time evolution was calculated using a Runge-Kutta method with adaptive step size in time, to keep the relative error less than 10^{-6}. I used $h = \pm 10$ to approximate $h \to \pm\infty$, and I tested that the numerical results are stable, and do not change if I used $h = \pm 20$.

Numerical results of the excitation probability as a function of the time-scale τ can be seen in figure 7.3. The excitation probability shows a power-law dependence in both cases:

$$P_t(\tau) \sim A_t(\tau)\tau^{-\kappa} , \tag{7.9}$$

but the prefactors, $A_t(\tau)$ have different functional forms.

When the quench ends at $t = 0$, and the localization-delocalization transition is crossed only once, the prefactor shows log-periodic oscillations: $A_0(\tau) \sim \sin^2(\log(\tau/\tau_0))$. This type of log-periodic oscillations are common in quasi-periodic systems [177]. Due to the oscillations, the exponent can be determined with some uncertainty:

$$\kappa = 0.45(5) . \tag{7.10}$$

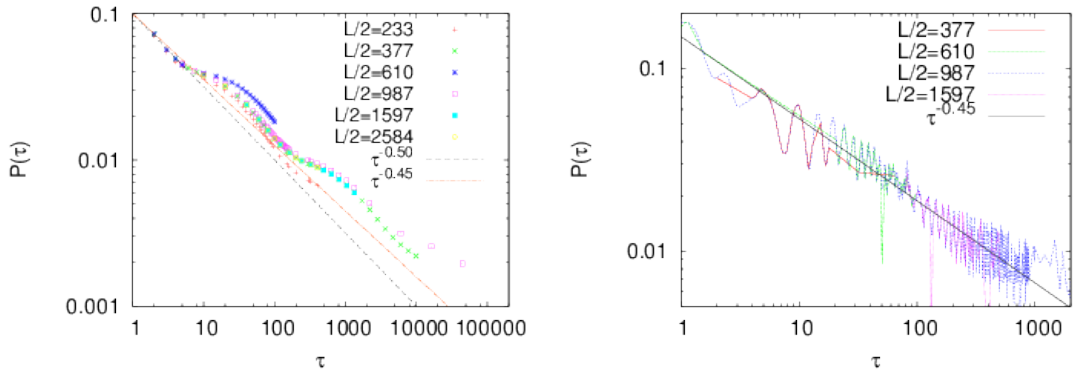

Figure 7.3. Excitation probability as a function of the time-scale, τ, after an adiabatic process from $h = -\infty$ to $h = 0$ (upper panel) and to $h = \infty$ (lower panel) calculated in finite systems of sizes $L = 2F_n$ with $n = 13, 14, \ldots, 18$.

If the localization-delocalization transition is crossed twice (at $h = -1$ and $h = 1$) the prefactor has fast oscillations in τ: $A_\infty(\tau) \sim \sin^2(\tau/\tau_\infty + cst.)$ with $\tau_\infty \approx 0.15$, and a slower log-periodic oscillation is also present. The fast oscillations are analogous to the Stückelberg oscillations [178,179]. It is hard to obtain the exponent of the second protocol, due to the fast oscillations, however the numerical data is compatible with the estimate for κ in equation (7.10).

Now we will build a scaling picture to interpret the measured $\kappa = 0.45$ value.

First the traditional Kibble-Zurek scaling (described in section 7.1) is used for the Aubry-André model. In the Aubry-André model $d = 1$ and $\nu = z = 1$ so the prediction of the Kibble-Zurek scaling theory is $\kappa_{\rm sc} = 0.5$, which is close to the numerical estimate, but sightly different. The rigorous derivations of the Kibble-Zurek scaling assume translational invariance, so the Kibble-Zurek prediction is not guaranteed to be precise for an inhomogeneous system. Here a scaling is developed specially for the Aubry-André model. The concept of the Kibble-Zurek time scale $t_{KZ} = |\tilde{t} - t_{crit}|$ (7.5) is used, however, the t_{KZ} time scale is connected with a more special way to the excitation probability than in the usual Kibble-Zurek scaling. The elementary transition probabilities $p_{q,q'}$, calculated at $t = 0$ (for the first protocol) will be investigated. The $p_{q,q'}$-s are arranged in decreasing order, then the first (biggest) N is summed up:

$$P(N, L, \tau) = \frac{2}{L} \sum_{q \in Q^+ q' \in Q^-}^{N'} p_{q,q'} \ . \tag{7.11}$$

This quantity is called partial excitation probability. (The prime on the sum denotes that the summation involves not all terms, just the N largest.)

I calculated the fraction of the partial excitation probability, and the full excitation probability $P(N, L, \tau)/P_0(\tau)$, for several system sizes and decay parameters (τ-s). For large systems the $P(N, L, \tau)$ is a function of N/L^2

$$P(N, L, \tau) = \pi(N/L^2) P_0(\tau) \ , \tag{7.12}$$

for large enough τ.

As it is shown on the right part of Fig.7.4 in the log-log plot $\pi(N/L^2)$ there is a linear section over many decades, and for large arguments it saturates. Thus $P(N, L, \tau)/P_0(\tau)$ can be approximated as

$$\frac{P(N,L,\tau)}{P_0(\tau)} \approx \begin{cases} \frac{P(N,L,\tau)}{P(N_{\text{eff}},L,\tau)} \sim (N/N_{\text{eff}})^{\omega} & N \leq N_{\text{eff}} \\ 1, & N > N_{\text{eff}} \end{cases} \tag{7.13}$$

From the data in the right panel of Fig.7.4 we estimate $\omega = 0.90(2)$. By definition of N_{eff}:

$$P_0(\tau) \sim (N_{eff}/L^2)^{\omega} \ . \tag{7.14}$$

We have to connect N_{eff}/L^2 with the time scale. To do this, we investigate the spectra of the Aubry-André model near to the Fermi - energy. In figure 7.5 the number of eigenstates between the Fermi level E_F and $E > E_F$ are shown in a finite chain, as function of the $E - E_F$ difference. The number of states between E_F and $E > E_F$ are denoted by $n(E - E_F)$. It can be seen that the eigenstates form 'branches'. These branches show a fractal-like structure. In figure 7.5 there is a finite number of branches, since it represents the spectra of a finite system. In an infinite system there would be an infinite number of branches. In an infinite system there are infinite number of branches. Investigating the position of the branches we found that

$$n(\epsilon) \sim \epsilon^{X_e} \tag{7.15}$$

where $X_e \approx 0.5 \pm 0.02$. Note, that this numerical result is in agreement with the more exact results of Wilkinson [102] about the box counting dimension. If two states (m and n) are close enough to the Fermi level, say closer than an energy scale ϵ, than the partial excitation probability $p_{m,n}$ gives an important part of a full excitation probability. There is $n(\epsilon)$ states in the ϵ neighborhood of the Fermi level E_F, so the effective number of partial excitations scales as:

$$N_{eff}/L^2 \sim n(\epsilon)^2 = \epsilon^{2X_e} \tag{7.16}$$

Using equation (7.14) one gets:

$$P_0(\tau) \sim (N_{eff}/L^2)^{\omega} = \epsilon^{2X_e\omega} \ . \tag{7.17}$$

Using $\epsilon \sim 1/t_{KZ}$ and equation (7.5) the expression of the Kibble-Zurek time:

$$P_0(\tau) \sim \tau^{-\frac{2\omega\nu z X_e}{\nu z+1}} \tag{7.18}$$

Substituting the values of the various exponents ($z = 1$, $\nu = 1$, $\omega = 0.9$, $X_e = 0.5$) one gets:

$$P_0(\tau) \approx 0.45 \ , \tag{7.19}$$

in good agreement with the numerical result.

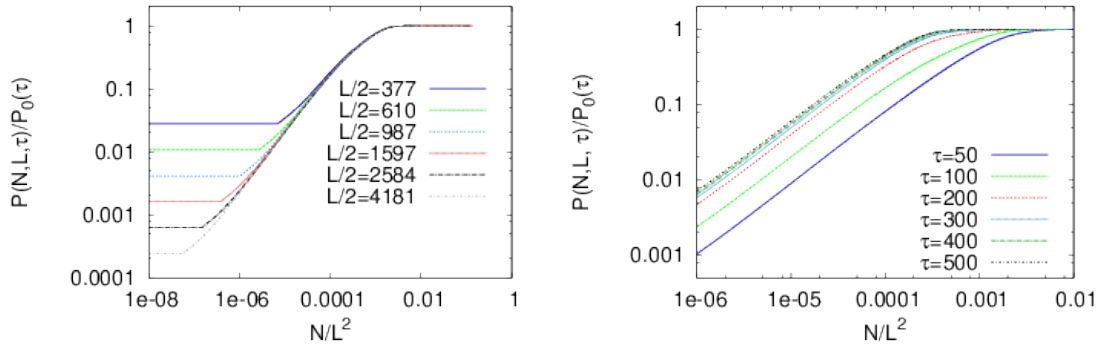

Figure 7.4. Normalized partial excitation probabilities as a function of $(N/L)^2$ for different sizes: $L = 2F_n$ with $n = 13, 14, \ldots, 18$ at $\tau = 100$ (upper panel) the same at $L = 2F_{18}$ for different values of τ (lower panel) both in log-log scale.

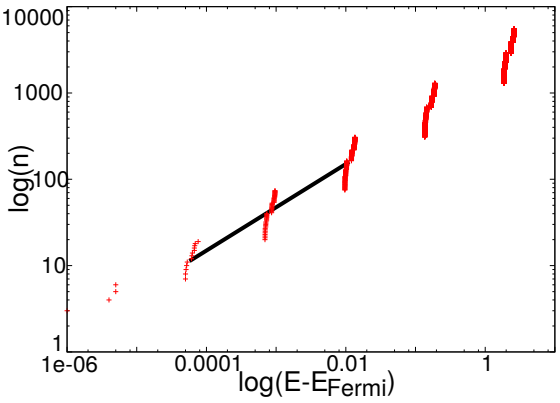

Figure 7.5. Number of eigenstates between the Fermi energy (E_F) and $E > E_F$, as a function of the $E - E_F$ difference. There are logarithmic scales of both axis. The eigenstates are result of numerical calculation in a chain of length $L = 2 \times 6765$.

7.4 Discussion

In this chapter we studied a nearly adiabatic process in the Harper model. The amplitude of the magnetic field $h(t)$ was varied linearly in time with a rate $1/\tau$ and studied the density of defects in the ground state created during this process. If the localization-delocalization transition point is passed once the density of defects follows a power-law dependence, $\sim \tau^{-\kappa}$, while if two symmetrically placed transition points are passed then the density of defects has a multiplicative oscillating correction, similar to the Stückelberg phase of periodically driven two-level systems. Using scaling arguments we have related κ to another critical exponents as given in equation(7.18). In this expression also the scaling dimension ω of the excitation probability enters. For homogeneous systems it is generally expected that $\omega = 1$. In our case, when the spectrum of the Hamiltonian is not continuous at the transition point, as well as the spectrum of the critical Hamiltonian is singular continuous we have $\omega < 1$. It is expected that $\omega \neq 1$ is a general rule for quasi-periodic and aperiodic Hamiltonians.

Finally, we discuss the question of the non-equilibrium dynamics of the Hamiltonian in equation (2.17) for different values of the quasi-periodicity parameter β in equation (6.2). If β is a rational number of the form $\beta = 1/(2q)$ with q being an integer, then in the

adiabatic process the decay exponent is given by [74] $\kappa = q/(q+1)$. The same result holds for $\beta = p/(2q)$, when p is an odd integer and p and q are relative primes, at least for not too large values of q. Thus these results cannot be analytically continued to the case, when β is an irrational number. If β is an irrational number and different from the inverse of the golden mean ratio studied in this paper, than the critical exponents of the non-equilibrium dynamics are expected to be β dependent. Some hint in favor of this assumption can be found in the diffusion properties of the quasi-particles, see in section 6.4. Indeed the diffusion exponent, D, is measured to be β dependent [102] and the same is expected to hold for the non-equilibrium exponents σ and μ.

This chapter is based on the following article:
G. Roósz., U. Divakaran, H. Rieger, F. Iglói *Non-equilibrium quantum relaxation across a localization-delocalization transition* Phys. Rev. B 90, 184202 (2014)
The numerical simulations presented in this chapter was done by me. Dr. Uma Divakaran did stability investigations about the numerical method. The modified scaling theory represented in the above chapter is also my work.

Chapter 8

Quench dynamics of the disordered Ising model

8.1 Introduction

In this chapter we investigate the dynamics of the magnetization of the disordered transverse field quantum Ising chain after a global quench. Concerning the functional form of the relaxation process after a quench in random quantum systems, there have been detailed studies about the time-dependence of the entanglement entropy [78–81, 180]. If the system consists of non-interacting fermions - such as the random XX-spin chain or the critical random transverse-field Ising chain - the dynamical entanglement entropy grows ultra slowly in time as

$$\mathcal{S}(t) \sim a \ln \ln t \,, \tag{8.1}$$

and saturates in a finite system at a value

$$\mathcal{S}(\ell) \sim b \ln \ell \,, \tag{8.2}$$

where ℓ denotes the size of a block in a bipartite system and can be chosen to be proportional to the size of the system L [79, 180]. These scaling forms can be explained by a strong disorder renormalization-group (SDRG) approach [103]. Recently, the SDRG method, which was designed as a ground state approach, has been generalized to take into account excited states [181–183]; this generalized RG method is often abbreviated as RSRG-X [181]. By this generalized SDRG method the ratio of the prefactors in (8.1) and (8.2) is predicted as $b/a = \psi_{\rm ne}$, where $\psi_{\rm ne} = 1/2$ is a critical exponent in the non-equilibrium process and describes the relation between time-scale and length-scale as

$$\ln t \sim L^{\psi_{\rm ne}} \,. \tag{8.3}$$

For interacting fermion models due to many-body localization the time-dependence of the dynamical entropy is $\mathcal{S}(t) \sim \ln^{\omega} t$ with $\omega \geq 1$, while the saturation value follows the volume law, $\mathcal{S}(\ell) \sim \ell$ [81].

We consider relaxation processes from an initial ferromagnetic state and from a fully

paramagnetic state by a sudden change of the strength of the transverse field. To circumvent numerical instability as observed in previous calculations for large systems using eigenvalue solver routines [79,180], we use multiple precision arithmetic to study the time-evolution through direct matrix multiplications.

8.2 The model

The model was introduced in Section 2.4, and the properties of the model also summarized there. The model we consider is the quantum Ising chain of length L defined by the Hamiltonian:

$$\mathcal{H} = -\frac{1}{2}\sum_{i=1}^{L-1} J_i \sigma_i^x \sigma_{i+1}^x - \frac{1}{2}\sum_{i=1}^{L} h_i \sigma_i^z \ , \tag{8.4}$$

in terms of the Pauli matrices $\sigma_i^{x,z}$ at site i. In this Chapter I will take free boundary conditions. The homogeneous model with the uniform coupling $J_i = 1$ and the uniform transverse field, $h_i = \tilde{h}$, is in the disordered (ordered) phase for $\tilde{h} > 1$ ($\tilde{h} < 1$), and the quantum critical point is located at $\tilde{h} = 1$. [111] The critical point of the model is described by a conformal field theory with a central charge $c = 1/2$. In the random model with quenched disorder, the J_i and the h_i are position dependent, and are independent random numbers taken from uniform distributions in the intervals $[0, 1]$ and $[0, h]$, respectively. The random model is in the disordered (ordered) phase for $h > 1$ ($h < 1$) and the random quantum critical point is at $h = 1$.

The free fermion representation of the Hamiltonian is:

$$H = -\sum_{i=1}^{L} h_i (c_i^\dagger c_i - \frac{1}{2}) - \frac{1}{2}\sum_{i=1}^{L-1} J_i (c_i^\dagger - c_i)(c_{i+1}^\dagger + c_{i+1}) \ , \tag{8.5}$$

which is a special case of equation (2.2). The usual description of the dynamics is to transform (8.5) to diagonal form, as it can be read in Appendix A, and as it was done in the previous chapters. This method was applied to the disordered Ising chain, and it was found that the eigenvalue solver routine fails to converge for some samples. The root of the problem is that nearly degenerate eigenstates occur in some samples. The difference between the energy levels of the states is comparable with the used numerical precision. This causes that the eigenvalue solver routine returns false eigenstates. These events cause a significant numerical error. To avoid instabilities, we follow a sightly difference procedure, where only matrix products are used, and the rounding errors are controlled by using multiple precision arithmetic.

8.2.1 Numerical calculation of time evolution

The Hamiltonian can be written in terms of Majorana operators:

$$H = \frac{1}{4}\sum_{n=1}^{2L}\sum_{m=1}^{2L} \breve{a}_m \left[\ T_{m,n}(i)^{(n-m)\mathrm{mod}(2)} \right] \breve{a}_n \ , \tag{8.6}$$

where

$$\begin{aligned} \check{a}_{2l-1} &= \sum_{k=1}^{L} \Phi_k(l)(\eta_k^\dagger + \eta_k) \ , \\ \check{a}_{2l} &= -\imath \sum_{k=1}^{L} \Psi_k(l)(\eta_k^\dagger - \eta_k) \ , \end{aligned} \tag{8.7}$$

are the Majorana operators. Some basic properties of these operators are included in Appendix A.5. The T matrix is given as:

$$T = \begin{bmatrix} 0 & h_1 & & & & \\ h_1 & 0 & J_1 & & & \\ & J_1 & 0 & h_2 & & \\ & & h_2 & 0 & \ddots & \\ & & & \ddots & \ddots & h_L \\ & & & & h_L & 0 \end{bmatrix} \tag{8.8}$$

Using the canonical anti-commutators, one can derive the Heisenberg equation of motion of the Majoranna operators:

$$\frac{d\check{a}_n(t)}{dt} = \sum_{m=1}^{2L} M_{n,m}\check{a}_m(t) \ . \tag{8.9}$$

here M is a $2L \times 2L$ real matrix. In the upper triangle the elements of M and T are equal, in the lower triangle the elements of T and M are opposite of each other.

$$M = \begin{bmatrix} 0 & h_1 & & & & \\ -h_1 & 0 & J_1 & & & \\ & -J_1 & 0 & h_2 & & \\ & & -h_2 & 0 & \ddots & \\ & & & \ddots & \ddots & h_L \\ & & & & -h_L & 0 \end{bmatrix} \tag{8.10}$$

One can expand the time dependent Majorana operators in the bases of the initial Majorana operators as follows:

$$\check{a}_m(t) = \sum_{n=1}^{2L} P_{mn}(t)\check{a}_n(0) \ . \tag{8.11}$$

$$P_{mn}(0) = \delta_{mn} \tag{8.12}$$

One obtains the following equations for the time evolution of the $P_{mn}(t)$ coefficients:

$$\frac{dP_{n,k}(t)}{dt} = \sum_{m=1}^{2L} T_{n,m}(-1)^{n-m}P_{m,k}(t) = \sum_{m=1}^{2L} M_{n,m}P_{m,k}(t) \ , \tag{8.13}$$

which can be written with short-hand matrix notation:

$$\frac{dP(t)}{dt} = MP(t) \ , \tag{8.14}$$

with the initial condition $P_{n,m}(0) = \delta_{n,m}$. The solution is $P(t) = \exp(Mt)$. It is possible to evaluate the exponential using the eigenvalue decomposition of M, however there are realizations where the eigenvalue solver routines fail to converge. To avoid the convergence problems we evaluate the exponential for a unit time step $t_{step} = 1$ using the Taylor series $\exp(Mt_{step}) = \sum_{n=0}^{\infty} \frac{M^n}{n!} t_{step}^n$. In the numerical calculations, we used multiple precision arithmetic to evaluate the Taylor-expansion, and summed the first 100 term in the expansion. The first 100 term is enough to make the truncation error smaller than the used numerical precision. The absolute value of the eigenvalues of M are smaller than 2 [120], so the nth term is the Taylor expansion is smaller than $2^n t_{step}^n / n!$ in operator norm. The time evolution is then calculated with matrix products,

$$P(2^n t_{step}) = P(2^{n-1} t_{step}) P(2^{n-1} t_{step}) \ . \tag{8.15}$$

I used two kinda of initial states, one ferromagnetic ($h_0 \to 0^+$) state and one paramagnetic ($h_0 \to +\infty$) state.
In the ferromagnetic state $\Psi^{(0)}(k)_j = \delta_{j,(k+1)mod(L)}$ and $\Phi^{(0)}(k)_j = -\delta_{k,j}$. One gets for the initial correlation matrix $G^{(0)}_{m,n} = -\sum_{k=1}^{L} \Psi^{(0)}(k)_m \Phi^{(0)}(k)_j = \delta_{m,(n+1)mod(L)}$.
In the paramagnetic state $\Psi^{(0)}(k)_j = \delta_{j,k}$ and $\Phi^{(0)}(k)_j = -\delta_{k,j}$, and one gets for the initial correlation matrix $G^{(0)}_{m,n} = \delta_{m,n}$.

8.3 From fully ordered initial state to the ferromagnetic phase

The fully ordered state is defined by $h \to 0^+$. We investigated various after quench magnetic field $h = 0.5 \ldots 0.9$, and different lengths of the chain $L = 16 \ldots 128$. The numerical results are shown in figure 8.1. Let us first investigate the (a) panel of Figure 8.1. The bulk

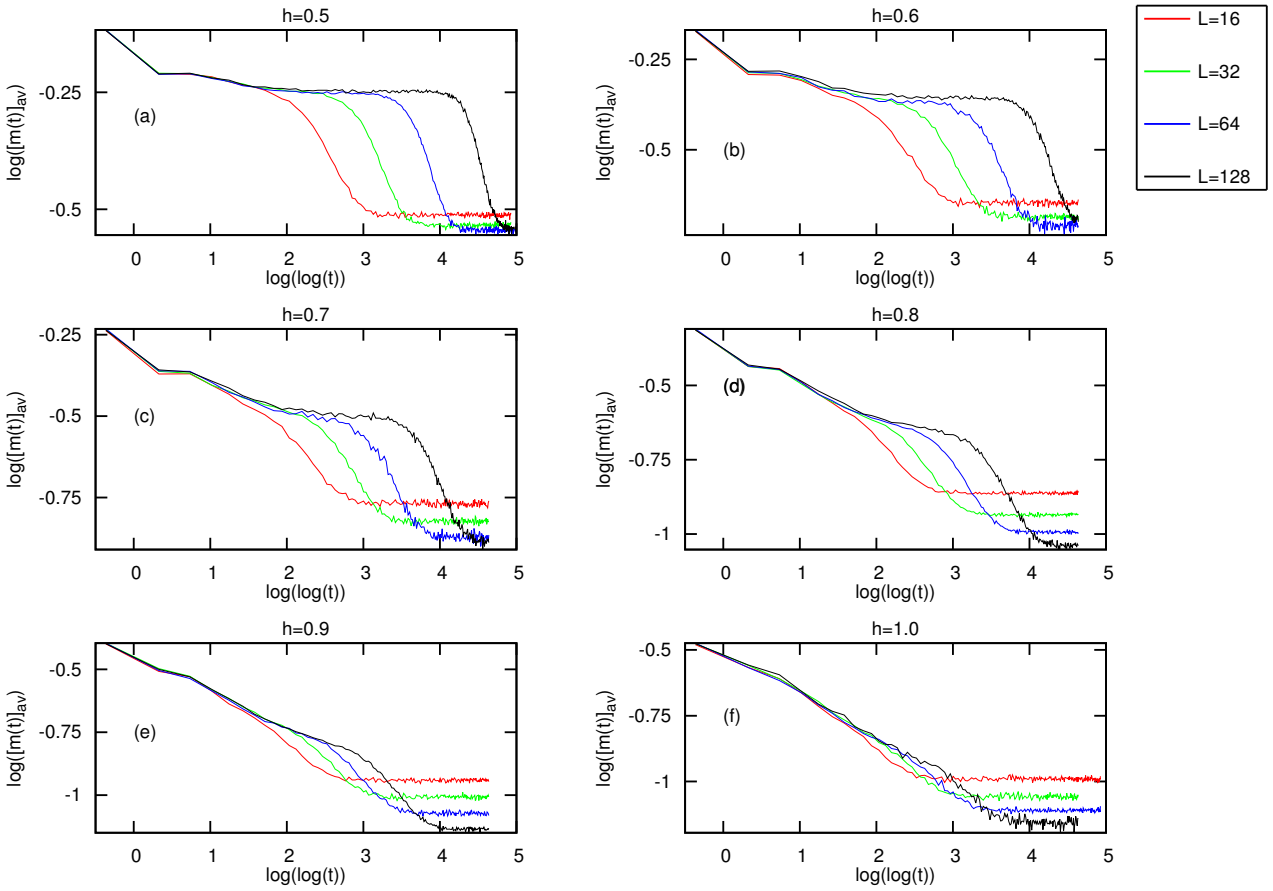

Figure 8.1. Quenches from the fully ordered initial state $h_0 = 0$, to the ferromagnetic phase and the critical point. Each sub-figure corresponds to a different magnetic field. (See the labels above the sub-figures.) The different colors denote the different chain lengths. The quench shown in the right bottom sub-figure ends in the critical point ($h = 1$), the others ends in the ferromagnetic phase ($h < 1$). The magnetization was calculated in the middle of the spin chain at site $l = L/2$.

magnetization decreases, first reach the first plateau, and after a system-size dependent time, t_{p2} a fast decrease happens, and the magnetization reaches a second plateau. The t_{p2} time goes to infinity in the thermodynamic limit: Therefore in the thermodynamic limit the second plateau is absent. The end time of the first plateau scales in a finite system as $\log(\log t_{p2}) \sim \log L$, and the average magnetization in the second plateau scales as $\log[m_{p2}(L)/m_{p2}(\infty)] \sim \xi/L$, where ξ is the correlation length of the second plateau. The other quenches ending in the ferromagnetic phase ((b)-(e) panels in Figure 8.1) show similar behavior. The end time of the first plateau t_{p2} become smaller and smaller as the after quench magnetic field approaches the critical value 1, and if the quench ends in the

critical point (Figure 8.1 (f) panel), there is no first plateau.

The double plateau behavior can be described in the framework of the semiclassical theory. Quasi-particles are created at the time of the quench, and the magnetization on a given site decrease, if a quasi-particle crosses the given site. In the ferromagnetic phase of the disordered Ising chain, there is a finite correlation length ξ, and the quasi-particles travels only ξ distance after the quench. When the quasi-particles traveled ξ distance from the site of their creation, the decrease of the magnetization stops, and the first plateau is created. If the after quench magnetic field h is closer to the critical point, the localization length ξ becomes larger, and the average magnetization in the first plateau becomes smaller.

The second plateau and the second fast decrease of the magnetization are the results of another, strictly finite-size effect. There is a special excitation in the ferromagnetic phase, with exponentially small energy: $\epsilon_0(L) \sim \exp(-L/\xi)$. The time scale where the first decrease occur is $t_{p2} \sim 1/\epsilon_0$, in correspondence with the numerical simulations. This special excitation is also localized, and the average values of the second plateau goes to a finite value in the thermodynamic ($L \to \infty$) limit. There is no such low energy excitation in the critical point: There the lowest excitation is $\epsilon_0(L) \sim \exp(-AL^{1/2})$.

8.4 Quench to the critical point

8.4.1 Ferromagnetic initial state

In Figure 8.2 the decay of the magnetization is shown after a quench from the ferromagnetic initial state ($h_0 \to 0^+$) to the critical point ($h = 1$). There is an asymptotic region where $\log(m(t))$ is proportional with $\log(\log t)$, $\log(m(t)) \sim a \log(\log t)$, where $a \approx 0.14$.

$$m(t) \sim (\log(t))^{-a} \tag{8.16}$$

The asymptotic region ends after a finite size dependent time, $t_a(L)$. For the quasi-particles emitted from the neighborhood of the boundaries, $t_a(L)$ amount of time is needed to reach the investigated bulk spin at $l = L/2$. Before $t_a(L)$ the boundaries does not effect the magnetization at site $l = L/2$, after $t_a(L)$ one observes finite-size effects in the dynamics of the bulk magnetization. After this asymptotic region there is a short period of fast decrease, and at the end there is the plateau region. For critical quenches there is only one plateau region. The average magnetization of the plateau region ($m_p(L)$) decreases with the increasing system size (see Figure 8.3). The $m_p(L)$ average magnetization is a power law of the system size (L)

$$m_p(L) \sim L^{-b} \,, \tag{8.17}$$

where $b \approx 0.068(5)$. Here the estimated error is the error of the numerical fit. The two formulas (8.16) and (8.17) have to give the same result for $t = t_a(L)$, so one gets:

$$\log t_a(L) \sim L^{b/a} \quad \text{where} b/a \approx 0.489 \pm 0.02 \,. \tag{8.18}$$

Comparing this result with the definition of the Ψ exponent:

$$\Psi = b/a \ . \tag{8.19}$$

This agrees with the result of RSRG-X. The scaling described above is illustrated in the right panel of Figure 8.2, where $\ln(L^b m(t))$ is plotted against $\ln(\ln t/L^\Psi)$.
The distributions of the variables in a disordered system are usually non-trivial, and often contains important informations about the system.

We investigate the distribution of the log-magnetization in the plateau regime. The probability distribution can be seen in Figure 8.3. The distribution is broad, and becomes broader with larger system sizes. One gets a data collapse with the scaling variable $y = \log m_p L^{-\alpha}$, thus

$$P_L(\log m_p) = L^{-\alpha}\tilde{p}(\log m_p L^{-\alpha}), \quad \alpha = b = 0.0685 \ . \tag{8.20}$$

as can be seen in Figure 8.3. The typical value of the magnetization in the plateau region is $\exp(-AL^\alpha)$, which is much smaller than the average value, $m_p(L) \sim L^{-b}$ (see Equation (8.17)). The contribution of the typical samples is very small, negligible in the thermodynamic limit. The important contribution to the average of the magnetization comes from the atypical samples, i.e. from the rare realizations. In those rare realizations the long time limit of the magnetization is large $m_p(L) = \mathcal{O}(1)$. The average of the magnetization is given by the $y \to 0^-$ behavior. It is assumed that for small values of y, $\tilde{p}$ follows a power law:

$$\tilde{p}(y) \sim (-y)^\chi \ . \tag{8.21}$$

The average of m_p is given by:

$$[m_p]_{av} = L^{-\alpha} \int dm_p \tilde{p}(\log m_p L^{-\alpha}) \tag{8.22}$$

$$\sim L^{-\alpha} \int dm_p [\log m_p L^{-\alpha}]^\chi \sim L^{-\alpha(1+\chi)} \tag{8.23}$$

with $\alpha = b$ and $\chi = 0$ (see figure 8.3) one gets $[m_p]_{av} \sim L^{-b}$, in agreement with the results of the numerical calculations summarized in Equation (8.17).

8.4.2 Paramagnetic initial state

The fully paramagnetic initial state means, that the initial magnetic field is very large $h_0 \to \infty$, or equivalently all of the couplings vanish. In this state, all of the spins point to the z direction, the magnetization is zero in the x direction, the initial correlation matrix is diagonal: $G^{(0)}_{m,n} = \delta_{m,n}$. I investigate quenches from the above described paramagnetic state to the critical point $h = 1$. The time dependence of the average magnetization are shown in Figure 8.4. The initial value is zero of the magnetization, which cannot be represented on the logarithmic scale of equation (8.4). The magnetization decreases for all global quenches in homogeneous or quasi-periodic chains. Surprisingly in the quench

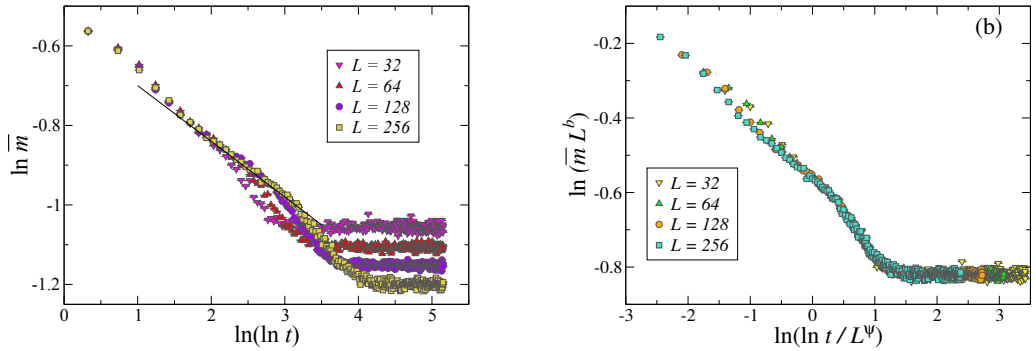

Figure 8.2. Left: Time evolution of the magnetization after a quench from $h_0 = 0.0$ to the critical point $h = 1$. The broken line denote a fit to the asymptotic region. Right Scaling plot of the relaxation of the magnetization after a quench from $h_0 = 0$ to the critical point in the disordered Ising chain the fitting parameters are $b = 0.0685$, $\Psi = 0.5$.

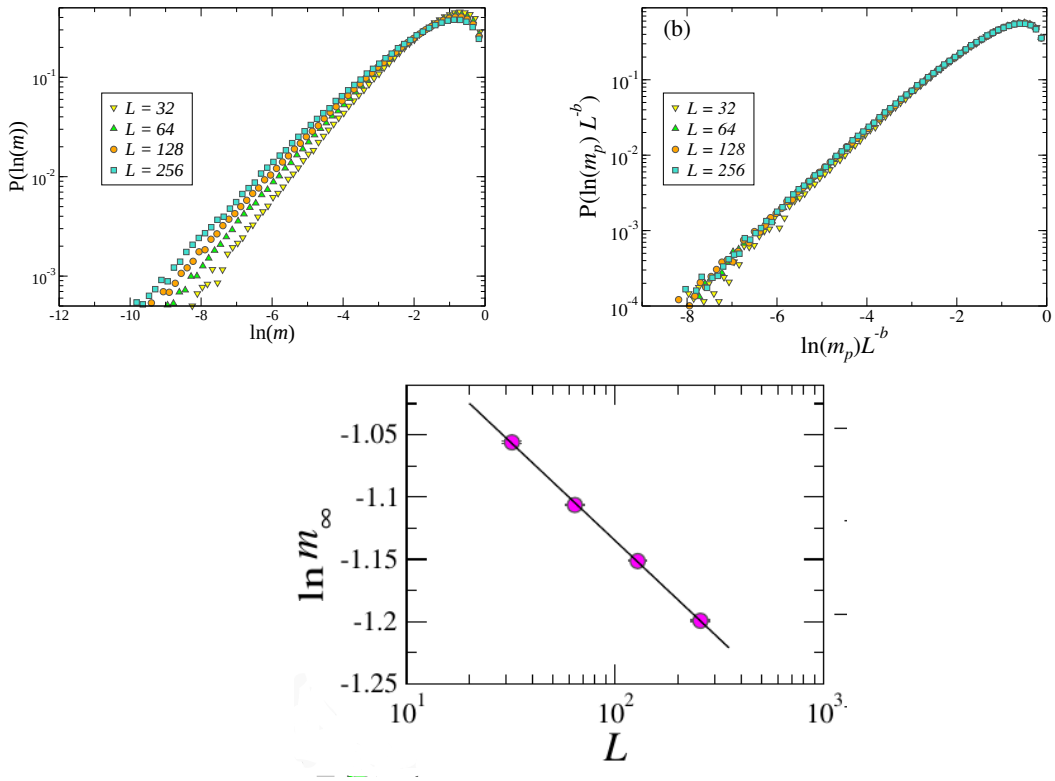

Figure 8.3. Left: Histogram of the plateau values after a quench from $h_0 = 0.0$ to the critical point. Right: Scaling plot of the histogram of the plateau values after a quench from $h_0 = 0$ to $h_1 = 1$. Bottom: Average of the magnetization after a quench from $h_0 = 0$ to $h = 1$ in the plateau region.

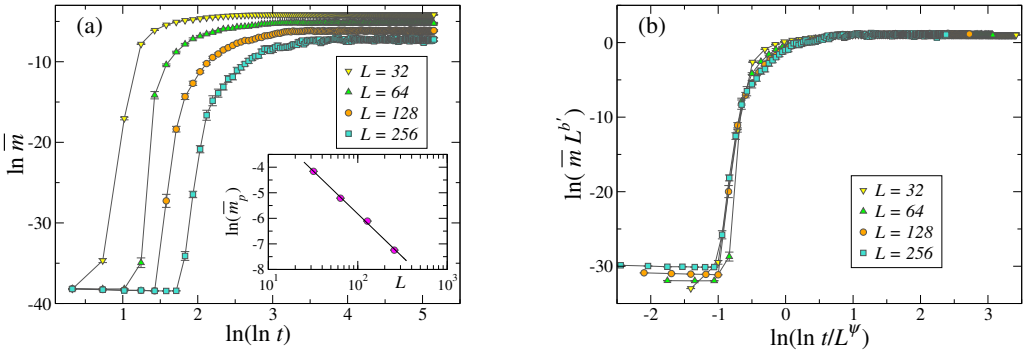

Figure 8.4. Panel (a): Time evolution of the order parameter after a quench from the paramagnetic state ($h_0 = \infty$), to the critical point $h = 1$ for different system sizes. In inset the average asymptotic (plateau) values can be seen. Panel (b): Scaled plot of the time evolution of the order parameter after a quench from the paramagnetic state ($h_0 = \infty$), to the critical point $h = 1$ for different system sizes. The values of the scaling exponents are $b' = 1.46$ $\Psi = 0.5$

investigated in this chapter the magnetization starts to increase and for long times reaches an asymptotic plateau value. The average plateau values decay with the system size L, and follow a power law:

$$[m_p]_{av}(L) \sim L^{-b'}, \quad b' = 1.4 \; . \tag{8.24}$$

This behavior is shown in the inset of Figure 8.4. The dynamical magnetization shows good scaling collapse, when $m_p L^{b'}$ is plotted against $\log t/L^{\Psi}$, as it is shown in Figure 8.4 . The large time limiting value of the dynamical magnetization, $m_p(L)$ was also studied, and it is shown in Figure 8.5. It can be seen, that the logarithm of the magnetization is broadly distributed. A good scaling collapse can reached with the scaling variable $y = \log m_p L^{-\alpha'}$, with $\alpha' = 0.5$. The scaling is shown in Figure 8.5. It follows, that the typical values of the magnetization scales with L as $m_p^{typ} \sim \exp(-CL^{\alpha})$, and it is much smaller than the average. The average value is determined by rare events with contributions of $\mathcal{O}(1)$.

$$P_L(\log m_p) = L^{-\alpha} \check{p}(\log m_p L^{-\alpha'}) \; . \tag{8.25}$$

The average of $m_p(L)$ is determined by the behavior of the $\check{p}(y)$ function on small negative arguments. (The function $\check{p}(y)$ is introduced in equation 8.25.) we assume that for small y:

$$\check{p}(y) \sim (-y)^{\chi'} \; . \tag{8.26}$$

From figure 8.5 one can see $\chi' = 2$ and with similar reasoning as in equation (8.23) one gets

$$[m_p]_{av}(L) \sim L^{-\alpha'(1+\chi')} \; , \tag{8.27}$$

in agreement with the numerical results.

With the investigation of the surface magnetization measured on the boundary site ($l = 1$) of an open chain enables a better understanding of the scaling behavior of the

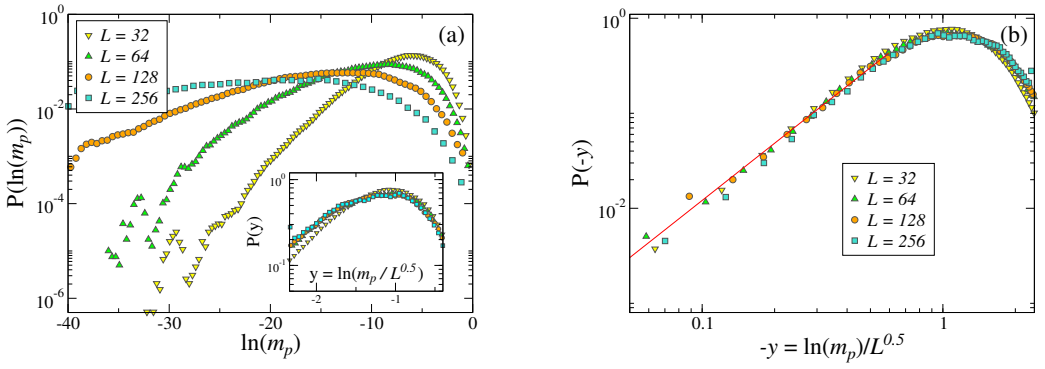

Figure 8.5. (a): Histogram of the plateau values after a quench from $h_0 = \infty$ to the critical point. (b): Histogram of the plateau values after a quench from $h_0 = \infty$ to the critical point. The $P(\log(mL^{1/2}))$ - $\log(m)L^{1/2}$ scaling gives a good data collapse.

long-time limiting value of the dynamical order parameter. With the results of Ref. [176]) (see equation (16)) the long-time limiting value of the surface magnetization, m_p^s, can be calculated exactly:

$$m_p^s = \Phi_1(1) \sum_{j=1}^{L} \Phi_1(j) \Phi_1^{(0)}(j) \; . \tag{8.28}$$

Here:

$$\begin{aligned} \Phi_1(j) &= \Phi_1(1) \prod_{i=1}^{j-1} \frac{h_i}{J_i} \, , \\ \Phi_1(1) &= \left[1 + \sum_{l=1}^{L-1} \prod_{j=1}^{l} \left(\frac{h_j}{J_j} \right)^2 \right]^{-1/2} \; . \end{aligned} \tag{8.29}$$

In the large-h_0 limit for $\Phi_1^{(0)}(j)$ one gets $\Phi_1^{(0)}(j) = \delta_{l_m,j}$. Here l_m is the position of the largest transverse field in the sample [184]. Thus

$$m_p^s = [\Phi_1(1)]^2 \prod_{j=1}^{l_m - 1} \left(\frac{h_j}{J_j} \right) \; , \tag{8.30}$$

where $\Phi_1(1) = m_{\rm eq}^s$ is the equilibrium value of the surface magnetization of the chain [117, 185], evaluated in the final state, i.e. with $h = h_c$.

The typical value of $m_{\rm eq}^s$ at the critical point scales as $\exp(-CL^{1/2})$ [117, 186]. The same scaling combination holds for m_p^s. As a consequence the right scaling combination for m_p^s is $y = \ln(m_p^s)L^{-1/2}$. It is the same form that has been obtained for the bulk spins above. From the scaling behavior of the average value $\overline{m_p^s}$ it can be seen, that the rare events are dominant.

The scaling of the surface magnetization can be calculated using an analogy with random walks. There is a direct connection between the random transverse-field Ising chain and a one-dimensional random walk ([117]): to a given sample (given magnetic fields h_i

and couplings J_i for $i = 1, 2, \dots L$) a one-dimensional random walk is associated. The associated random walk starts at the origin and takes consecutive steps, the length of the i-th step being $\ln(h_i/J_i)$.

The associated random walk stays at positive positions for all steps (In other words it is a surviving walk.) for rare realizations of $m^s_{\rm eq}$. Concerning m^s_p, here for a rare realization both $m^s_{\rm eq}$ and the product $\prod_{j=1}^{l_m-1}\left(\frac{h_j}{J_j}\right)$ should be of order of $\mathcal{O}(1)$. In the random walk language it means that the walk is surviving and returns after l_m steps.

The probability of this particular event is: $\mathcal{P}(l_m) \sim l_m^{-3/2}(L-l_m)^{-1/2}$. The average value scales as: $\sum_{l_m}\mathcal{P}(l_m)/L \sim L^{-3/2}$, which means that $\overline{m^s_p}(L) \sim L^{-3/2}$. The scaling behavior, extracted from the numerical data is similar to the last form.

8.5 Discussion

In this section we investigated numerically the dynamics of the local magnetization after a quench in the transverse quantum Ising chain. In order to get precise numerical results we avoided to use eigenvalue solver routines, since routine stability problems were reported in the literature [122] [187]. I calculated the time evolution of Majorana operators using only matrix products and multiple precision arithmetic.

If the quench starts from the ferromagnetic state and ends in the ferromagnetic phase the magnetization first reaches a plateau value, and after a delay time a second relaxation occurs, and the magnetization reaches a second plateau value. The second relaxation is generated by quasi-localized modes which are present in the ferromagnetic phase of a finite system. In an infinite system only the first plateau exists. The average magnetization is h dependent and finite in both plateaus.

If the system is quenched from the ferromagnetic phase to the critical point the magnetization goes to zero in an infinite system, as $m_l(t) \sim (\ln(t))^{-a}$. In a finite system the magnetization reaches a finite L dependent limiting value. The distribution of the long-time limiting value of the magnetization was investigated. The typical value goes to zero starched exponentially with the system size ($\exp(-CL^\alpha)$), but the average is dominated by rare events, and decays with a power law of the system size.

If the quench start from the paramagnetic state and ends in the critical point a rapid increase of the average magnetization was found, which is a unique property of the random chain: After any quench in the homogeneous or quasi-periodic Ising chain the magnetization decays.

This chapter is based on the following article:

G. Roósz., Y.-C. Lin, F. Iglói *Critical quench dynamics of random quantum spin chains: Ultra-slow relaxation from initial order and delayed ordering from initial disorder* New J. Phys. **19**, 023055 (2017)

I did the numerical simulations presented in the above chapter, and the scaling analysis about the bulk magnetization is also my own work. The analysis of the surface magnetization was did by Prof. Dr. Ferenc Igloi.

Chapter 9

Conclusion

In this dissertation I investigated the dynamics of inhomogeneous one dimensional systems with free-fermion techniques. Different types of inhomogeneities were investigated (local defect, two types of quasi periodic modulation, and a disordered system). The main results are the following:

1. For the generalized local defect I checked using large scale numerical simulations the conjuncture about the dynamics of the local magnetization at the defect site. Here the term generalized means, that a coupling and the two neighboring magnetic fields differs from the critical value. The dynamics is function of the quench parameter κ_i which is a combination of the coupling, and the magnetic fields: $\kappa_i = \frac{J_i}{h_{1i}h_{2i}}$. Here κ_1 describes the pre-quench system, and κ_2 describes the after quench system. The time evolution of the magnetization in a finite system of length L is:

$$m_d(t,L) \sim L^{-x_1} \left[L \sin\left(\pi \frac{t}{L}\right) \right]^{2(x_{12}-x_2)}, \; 0 < t < L \, .$$

   where the exponents are $x_i = \frac{\sqrt{2}}{\pi} \arctan(\frac{1}{\kappa_i})$ and $x_{12} = \sqrt{x_1 x_2}$. $(i = 1, 2)$

2. For the Fibonacci Ising chain I investigated the after dynamics of the local magnetization numerically using free fermion methods. I found that the magnetization follows a stretched exponential decrease:

$$m_{\mathrm{b}}(t) \sim A(t) \exp\left(-Ct^{\mu}\right) \, .$$

   I also found a dynamical phase transition in the behavior of the magnetization: There is a critical magnetic field h^* if the after quench magnetic field is bigger than h^*, the $A(t)$ prefactor of the magnetization oscillates, if the after quench magnetic field is below h^* the prefactor $A(t)$ remains positive. In a homogeneous system $h^* = 1$, in the Finonacci Ising chain $h^* < 1$, and h^* is power law of the inhomogeneity strength. For the entanglement entropy and for the wave-packet power-law increase were found. The exponents of the magnetization, entropy, and wave packet are close to each other in the non-oscillatory phase. This phenomenon was understood using a quasi-classical reasoning.

3. I investigated the quench dynamics of the Harper model, which shows a localization-delocalization phase transition. I calculated the after-quench dynamics of the entanglement entropy and the local magnetization. If the quench ends in the localized phase, the dynamics is similar to the dynamics of an homogeneous system: The entanglement entropy grows linearly in time, the magnetization decrease exponentially, the wave packet shows a ballistic spread. If the quench ends in the localized phase, the entropy and the magnetization both remains finite in the long-time limit, and the width of the wave packet remains small, comparable with the static localization length.
   If the quench ends at the critical point, the magnetization decreases with a stretched exponential function $m_{\mathrm{b}}(t) \sim A(t)\exp\left(-Ct^{\mu}\right)$, and the entropy grows with a power function $S \sim t^{\sigma}$ of the time. The spreading of the wave packet follows a power law $d(t) \sim t^{0.477}$ [102]. The exponents μ and σ are close to the exponent of the wave-packet spread. This fact has been understood based on a quasi-classical reasoning.

4. I investigated a Kibble-Zurek process in the Harper model. The defect density scales with a power of the speed of the process $P \sim 1/\tau^{\kappa}$. The prediction of the standard Kibble-Zurek scaling for the exponent is $\kappa = 1/2$. My numerical data suggest smaller exponent, $\kappa \approx 0.45$. I developed a modified version of the Kibble-Zurek scaling for the Harper model. This modified scaling is in good agreement with the numerical data.

5. I investigated the after quench dynamics of the magnetization in the disordered transverse Ising model. I investigated three types of quenches: from a totally ferromagnetic ($h_0 = 0$) state to the ferromagnetic phase ($0 < h < 1$), from the totally ferromagnetic phase ($h_0 = 0$) to the critical point ($h = 1$), and from the totally paramagnetic state ($h_0 \to \infty$) to the critical point ($h = 1$).
   If the quench starts from the totally ferromagnetic state, and ends at the critical point, the magnetization remains constant in the long time limit.
   If the quench starts from the infinitely paramagnetic phase and ends at the critical point, the magnetization of the finite system increases, which is a unique fact of this disordered system. If $L \to \infty$, the asymptotic magnetization goes to zero in the aforementioned quench.
   If the quench starts from the totally ferromagnetic phase ($h_0 = 0$) and ends at the critical point, the magnetization shows an extremely slow decrease of the form:

$$m(t) \sim (\log(t))^{-a}$$

   where $a \approx 0.14$.

10. fejezet

Összefoglaló

10.1. Bevezetés

A zárt kvantumrendszerek külső paraméterek megváltoztatását követő dinamikája aktívan kutatott terület, mind kísérleti, mind elméleti tekintetben. A paraméter megváltoztatásának sebessége szerint két szélsőséges esetről beszélhetünk. A külső paraméter hirtelen megváltoztatását "kvencs"-nek nevezzük. A változtatás utáni dinamikát *kvencs utáni dinamikának* Kísérletileg a kvencs utáni dinamika a Feshbach rezonancia segítségével valósítható meg [1–11].

A kvencsekkel kapcsolatban az egyik kérdéskör az, hogy a fizikai mennyiségek hogyan változnak röviddel a paraméter megváltoztatása után. A másik kérdéskör azt vizsgálja, hogy a kvencs után nagyon hosszú idő elteltével milyen állandósult állapot alakul ki, mi a kapcsolata a kialakult állandósult állapotnak a rendszerben létező megmaradó mennyiségekkel. [12–57]. A másik határeset a paraméter nagyon lassú változtatása, a *közel adiabatikus dinamika*. A külső paramétert a legtöbbször időben lineárisan változtatják $\sim t/\tau$ módon, és a változtatás során átvisszük a rendszert egy fázisátalakulási ponton. A folyamat elején a rendszer a pillanatnyi Hamilton-operátor alapállapotában van. Ha a paraméter változtatásának sebessége $(1/\tau)$ sokkal kisebb mint a rendszerben található legkisebb energia különbséghez tartozó időskála, a rendszert jellemző állapotvektor mindvégig közel marad a pillanatnyi alapállapothoz. Azonban a legkisebb energia különbség (legkisebb gap) nullához tart, ahogy a rendszer közelít a fázisátalakulási ponthoz, így a külső paraméter változása nem lesz a folyamat egész ideje alatt "elég lassú".
A kérdés, hogy milyen messze lesz a lassú dinamikával kapott állapot az alapállapottól a fázisátalakulási pont keresztezése után, intenzív vizsgálatok tárgyát képezte [50, 56, 58–74]. Kibble és Zurek [58] [59] megadott egy összefüggést, amely a két állapot "távolságát" a $P(\tau) \sim$ (density of deffects) $\sim \frac{1}{\xi^d} \sim \tau^{-\frac{d\nu}{\nu z+1}}$ módon jellemzi, ahol d a rendszer dinamikája, ν a korrelációs hossz kritikus exponense, z a dinamikai exponens. A formula eredeti indoklása heurisztikus, azóta perturbatív és numerikus módszerekkel vizsgálták az érvényességét különböző rendszerekben.
Az itt kiemelt kétféle folyamat mellett az irodalomban más nemegyensúlyi dinamikával kapcsolatos kérdéseket is vizsgáltak, ilyen például egy izolált rendszer időfejlődése időben periodikusan [75] [76], kvázi-periodikusan vagy véletlenszerűen [77] változó külső potenciálban.

A kvencs dinamikával kapcsolatban kiterjedt irodalom létezik, amelyben azonban leginkább a homogén (transzláció invariáns) rendszerek dinamikáját vizsgálták [12,16–33,50,51,55]. A homogén rendszerekkel kapcsolatban az egyik legszebb eredmény a kvencs utáni dinamika kvázi-klasszikus leírása. A kvencs során a rendszer minden pontjában kvázirészecske párok keletkeznek ellentétes impulzussal. Ezek a részecskék a későbbiek során állandó sebességgel haladnak, a rendszert határoló felületekről visszaverődnek [38, 51, 56]. A kváziklasszikus leírás segítségével a homogén rendszerekre aszimptotikusan egzakt eredmények kaphatóak. Az inhomogén rendszerek kvencs utáni dinamikájával kapcsolatban csak néhány speciális esetet vizsgáltak az irodalomban, például az összefonódási entrópia viselkedését rendezetlen spinláncokban [78–80], vagy a soktest-lokalizáció modelljeiben [81] [82]. Az inhomogenitás egy speciális típusa a kvázi-periodikus rend, ami a homogén és a rendezetlen rendszerek "között" helyezkedik el: bonyolultabb az előbbinél, hisz nem transzláció invariáns, de egyszerűbb az utóbbinál, mert rendezett, determinisztikus [83–85].
A kváziperiodikus rendszerek szokatlan transzporttulajdonságokkal bírnak, bennük a hullámcsomag kiterjedése nem "ballisztikus" mint a homogén rendszerekben, hanem anomális diffúziót követ [86, 87].
A disszertáció az alábbi négy cikken alapul:

1. F. Iglói, G. Roósz, Y.-C. Lin *Nonequilibrium quench dynamics in quantum quasicrystals* New J. Phys. 15, 023036 (2013)

2. F. Iglói, G. Roósz, L. Turban *Evolution of the magnetization after a local quench in the critical transverse-field Ising chain* J. Stat. Mech. (2014) P03023

3. G. Roósz., U. Divakaran, H. Rieger, F. Iglói *Non-equilibrium quantum relaxation across a localization-delocalization transition* Phys. Rev. B 90, 184202 (2014)

4. G. Roósz., Y.-C. Lin, F. Iglói *Critical quench dynamics of random quantum spin chains: Ultra-slow relaxation from initial order and delayed ordering from initial disorder* 2017 New J. Phys. https://doi.org/10.1088/1367-2630/aa60e6

A következő alfejezetekben a disszertáció saját eredményeket ismertető részeinek magyar nyelvű kivonata olvasható.

10.2. Általánosított lokális kvencs

Ebben a fejezetben az angol nyelvű szöveg 4 fejezetét foglalom össze, amely a [188] cikken alapul. Az irodalomban a legtöbbet vizsgált kérdéskör az un. globális kvencs: Ekkor a rendszer egy paramétere globálisan, az egész rendszerre kiterjedő homogén módon változik meg: Ilyen például egy külső mágneses tér bekapcsolása, amelynek értéke az egész rendszer területén homogén. Egy másik érdekes kérdéskör a lokális kvencsek területe, amikor a Hamilton operátor egy rácshely környezetében változik meg pillanatszerűen. Kísérletekben a lokális kvencset valósít meg például a röntgensugarak fémbeli elnyelődése [141].

Az elméleti vizsgálatok többsége kritikus egydimenziós rendszerekkel foglalkozik, amelyekre vonatkozóan a konform térelmélet segítségével egzakt eredményeket lehet megfogalmazni. A konform térelmélet a modell folytonos határesetét írja le, ahol a rendszer egy kétdimenziós (x,t) téridőben él. Ebben a fejezetben egy kritikus transzverzális terű kvantum Ising láncot vizsgálunk, amelyben egy általánosított hibahely paramétereit pillanatszerűen megváltoztatjuk. Az általánosított jelző arra vonatkozik, hogy egy csatolás és a két szomszédos mágneses tér értéke is különbözik a kritikus láncra jellemző tömbi értéktől.

Az általunk vizsgált rendszer Hamilton-operátora:

$$\mathcal{H}_i = -\frac{1}{2}\left[\sum_{n=1}^{L-1}\sigma_n^x\sigma_{n+1}^x + (J_i-1)\sigma_{L/2}^x\sigma_{L/2+1}^x + \sum_{n=1}^{L}\sigma_n^z + (h_{i1}-1)\sigma_{L/2}^z + (h_{i2}-1)\sigma_{L/2+1}^z\right], \quad (10.1)$$

ahol σ_n^x, σ_n^y, σ_n^z a pauli mátrixok. A hibahely a lánc közepén található, és a kvencs előtt $(t<0)$ J_1 csatolás, attól balra h_{11} mágneses tér, a J_1 csatolástól jobbra h_{12} mágneses tér jellemzi. A kvencs utáni paraméterek J_2, h_{21}, h_{22}. A kvencs után a hibahelyen mért lokális mágnesezettség időbeli fejlődését vizsgáljuk. A lokális mágnesezettséget a σ^x operátor alapállapot és első gerjesztett állapot közötti mátrixelemeként számíthatjuk [167] $m_n(t)\langle\Phi_0|\sigma_n^x(t)|\Phi_1\rangle$ egy tetszőleges rácsponton. A mágnesezettség a hibahelyen: $m_d(t) = m_{n=L/2}(t)$. A rendszer megfeleltethető egy kétdimenziós klasszikus spin modell extrém-anizotrop esete transzfermátrixának. A megfeleltetés segítségével levezethető a lokális mágnesezettség imaginárius időbeli dinamikája a termodinamikai határesetben ($L\to\infty$ határesetben). Az eredmények a következőképen foglalhatók össze: A dinamika a $\kappa_i = \frac{J_i}{h_{i1}\,h_{i2}}$ $\quad (i=1,2)$ effektív kölcsönhatások függvénye, a mágnesezettség imaginárius időbeli változása hatványfüggvényt követ a

$$m_d(\tau) \sim \tau^{x_{12}-x_2}, \quad 0<\tau\ll L \quad (10.2)$$

alakban, ahol az exponensek értékei: $x_i = \frac{\sqrt{2}}{\pi}\arctan(\frac{1}{\kappa_i})$ és $x_{12} = \sqrt{x_1x_2}$. A valós idejű dinamikára ismertek az irodalomból eredmények ha $h_{11} = h_{12} = h_{21} = h_{22} = 1$, és a $J_1 = \infty$ (a kezdeti állapotban a hibahely spinjei rögzítettek) vagy $J_1 = 1$ és $J_2 = 0$ (egy homogén lánc szétvágása).

A rögzített spinű esetre [142] konform térelmélet segítségével meghatározták hogy a mágnesezettség relaxációja:

$$m_d^{(+)}(t) \sim t^{-2x_m} \quad 0<t\ll L\,. \quad (10.3)$$

ami numerikus szimulációkkal is tesztelve lett a transzverzális terű kvantum Ising láncban [94]. Egy nyílt láncban [94] eredményei a következő formulával összegezhetőek:

$$m_d^{(+)}(t,L) \sim \left[L\sin\left(\pi\frac{t}{L}\right)\right]^{-2x_m}, \quad 0<t<L\,. \quad (10.4)$$

Abban az esetben, amikor a két félrendszer a kvencs után nincs összekapcsolva [94] nume-

rikus eredményeit az alábbi formulával lehet összefoglalni:

$$m_d^{(fb)}(t,L) \sim L^{-1/2}\left[L\sin\left(\pi\frac{t}{L}\right)\right]^{1/4}, \quad 0<t<L\,. \tag{10.5}$$

ami rövid időkre a következő alakot veszi fel:

$$m_d^{(fb)}(t) \sim m_0(L)\,t^{1/4}, \quad 0\le t\ll L\,, \tag{10.6}$$

ahol $m_0(L) \sim L^{-x_{ms}}$ az egyensúlyi értéke a hibahelyi mágnesezettségnek a kiindulási állapotban. Az exponens a (10.6) egyenletben megegyezik $1/4 = 2(x_{ms}/2 - x_m)$ -vel, ahol $x_2 = x_m$ and $x_{12} = x_{ms}/2$. A rögzített spinű kezdőállapotra, (10.4) egyenlet, ugyanez teljesül $x_{12} = 0$-el. Ha t^2-et helyettesítünk τ helyére az imaginárius időre vonatkozó egyenletekbe akkor a (10.2) egyenletből megkaphatjuk a valós időre vonatkozó eredményeket, a (10.4) és (10.6) egyenleteket. Ezért megfogalmazhatjuk a hibahelyi mágnesezettség kvencs utáni viselkedésére (az $L \gg 1$ határesetben) az alábbi sejtést:

$$m_d(t) \sim m_0(L)\,t^{2(x_{12}-x_2)}, \quad 0<t\ll L\,, \tag{10.7}$$

ahol $m_0(L) \sim L^{-x_1}$. Egy véges rendszerben sejtésünk szerint a mágnesezettség a következő (periodikus) módon változik a kvencs után:

$$m_d(t,L) \sim L^{-x_1}\left[L\sin\left(\pi\frac{t}{L}\right)\right]^{2(x_{12}-x_2)}, \; 0<t<L\,. \tag{10.8}$$

A fenti két egyenlet a fejezet fő eredménye. A sejtésként megfogalmazott formulákat numerikus szimulációval ellenőriztem.

10.3. A Finonacci Ising kvázikristály nem egyensúlyi dinamikája

Ebben a fejezetben a kvantum Ising lánc egy kváziperiodikus változatának dinamikáját vizsgáljuk. A modellt definiáló Hamilton-operátor a következő:

$$\mathcal{H} = -\frac{1}{2}\left[\sum_i J_i\sigma_i^x\sigma_{i+1}^x + h\sum_i \sigma_i^z\right], \tag{10.9}$$

(σ_i^x, σ_i^z a Pauli mátrixok az i. helyen) A J_i csatolások helyfüggőek, és az alábbi módon vannak paraméterezve:

$$J_i = Jr^{f_i}\,, \tag{10.10}$$

itt $r > 0$ az inhomogenitás erősségét jellemzi, $r = 1$ megfelel a homogén rendszernek, minél kisebb r annál erősebb az inhomogenitás. Az f_i számok 0 vagy 1 értéket vehetnek fel, és kváziperiodikusan váltakoznak az un. Fibonacci sorozatnak megfelelően.

A J kölcsönhatás erősség a (10.10) egyenletben $J = r^{-\rho}$, ahol

$$\rho = \lim_{L\to\infty} \frac{\sum_{i=1}^{L} f_i}{L} = 1 - \frac{1}{\omega} \, , \tag{10.11}$$

az 1 számok aránya egy nagyon hosszú (végtelen sorozatban).

A Fibonacci sorozatot a következő algebrai kifejezés definiálja:

$$f_i = 1 + \left[\frac{i}{\omega}\right] - \left[\frac{i+1}{\omega}\right] \, , \tag{10.12}$$

ahol $[x]$ az x szám egészrésze, és $\omega = (\sqrt{5}+1)/2$. A fenti definícióval a modell kritikus pontja $h = 1$-ben van, $h < 1$ a ferromágneses fázis, $h > 1$ a paramágneses fázis. A Fibonacci sorozat a Harris-Luck kritérium szerint [204] irreleváns perturbáció: A kritikus exponensek folytonosan változnak a rendezetlenség erősségének függvényben.
A kvencset a mágneses tér hirtelen változtatásával valósítottam meg. A kvencs előtt a mágneses tér h_0 a kvencs után a mágneses tér értéke h. Vizsgáltam a lokális mágnesezettség viselkedését a határfelületektől távol, a tömbi részben, az összefonódási entrópia időbeli változását, és az un. hullámcsomag kiszélesedését. Az összefonódási entrópia definíciója a következő. A rendszer a $|\Psi\rangle$ tiszta állapotban van, amit a $\rho = |\Psi\rangle\langle\Psi|$ diadikus sűrűségmátrixszal is jellemezhetünk. A rendszert két részre osztjuk (A és B). Definiáljuk a redukált sűrűség mátrixokat $\rho_A = \mathrm{Tr}_B\rho$ és $\rho_B = \mathrm{Tr}_A\rho$. Az összefonódási entrópia a redukált sűrűségmátrixok von Neumann entrópiája: $S = -\mathrm{Tr}_B\rho_B \ln\rho_B = -\mathrm{Tr}_A\rho_B \ln\rho_A$ Az összefonódási entrópia a két rész közötti összefonódást jellemzi. Numerikus szimulációk segítségével a következő eredményekre jutottam: A mágnesezettség kvencs utáni dinamikája nyújtott exponenciális viselkedést mutat:

$$m_{\mathrm{b}}(t) \sim A(t)\exp\left(-Ct^{\mu}\right) \, . \tag{10.13}$$

az $A(t)$ prefaktor egységnyi nagyságrendű. Az $A(t)$ prefaktor viselkedésében két tartományt különíthetünk el $h < h^*(r)$, akkor $A(t) > 0$ ha $h < h^*(r)$ akkor $A(t)$ oszcillál. A $h^*(r)$ dinamikai fázisátalakulási pont az r paraméternek hatványfüggvénye: $h^*(r) \sim r^{\omega}$ ahol $\omega \approx 0.24$ adódik. A $h^*(r) \sim r^{\omega}$ összefüggés azzal a feltevéssel áll összhangban,hogy a mágnesezettség akkor marad pozitív, ha a vizsgált rácshely környezete lokálisan ferromágneses, és akkor csökken oszcillálva, ha a környezet lokálisan paramágneses. Az összefonódási entrópia a kvencs után az idő hatványfüggvényeként nő:

$$\mathcal{S}(t) \sim t^{\sigma} \, , \tag{10.14}$$

a σ exponens közel megegyezik a mágnesezettségnél bevezetett μ exponenssel abban a tartományban, ahol a mágnesezettség oszcilláció nélkül tart 0-hoz. Ezt a numerikus megfigyelést kvalitatíven a kvázi-klasszikus elmélettel értelmeztem.

10.4. A Harper-modell nem egyensúlyi dinamikája

A Harper-modellt definiáló Hamilton-operátor:

$$\mathcal{H} = -\frac{1}{4}\sum_{n=1}^{L}(\sigma_n^x\sigma_{n+1}^x + \sigma_n^y\sigma_{n+1}^y) - \sum_{n=1}^{L} h_n\sigma_n^z \ . \tag{10.15}$$

ahol $\sigma_n^{x,y,z}$ a Pauli-mátrixok az n. rácshelyen és h_n egy kváziperiodikus potenciál:

$$h_n = h\cos(2\pi\beta n) \ , \tag{10.16}$$

ahol $\beta = (\sqrt{5}-1)/2$ az aranymetszés inverze. A Harper-modell lokalizációs fázisátalakulást mutat [102], $|h| < 1$-re a modell saját állapotai kiterjedtek, a spektrum abszolút folytonos, $|h| > 1$-re a saját állapotok lokalizáltak, a modell pontspektrummal bír. A kritikus pontban ($|h| = 1$) a modell spektruma fraktál-szerű, szinguláris-folytonos [113]. A kvenccsel kapcsolatos numerikus eredményeket aszerint írom le, hogy a kvencs utáni h mágneses tér melyik fázisban van.

Ha a kvencs a kiterjedt fázisban végződött, a Harper-modell dinamikája a homogén rendszerekére emlékeztet: A lokális mágnesezettség exponenciálisan csökken, az összefonódási entrópia az idővel lineárisan nő, a hullámcsomag ballisztikusan szélesedik. Ha a kvencs a lokalizált fázisban végződik, a lokális mágnesezettség és az entrópia is véges értékű marad. Ha a kvencs a kritikus pontban végződik, a lokális mágnesezettség nyújtott exponenciális viselkedést mutat $m_{\mathrm{b}}(t) \sim A(t)\exp\left(-Ct^{\mu}\right)$ ahol $\mu \approx 0.43(5)$, az entrópia $S(t) \sim t^{\sigma}$ viselkedést mutat, ahol $\sigma \approx 0.47(5)$. Mind a σ mind a ν exponens közel esik a [102] cikkeben a hullámcsomag kiszélesedésére meghatározott 0.477 értékhez. Az exponensek közeli értéke arra enged következtetni, hogy a kvázi-klasszikus kép kvázi-periodikus rendszerek esetében is helyes, csupán a kvázi-részecske párok homogén rendszerbeli ballisztikus mozgását kell a megfelelő anomális diffúzióval helyettesíteni.

10.5. Közel adiabatikus dinamika a Harper modellben

Ebben a fejezetben a Harper-modell közel adiabatikus dinamikájával kapcsolatos eredményeket összegzem. Az adiabatikus dinamikával kapcsolatban kétféle "protokollt" használtam: Az első során a h mágneses tér értéke $-\infty$-ből indul, és $h = t/\tau$ módon növekszik ∞ értékig. A második protokoll során a mágneses tér szintén $-\infty$-ből indul, és $h = t/\tau$ módon növekszik, de csak $h = 0$-ig. Az első protokoll során a fázisátalakulási pontot kétszer keresztezzük, a második protokoll során egyszer.

A fázisátalakulási pontokon való áthaladás során a rendszerben gerjesztések keletkeznek. Annak valószínűségére, hogy a rendszer gerjesztett állapotban lesz, a hagyományos Kibble-Zurek skálázás $P \sim 1/\tau^{1/2}$-et jósol [58]. A numerikus adataim $P \sim 1/\tau^{0.45}$-el kompatibilisek. A Kibble-Zurek skálázás egy módosított formáját alkottam meg, ami jól illeszkedik a numerikus eredményeimhez.

10.6. A rendezetlen kvantumos Ising modell nem egyensúlyi dinamikája

Ebben a fejezetben a mágnesezettség kvencs utáni dinamikáját vizsgáljuk a rendezetlen Ising láncban. Az összefonódási entrópia kvencs utáni dinamikájával kapcsolatban részletes vizsgálatokat olvashatunk az irodalomban [78–81, 180].

Ha a rendszer nemkölcsönható fermionokból áll - mint a rendezetlen XX vagy a rendezetlen kritikus Ising lánc - a dinamikus összefonódási entrópia az idő második logaritmusával arányosan, rendkívül lassan növekszik:

$$\mathcal{S}(t) \sim a \ln \ln t \,, \tag{10.17}$$

és hosszú idő eltelte után szaturálódik egy aszimptotikus értékhez:

$$\mathcal{S}(\ell) \sim b \ln \ell \,, \tag{10.18}$$

ahol ℓ a blokkméret a kétfelé vágott rendszerben, amit a teljes L hosszal arányosnak választottak a vizsgálatokban [79,180]. Ezek az összefüggések értelmezhetőek az erős rendezetlenség renormálási csoport (strong disorder renormalization-group, SDRG) segítségével [103]. Az erős rendezetlenség renormálási csoport (SDRG), ami eredetileg az alapállapot tulajdonságainak leírására lett megalkotva, a közelmúltban megjelent munkákban [181–183] általánosítva lett a gerjesztett állapotokra is, erre az általánosított verzióra gyakran hivatkoznak RSRG-X -ként [181].

Az RSRG-X módszer jóslata a (10.17) és (10.18) egyenletekben szereplő prefaktorok arányáról $b/a = \psi_{\rm ne}$, ahol $\psi_{\rm ne} = 1/2$. A nem-egyensúlyi folyamatban a hossz és időskála összefüggése:

$$\ln t \sim L^{\psi_{\rm ne}} \,. \tag{10.19}$$

Az általam vizsgált modlet definiáló Hamilton-operátor:

$$\mathcal{H} = -\sum_{i=1}^{L-1} J_i \sigma_i^x \sigma_{i+1}^x - \sum_{i=1}^{L} h_i \sigma_i^z \,, \tag{10.20}$$

ahol J_i a $[0,1]$ intervallumból és h_i a $[0,h]$ intervallumból kerül kiválasztásra egyenletes eloszlás szerint.

A vizsgálatok során kétféle kezdőállapotot használtam. Az egyik a teljesen ferromágneses állapot, ami a $h \to 0$ határesetnek felel meg, a másik a teljesen paramágneses állapot, ami az összes csatolás kikapcsolásának felel meg $J_i = 0$. Ha a kvencs a teljesen ferromágneses állapotból indult a ferromágneses fázis "belsejébe" $(0 < h < 1)$ vezetett, a mágnesezettség véges maradt a hosszú idők határesetében.

Ha a kvencs előtt a rendszer a teljesen paramágneses állapotban volt és a kritikus pontba vittük a kvenccsel, akkor a mágnesezettség egy gyors *növekedés* után ért el egy állandósult értéket. Az állandósult érték az $L \to \infty$ limeszben zéróhoz tart.

Ha a kvencs a teljesen ferromágneses állapotból indult, és a kvencs utáni Hamilton operátor

kritikus volt, a mágnesezettség egy nagyon lassú relaxációt mutatott:

$$m(t) \sim (\log(t))^{-a} \,, \tag{10.21}$$

ahol $a \approx 0.14$. A csökkenő tartomány után a mágnesezettség egy konstans értéket vett fel, aminek a véges méret függése:

$$m_p(L) \sim L^{-b} \,, \tag{10.22}$$

ahol $b \approx 0.068(5)$. A két exponens aránya $b/a = 0.48(5) \approx 1/2$ jó összhangban az RSRG-X eredményekkel.

10.7. Konklúzió

A disszertációmban egydimenziós inhomogén kvantum rendszerek nem-egyensúlyi dinamikáját vizsgáltam szabad fermionos módszerek segítségével. Különböző típusú inhomogenitásokat vizsgáltam (lokális hibahely, kétféle kváziperiodikus rendszer, rendezetlen rendszer.) Az elért eredmények a következőek:

1. Általánosított lokális kvencs. Az általánosított kifejezés arra vonatkozik, hogy nem csak egy csatolás, hanem a csatolással szomszédos mágnese terek is megváltoznak a kvencs időpontjában. Precíz numerikus szimulációk segítségével ellenőriztem a lokális mágnesezettség kvencs utáni dinamikájára vonatkozó sejtést. A dinamika a κ_i kvencs paraméter függvénye, ami a hibahelyet jellemző csatolás és mágneses terek kombinációja: $\kappa_i = \frac{J_i}{h_{1i}h_{2i}}$. A κ_1 paraméter a kvencs előtti, a κ_2 paraméter a kvencs utáni rendszerre vonatkozik. A mágnesezettség időfejlődése egy véges, L spinből álló rendszerben:

$$m_d(t,L) \sim L^{-x_1} \left[L \sin\left(\pi \frac{t}{L} \right) \right]^{2(x_{12}-x_2)}, \; 0 < t < L \,.$$

   ahol az exponensek $x_i = \frac{\sqrt{2}}{\pi} \arctan(\frac{1}{\kappa_i})$ és $x_{12} = \sqrt{x_1 x_2}$.

2. Fibonacci Ising kvázi kristályban a mágnesezettség, az összefonódási entrópia és a propagátor kvencs utáni dinamikáját vizsgáltam. A lokális mágnesezettség a kvencs után nyújtott exponenciális függvény szerint csökken:

$$m_{\mathrm{b}}(t) \sim A(t) \exp\left(-C t^{\mu}\right) \,.$$

   Itt $A(t)$ egy $O(1)$ nagyságrendű prefaktor. Az $A(t)$ prefaktoral kapcsolatban egy dinamikai fázisátalakulást találtam. Van egy kritikus mágneses tér érték h^*, ha a kvencs utáni mágneses tér kisebb mint h^* az $A(t)$ prefaktor pozitív minden t-re, ha nagyobb akkor oszcillálva pozitív és negatív értékeket is felvesz. A homogén rendszerben ez a fázishatár egybeesik a (statikus) kritikus ponttal. Az inhomogén rendszerben h^* a ferromágneses fázisban van, és folytonos függvénye az inhomogenitás erősségének. Az összefonódási entrópia a kvencs után kezdetben hatványfüggvény módon növekszik $S \sim t^{\sigma}$, majd (véges rendszerben) beáll egy aszimptotikus értékre,

ami a rendszerméret függvénye. A propagátorból készített "hullámcsomag" kezdetben szintén hatványfüggvény módon szélesedik,$d(t) \sim t^D$. A három exponens (μ, σ, D) numerikusan megállapított értéke (a számítások pontosságát figyelembe véve) megegyezik abban a tartományban, ahol a mágnesezettség előjel nélkül csökken. Ezt az egyezést kvázi-klasszikus leírás segítségével értelmeztem.

3. Vizsgáltam a Harper-modell kvencs utáni dinamikáját. Ebben a modellben lokalizáció-delokalizáció átalakulás figyelhető meg. Numerikus számolással követtem az összefonódási entrópia és a lokális mágnesezettség dinamikáját. Ha a kvencs utáni Hmailton-operátor a delokalizált fázisban van, a dinamika hasonló egy homogén rendszer dinamikájához: A mágnesezettség exponenciálisan csökken, az összefonódási entrópia lineárisan nő az idővel. Ha a kvencs a lokalizált fázisban végződik, a mágnesezettség és az entrópia is véges marad.
   Ha kvencs a kritikus pontban végződik, a mágnesezettség nyújtott exponenciális függvény szerint csökken: $m_{\mathrm{b}}(t) \sim A(t)\exp\left(-Ct^{\mu}\right)$, és az entrópia hatványfüggvényként nő $S \sim t^{\sigma}$. A hullámcsomag szélessége szintén hatványfüggvény szerint növekszik $d(t) \sim t^{0.477}$, összhangban az irodalomban fellelhető eredményekkel [102]. A μ és σ exponensek értéke közel esik a hullámcsomag exponenséhez, amit a kvázi-klasszikus kép segítségével értelmeztem

4. Vizsgáltam egy közel adiabatikus folyamatot a Harper-modellben. A folyamat során a rendszert lassan visszük át a lokalizációs-delokalizációs kritikus ponton, a mágneses tér időfüggése $h(t) = t/\tau$ ahol $\tau \gg 1$ a folyamat sebessége. Azt vizsgáltam, a rendszer milyen közel lesz a pillanatnyi Hamilton-operátor alapállapotához a kritikus ponton való áthaladás után- A Kibble-Zurek skálázás jóslata az, hogy pillanatnyi Hamilton-operátor alapállapotától vett távolság $P \sim 1/\tau^{\kappa}$ módon függ a folyamat sebességétől, ahol $\kappa = 1/2$. A numerikus adataim $\kappa \approx 0.45$-el kompatibilisek. Megadtam a Kibble-Zurek skálázásnak a Harper-modellre vonatkozó, speciálisan módosított változatát, ami jól illeszkedik a numerikus adatokhoz is.

5. Vizsgáltam a rendezetlen egydimenziós kvantum Ising lánc globális kvencs utáni dinamikáját. A transzverzális tér a kvencs előtti h_0 értékről hirtelen h-ra változik. Kétféle kezdőállapotot vizsgáltam, a $h = 0$ ferromágneses kezdőállapotban mindegyik spin az X irányba mutat (ami a kölcsönhatás iránya), a paramágneses kezdőállapotban mindegyik spin a Z irányba (a transzverzális tér irányába) mutat. A két kezdőállapot segítségével háromféle kvencset vizsgáltam: A $h = 0$ ferromágneses állapotból a ferromágneses fázis $0 < h < 1$ belsejébe, a ferromágneses kezdőállapotból a kritikus pontba, illetve a paramágneses kezdőállapotból a kritikus pontba vittem a rendszert a kvencs során.
   Ha a ferromágneses kezdőállapotból a ferromágneses fázis belsejébe vezetett a kvencs, a mágnesezettség konstans maradt az $L \to \infty$, $t \to \infty$ határesetben is.
   Ha a paramágneses állapotból a kritikus pontba vezetett a kvencs, akkor egy véges rendszerben a mágnesezettség átlagértéke növekedett, majd egy aszimptotikus ($t \to \infty$) értékre állt be. A homogén és kvázi-periodikus rendszerekben minden kvencs

után csökkent a mágnesezettség értéke, a növekedés ennek a speciális kvencsnek a sajátossága. Az aszimptotikus ($t \to \infty$) mágnesezettség érték függ a rendszermérettől, és nullához tart az $L \to \infty$ határesetben.
Ha a kvencs a ferromágneses állapotból indul, és a kritikus pontban végződik, a mágnesezettség átlaga rendkívül lassan csökken:

$$m(t) \sim (\log(t))^{-a}$$

ahol $a \approx 0.14$.

Acknowledgements

I wish to express my sincere gratitude to those excellent people without whom it would not be possible to complete this thesis. First of all I would like to thank to my Father, my Brother and especially to my Mother that they always supported me during my studies.
I am grateful to all teachers and students of the Department of Theoretical Physics of the University of Szeged for creating inspiring atmosphere. I am specially grateful to Lóránt Szabó and Tamás Görbe for the great discussions about various fields of the physics.
I had the luck to spent my time partially in the Wigner Research Centre for Physics where I got to know excellent physicist. I would like to express my gratitude for Dr. Róbert Juhász and to Dr. István Kovács for the consultations. I rally learnt a lot from them.
During my studies I had the luck to enjoy the outstanding lectures of Prof. Dr. Iván Gyémánt, Prof. Dr. Iglói Ferenc, Dr. Habil. László Sasvári, Dr. Gergely Szirmai, Prof. Dr. Mihály Benedict and Prof. Dr. László Fehér. I am glad to Dr. Habil. Peter Földi, for his continuous support and for the great discussions.

I had the opportunity to work with real experts of statistical physics, namely with Prof. Dr. Yu-Cheng Lin, Prof. Dr. Loic Turban, Dr. Uma Divakaran Prof. Dr. Heiko Rieger, Dr. Róbert Juhász, and Dr. István Kovács. I am glad to them all for the common work, and for the valuable discussions.

I had the luck to work in the group of Prof. Dr. Heiko Rieger at the Universität des Saarlandes. I am really grateful for the hospitality to Dr. Prof. Heiko Rieger and every members of his group. This group was a great place to work and learn.
I am grateful to my supervisor Prof. Dr. Ferenc Igloi, for the continuous support, for raising interesting problems, and for introducing me to the impressive filed of statistical physics.
I would like to express my sincere gratitude to my wife, for her patience, for our home, which would be empty without She, and for her unique way of thinking, which is a complementary of mine. This thesis is dedicated to her.

Köszönetnyilvánítás

Sok nagyszerű embernek tartozom köszönettel, akik nélkül ez a dolgozat nem jöhetett volna létre. Először is köszönettel tartozom Édesapámnak, Bátyámnak, és különösen Édesanyámnak, amiért tanulmányaim során mindvégig támogattak és biztattak.
Köszönettel tartozom a Szegedi Tudományegyetem Elméleti Fizikai Tanszéke minden oktatójának és diákjának, a Tanszék inspiráló légköréért. Külön köszönettel tartozom Szabó Lórántnak és Görbe Tamásnak, akik a Tanszéken irodatársaim voltak, és számos alkalommal élvezetes beszélgetéseket folytattunk a fizika különböző területeiről.
Abban a szerencsében volt részem, hogy a doktori tanulmányaim éveit részben a Wigner Fizikai Kutató Intézetben töltöttem, ahol számos nagyszerű fizikust ismerhettem meg. Hálás vagyok Dr. Juhász Róbertnek és Dr. Kovács Istvánnak a konzultációkért, szakmai iránymutatásért, mindkettőjüktől sokat tanultam.
Meghatározó élmény volt Prof. Dr. Gyémánt Iván, Prof. Dr. Iglói Ferenc, Dr. Habil Sasvári László, Dr. Szirmai Gergely, Prof. Dr. Benedict Mihály és Prof. Dr. Fehér László előadásait látogatni. Hálás vagyok Dr. Habil Földi Péternek, aki a Bsc szakdolgozatom során témavezetőm volt, a konzultációkért, és a folyamatos támogatásáért, amelyben mindvégig részesültem. A doktori tanulmányok során kiváló szerzőtársakkal volt szerencsém együtt dolgozni. Hálával tartozom Dr. Juhász Róbertnek, Dr. Kovács Istvánnak, Prof. Dr. Loic Turban-nak Prof. Dr. Yu-Cheng Lin-nek, Dr. Uma Divakarannak és Prof. Dr. Heiko Rieger-nek a közös munkáért, amiből nagyon sokat tanultam. Dr. Prof. Heiko Riegernek külön köszönöm a lehetőséget, hogy két nyarat a kutatócsoportjában dolgozhattam az Universität des Saarlandes-en.
Köszönettel tartozom Prof. Dr. Iglói Ferencnek, témavezetőmnek, a folyamatos támogatásért, az érdekes témák felvetésért, és azért, hogy megismertette velem statisztikus fizika lenyűgöző világát.
Köszönettel tartozom feleségemnek, Máriának, a türelméért, az otthonért, amit Ő teremt meg, és a gondolkodásmódjáért, amivel úgy hiszem, kiegészít engem. Neki ajánlom ezt a dolgozatot.

Appendix A

Time Evolution, Eigenstates

In this chapter we summarize the basic facts about calculating the eigenstates of the inhomogeneous XY model, and the dynamics. The inhomogeneous XY model is defined in Equation (2.1).

A.1 Transformation to quadratic form

Jordan-Wigner transformation [105] [104]:

$$\sigma_l^{\pm} = \frac{1}{2}(\sigma_l^x \pm i\sigma_l^y) \tag{A.1}$$

$$\sigma_l^x = \sigma_l^+ + \sigma_l^- \quad \sigma_l^y = \frac{1}{i}(\sigma_l^+ - \sigma_l^-) \quad \sigma_l^z = 2\sigma_l^+\sigma_l^- - 1 \tag{A.2}$$

$$c_l = \exp(i\pi \sum_{j=1}^{l-1} \sigma_j^+\sigma_j^-)\sigma_l^- \tag{A.3}$$

$$c_l^\dagger = \exp(i\pi \sum_{j=1}^{l-1} \sigma_j^+\sigma_j^-)\sigma_l^+ \tag{A.4}$$

$$\tag{A.5}$$

The Hamiltonian is quadratic with the new c_l Fermion operators, expect the last term in the case of periodic boundary conditions.

$$H = -\sum_{l=1}^{L} h_l(c_l^\dagger c_l - 1/2) - \frac{1+\gamma}{2}\sum_{l=1}^{L-1} J_l(c_l^\dagger - c_l)(c_{l+1}^\dagger + c_{l+1}) - \frac{1-\gamma}{2}\sum_{l=1}^{L-1} J_l(c_l^\dagger + c_l)(c_{l+1} - c_{l+1}^\dagger) + J_L w\left[\frac{1+\gamma}{2}(c_L^\dagger - c_L)(c_1^\dagger + c_1) + \frac{1-\gamma}{2}(c_L^\dagger + c_L)(c_1^\dagger - c_1)\right] e^{-i\pi\sum_{j=1}^{L} c_j^\dagger c_j} \tag{A.6}$$

If one uses periodic boundary conditions, the Hamiltonian is not quadratic in the c_l, $c_l^\dagger$ operators. However the Hamiltonian commutes with the $P = e^{-i\pi\sum_{j=1}^{L} c_j^\dagger c_j}$ parity operator. The P operator has two eigenvalues: $\lambda_P = \pm 1$. When periodic boundary conditions are used the Hamiltonian can solved separately in the odd ($\lambda_P = -1$), and the even

($\lambda_P = +1$) sub spaces. After restricting to these (invariant) subspaces, the Hamiltonian becomes quadratic in the c_l, $c_l^\dagger$ operators. In the the invariant subspaces:

$$H_{\lambda_P} = -\sum_{l=1}^{L} h_l(c_l^\dagger c_l - 1/2) - \frac{1+\gamma}{2}\sum_{j=1}^{L-1} J_l(c_l^\dagger - c_l)(c_{l+1}^\dagger + c_{l+1}) - \frac{1-\gamma}{2}\sum_{j=1}^{L-1} J_l(c_l^\dagger + c_l)(c_{l+1} - c_{l+1}^\dagger) + wJ_L\lambda_P\left[\frac{1+\gamma}{2}(c_L^\dagger - c_L)(c_1^\dagger + c_1) - \frac{1-\gamma}{2}(c_L^\dagger + c_L)(c_1^\dagger - c_1)\right] . \quad \text{(A.7)}$$

A.2 Solution of a general quadratic operator

Consider a quadratic Hamiltonian [105] :

$$H = \sum_{i,j=1}^{L} A_{i,j} c_i^\dagger c_j + \frac{1}{2}\sum_{i,j=1}^{N} B_{i,j}(c_i^\dagger c_j^\dagger + h.c.) . \quad \text{(A.8)}$$

In the case of the XY chain $A_{i,i} = -h_i$, $A_{i+1,i} = A_{i,i+1} = -\frac{1}{2}J_i$, $B_{i+1,i} = -B_{i,i+1} = \frac{1}{2}\gamma J_l$ With the Bogoliubov transformation:

$$\eta_k = \sum_{i}^{N}\left(\frac{1}{2}(\Phi_k(i) + \Psi_k(i))c_i + \frac{1}{2}(\Phi_k(i) - \Psi_k(i))c_i^\dagger\right) , \quad \text{(A.9)}$$

the Hamiltonian becomes diagonal:

$$H = \sum_{k=1}^{N} \Lambda_k(\eta_k^\dagger \eta_k - 1/2) . \quad \text{(A.10)}$$

The η_k and $\eta_k^\dagger$ operators fulfill the canonical anti-commutation relations:

$$\begin{aligned} \left[\eta_k, \eta_q^\dagger\right]_+ &= \delta_{k,q} \\ \left[\eta_k, \eta_q\right]_+ &= \left[\eta_k^\dagger, \eta_q^\dagger\right]_+ = 0 \end{aligned} \quad \text{(A.11)}$$

The excitation energies and the $\Psi_k(i)$ $\Phi_k(i)$ coefficients are solutions of the following two equations:

$$(A-B)\Phi_k = \Lambda_k\Psi_k \quad \text{(A.12)}$$

$$(A+B)\Psi_k = \Lambda_k\Phi_k \quad \text{(A.13)}$$

By multiplying (A.12) with $A+B$, and (A.13) with $A-B$, one gets an eigenvalue problem:

$$(A+B)(A-B)\Phi_k = \Lambda_k^2\Phi_k \quad \text{(A.14)}$$

$$(A-B)(A+B)\Psi_k = \Lambda_k^2\Psi_k . \quad \text{(A.15)}$$

Usually the above two equations are used to calculate $\Psi_k(i)$, $\Phi_k(i)$ and Λ_k. The ground

state is the vacuum of the new fermion operators (η and $\eta^\dagger$):

$$\eta_k|GS\rangle = 0\ . \tag{A.16}$$

To calculate the expectation value of any operators in the ground state one usually express the operator using the η and η_k operators, and use the canonical anti-commutators and equation (A.16).

A.3 Solution of the homogeneous Ising chain

In this section the calculation of the elementary excitations and eigenenergies of the Ising chain are included. It is also included how the ground states of homogeneous Ising models with different transverse fields can be expressed with each other. This later relationship is useful in the investigation of the quenches in the homogeneous system. The Hamiltonian after the Jordan-Wigner transformation is:

$$H = -h\sum_{i=1}^{L} c_i^\dagger c_i - \frac{1}{2}\sum_{i=1}^{L}(c_i^\dagger - c_i)(c_{i+1}^\dagger + c_{i+1})\ , \tag{A.17}$$

where $h_i = h$ and $J_i = 1$. It is worth to introduce the Fourier transformation of the c_i, $c_i^\dagger$ fermion operators:

$$c_q = \frac{1}{\sqrt{L}}\sum_{j=1}^{N}\exp(iqj)c_j \tag{A.18}$$

$$c_q^\dagger = \frac{1}{\sqrt{L}}\sum_{j=1}^{N}\exp(iqj)c_j^\dagger\ , \tag{A.19}$$

where $q = 2\pi m/L$, $m = 0 \ldots L-1$. The c_q $c_q^\dagger$ operators are fermion operators ($\{c_q, c_k\} = \{c_q^\dagger, c_k^\dagger\} = 0$, $\{c_q, c_k^\dagger\} = \delta_{q,k}$). With these operators the Hamiltonian takes the following form:

$$H = -\sum_q (h + \cos q)c_q^\dagger c_q - \frac{1}{2}\sum_q (e^{-iq}c_q^\dagger c_{-q}^\dagger - e^{iq}c_q c_{-q})\ . \tag{A.20}$$

One introduces the η_q and $\eta_q^\dagger$ fermion operators with the Bogoliubov transformation:

$$\eta_q = u_q c_q + i v_q c_{-q}^\dagger \tag{A.21}$$

$$\eta_{-q}^\dagger = i v_q c_q + u_q c_{-q}^\dagger\ . \tag{A.22}$$

Where

$$u_h(p) = \sqrt{\frac{\varepsilon_h(p) + h - \cos p}{2\varepsilon_h(p)}}$$

$$v_h(p) = \sqrt{\frac{\varepsilon_h(p) - (h - \cos p)}{2\varepsilon_h(p)}}\ , \tag{A.23}$$

and the $\varepsilon_h(p)$ excitation energy is:

$$\varepsilon_h(p) = \sqrt{(h-\cos p)^2 + \sin^2 p}\,. \tag{A.24}$$

The η_q and $\eta_q^\dagger$ operators are fermion operators with the usual anti-commutator rules. $\{\eta_q, \eta_k\} = \{\eta_q^\dagger, \eta_k^\dagger\} = 0$, $\{\eta_q, \eta_k^\dagger\} = \delta_{q,k}$) The diagonal form of the Hamiltonian is:

$$H = \sum_q \varepsilon_h(q)\eta_q^\dagger\eta_q\,. \tag{A.25}$$

Ground states with different transverse fields
Let $|\Psi_0\rangle$ is the ground state of (A.17) with $h = h_0$ and $|0\rangle$ is the ground state with $h = h_1$. The η operators correspond to the h_0 magnetic field. The ground state corresponding to h_1 transverse field van be expressed as:

$$|\Psi_0\rangle = \prod_p \left[U_p + iV_p\eta_p^\dagger\eta_{-p}^\dagger\right]|0\rangle\,, \tag{A.26}$$

where

$$U_p = u_{h_0}(p)u_h(p) + v_{h_0}(p)v_h(p) \tag{A.27}$$
$$V_p = u_{h_0}(p)v_h(p) - v_{h_0}(p)u_h(p)\,. \tag{A.28}$$

A.4 Time evolution of the c_l, $c_l^\dagger$ operators

In the following non-equilibrium calculations, the α parameter will be time-dependent in the Hamiltonian:

$$H_{\rm odd} = \alpha(t)\sum_{l=1}^{L} h_l(c_l^\dagger c_l - 1/2) + \frac{1+\gamma}{2}\sum_{j=1}^{L-1} J_l(c_l^\dagger - c_l)(c_{l+1}^\dagger + c_{l+1}) + \frac{1-\gamma}{2}\sum_{j=1}^{L-1} J_l(c_l^\dagger + c_l)(c_{l+1} - c_{l+1}^\dagger) \tag{A.29}$$

We will use the Heisenberg picture to calculate the time evolution. Creation-annihilation operators in the Heisenberg picture:

$$c_l^H(t) = \mathrm{Texp}\left[\int_{t_0}^{t} iH(t')dt'\right] c\,\mathrm{Texp}\left[\int_{t_0}^{t} -iH(t')dt'\right] \tag{A.30}$$
$$c_l^{H\dagger}(t) = \mathrm{Texp}\left[\int_{t_0}^{t} iH(t')dt'\right] c^\dagger\,\mathrm{Texp}\left[\int_{t_0}^{t} -iH(t')dt'\right] \tag{A.31}$$

Here Texp denotes the time ordered exponential function. The Hamiltonian is quadratic in the creation-annihilation operators, as a consequence the time evolution only mixes this

$2L$ operator, higher order operator products does not occur:

$$\begin{aligned} c_l^H(t) &= \sum_{k=1}^{L} g_k(t)c_k + h_k(t)c_k^\dagger \\ c_l^{H\dagger}(t) &= \sum_{k=1}^{L} g_k^*(t)c_k^\dagger + h_k^*(t)c_k \end{aligned} \tag{A.32}$$

At the beginning of the time evolution, the system is in the ground state of the initial Hamiltonian. We will use two different types of $\alpha(t)$ functions. For quenches $\alpha(t)$ is step function of the time:

$$\alpha(t) = \begin{cases} h_0 & \text{if} \quad t < 0 \\ h & \text{if} \quad t > 0 \end{cases} \tag{A.33}$$

For quenches one solves the after quench Hamiltonian, and expresses the $c_l(t)$, $c_l^\dagger(t)$ operators using the well-known time evolution of the η_k, $\eta_k^\dagger$ operators.

$$H(t > 0) = \sum_k \epsilon_k \eta_k^\dagger \eta_k \tag{A.34}$$

$$\eta_k(t) = e^{-i\epsilon_k t}\eta_k \quad \eta_k^\dagger(t) = e^{-i\epsilon_k t}\eta_k^\dagger \tag{A.35}$$

$$c_l(t) = \sum_k \left\{ \frac{1}{2}(\Psi_k(l) + \Phi_k(l))\eta_k e^{-i\epsilon_k t} + \frac{1}{2}(\Phi_k(l) - \Psi_k(l))\eta_k^\dagger e^{i\epsilon_k t} \right\} \tag{A.36}$$

$$c_l^\dagger(t) = \sum_k \left\{ \frac{1}{2}(\Psi_k(l) + \Phi_k(l))\eta_k^\dagger e^{i\epsilon_k t} + \frac{1}{2}(\Phi_k(l) - \Psi_k(l))\eta_k e^{-i\epsilon_k t} \right\} \tag{A.37}$$

When investigating a Kibble-Zurek process, we will consider a smooth, continuous $\alpha(t)$ function. In this case, using the Heisenberg equation of motion and the canonical anti commutators one derives a set of differential equations for the $g_{m,l}$ and $h_{m,l}$ coefficients in (A.32).

$$\begin{aligned} \dot{g}_{m,l}(t) &= -i\alpha(t)h_m g_{m,l}(t) - iJ_m g_{m+1,l}(t) - iJ_m g_{m+1,l}(t) - \gamma J_{m-1}h_{m-1,l}(t) + \gamma J_m h_{m+1,l}(t) \\ \dot{g}_{m,l}(t) &= -i\alpha(t)h_m h_{m,l}(t) - iJ_m h_{m+1,l}(t) - iJ_m h_{m+1,l}(t) - \gamma J_{m-1}g_{m-1,l}(t) + \gamma J_m g_{m+1,l}(t) \end{aligned}$$

We will use the above equations to calculate the time evolution in the Harper model. In the Harper model $\gamma = 0$, the dynamics preserve the particle number, and the creation operators don't mix with the annihilation operators.
In this limit the $h_{k,l}(t)$ coefficients are zero, and the time evolution of the system is driven by the following equation:

$$i\frac{\mathrm{d}\tilde{\phi}_{q,n}}{\mathrm{d}t} = \frac{1}{2}\tilde{\phi}_{q,n-1} + \alpha(t)h_n\tilde{\phi}_{q,n} + \frac{1}{2}\tilde{\phi}_{q,n+1}\ , \tag{A.38}$$

where the notation $\tilde{\phi}_{k,n}(t) = g_{k,l}(t)$ was introduced, because this notation has been used in our article, and in the main text.

A.5 Majorana fermions

When investigating quench dynamics, it is convenient to introduce the so-called Majoranna fermions:

$$\check{a}_{2l-1} = c_l + c_l^\dagger \tag{A.39}$$

$$\check{a}_{2l} = i(c_l - c_l^\dagger) \; . \tag{A.40}$$

They are simply related to the η_k and $\eta_k^\dagger$ operators:

$$\begin{aligned} \check{a}_{2l-1} &= \sum_{k=1}^{L} \Phi_k(l)(\eta_k^\dagger + \eta_k) \; , \\ \check{a}_{2l} &= -\imath \sum_{k=1}^{L} \Psi_k(l)(\eta_k^\dagger - \eta_k) \; . \end{aligned} \tag{A.41}$$

Inserting $\eta_k^\dagger(t) = e^{\imath t \epsilon_k} \eta_k^\dagger$ and $\eta_k(t) = e^{-\imath t \epsilon_k} \eta_k$ into (A.41) one obtains

$$\check{a}_m(t) = \sum_{n=1}^{2L} P_{m,n}(t) \check{a}_n \; , \tag{A.42}$$

with

$$\begin{aligned} P_{2l-1,2k-1} &= \sum_q \cos(\epsilon_q t) \Phi_q(l) \Phi_q(k), \\ P_{2l-1,2k} &= -\sum_q \sin(\epsilon_q t) \Phi_q(l) \Psi_q(k) \; , \\ P_{2l,2k-1} &= \sum_q \sin(\epsilon_q t) \Phi_q(k) \Psi_q(l) \; , \\ P_{2l,2k} &= \sum_q \cos(\epsilon_q t) \Psi_q(l) \Psi_q(k) \; . \end{aligned} \tag{A.43}$$

The two-operator expectation values are given as:

$$\langle \check{a}_m(t) \check{a}_n(t) \rangle = \sum_{k_1,k_2} P_{m,k_1}(t) P_{n,k_2}(t) \langle \check{a}_{k_1} \check{a}_{k_2} \rangle \; . \tag{A.44}$$

Appendix B

Quantities of interest

B.1 Magnetization

B.1.1 Definition

Another quantity we consider is the *local magnetization*, $m_l(t)$, at a position l, of an open chain. Following Yang [167] this is defined for large L as the off-diagonal matrix-element:

$$m_l\left(t\right) = \left\langle \Psi_0^{(0)} \left|\sigma_l^x(t)\right| \Psi_1^{(0)} \right\rangle \ , \tag{B.1}$$

where $\left|\Psi_1^{(0)}\right\rangle$ is the first excited state of the initial Hamiltonian.

B.1.2 Calculation method

To calculate the local magnetization in (B.1), we need to first calculate the time dependence of the spin operator $\sigma_l^x(t)$ at site l in the Heisenberg picture. The spin operators are then expressed in terms of the Majoranna operators as:

$$\sigma_l^x \quad = \quad \imath^{l-1} \prod_{j=1}^{2l-1} \check{a}_j \ , \tag{B.2}$$

and the local magnetization in (B.1) is then given as the expectation value of a product of fermion operators with respect to the ground state:

$$m_l(t) = (\imath)^{l-1} \langle \Psi_0^{(0)}| \prod_{j=1}^{2l-1} \check{a}_j(t)\eta_1 |\Psi_0^{(0)}\rangle \ , \tag{B.3}$$

where we have used: $|\Psi_1^{(0)}\rangle = \eta_1|\Psi_0^{(0)}\rangle$. The expression in (B.3) - according to Wick's theorem - can be expressed as a sum of products of two-operator expectation values. This can be written in a compact form of a Pfaffian, which in turn can be evaluated as the square root of the determinant of an antisymmetric matrix:

$$m_l(t) = (-\imath)^{l-1} \begin{vmatrix} \langle \check{a}_1(t)\check{a}_2(t)\rangle & \langle \check{a}_1(t)\check{a}_3(t)\rangle & \cdots & \langle \check{a}_1(t)\check{a}_{2l-1}(t_1)\rangle & \langle \check{a}_1(t)\eta_1\rangle \\ & \langle \check{a}_2(t)\check{a}_3(t)\rangle & \cdots & \langle \check{a}_2(t)\check{a}_{2l-1}(t)\rangle & \langle \check{a}_2(t)\eta_1\rangle \\ & \ddots & & & \vdots \\ & & & \langle \check{a}_{2l-2}(t)\check{a}_{2l-1}(t)\rangle & \langle \check{a}_{2l-2}(t)\eta_1\rangle \\ & & & & \langle \check{a}_{2l-1}(t)\eta_1\rangle \end{vmatrix} = \pm \left[\det C_{ij}\right]^{1/2} , \quad \text{(B.4)}$$

where C_{ij} is the antisymmetric matrix $C_{ij} = -C_{ji}$, with the elements of the Pfaffian (B.4) above the diagonal. (Here and in the following we use the short-hand notation: $\langle \dots \rangle = \langle \Psi_0^{(0)}| \dots |\Psi_0^{(0)}\rangle$.)

Below we describe how the time evolution of the spin operator σ_l^x follows from the time dependence of the Majorana fermion operators. The *equilibrium* correlations in the initial state with a transverse field h_0 are:

$$\begin{aligned} \langle \check{a}_{2m-1}\check{a}_{2n-1}\rangle = \langle \check{a}_{2m}\check{a}_{2n}\rangle &= \delta_{m,n}, \\ \langle \check{a}_{2m-1}\check{a}_{2n}\rangle = -\langle \check{a}_{2m}\check{a}_{2n-1}\rangle &= \imath G^{(0)}_{n,m} , \end{aligned} \quad \text{(B.5)}$$

where the static correlation matrix $G^{(0)}_{m,n}$ is given as:

$$G^{(0)}_{m,n} = -\sum_q \Psi^{(0)}_q(m)\Phi^{(0)}_q(n) , \quad \text{(B.6)}$$

where $\Psi^{(0)}_q(m)$ and $\Phi^{(0)}_q(n)$ are the components of the eigenvectors in (A.9), calculated for the initial Hamiltonian. Then (A.44) can be written in the form:

$$\langle \check{a}_m(t)\check{a}_n(t)\rangle = \delta_{m,n} + \imath\Gamma_{m,n}(t) , \quad \text{(B.7)}$$

were

$$\begin{aligned} \Gamma_{2l-1,2m-1} &= \sum_{k_1,k_2} \left[G^{(0)}_{k_2,k_1} P_{2l-1,2k_1-1} P_{2m-1,2k_2} - G^{(0)}_{k_1,k_2} P_{2l-1,2k_1} P_{2m-1,2k_2-1} \right] \\ \Gamma_{2l-1,2m} &= \sum_{k_1,k_2} \left[G^{(0)}_{k_2,k_1} P_{2l-1,2k_1-1} P_{2m,2k_2} - G^{(0)}_{k_1,k_2} P_{2l-1,2k_1} P_{2m,2k_2-1} \right] \\ \Gamma_{2l,2m-1} &= -\sum_{k_1,k_2} \left[G^{(0)}_{k_2,k_1} P_{2l,2k_2} P_{2m-1,2k_1-1} - G^{(0)}_{k_1,k_2} P_{2l,2k_2-1} P_{2m-1,2k_1} \right] \\ \Gamma_{2l,2m} &= \sum_{k_1,k_2} \left[G^{(0)}_{k_2,k_1} P_{2l,2k_1-1} P_{2m,2k_2} - G^{(0)}_{k_1,k_2} P_{2l,2k_1} P_{2m,2k_2-1} \right] . \end{aligned} \quad \text{(B.8)}$$

In (B.4) there are also the contractions:

$$\begin{aligned} \Pi_m &= \langle \Psi_0^{(0)}|\check{a}_m(t)\eta_1|\Psi_0^{(0)}\rangle \\ &= \sum_n P_{m,n}\langle \Psi_0^{(0)}|\check{a}_n\eta_1|\Psi_0^{(0)}\rangle \end{aligned} \quad \text{(B.9)}$$

where

$$\begin{aligned}\langle\Psi_0^{(0)}|\check{a}_{2l-1}\eta_1|\Psi_0^{(0)}\rangle &= \Phi_1^{(0)}(l)\\ \langle\Psi_0^{(0)}|\check{a}_{2l}\eta_1|\Psi_0^{(0)}\rangle &= \imath\Psi_1^{(0)}(l)\ .\end{aligned} \tag{B.10}$$

B.2 Propagator

Let us denote the all spin down state as $|0\rangle$.

$$|0\rangle = |\downarrow\rangle \otimes |\downarrow\rangle \otimes \cdots \otimes |\downarrow\rangle \tag{B.11}$$

Where $|\downarrow\rangle$ is an eigenvector of σ^z: $\sigma^z|\downarrow\rangle = -|\downarrow\rangle$. This is the vacuum of the c_l, $c_l^\dagger$ operators:

$$c_l|0\rangle = 0 \quad \text{for all l.} \tag{B.12}$$

The definition propagator is:

$$\mathcal{G}(k,l,t) = \langle 0|c_k(t)c_l^\dagger(0)|0\rangle\ . \tag{B.13}$$

$|\mathcal{G}(k,l,t)|^2$ is the probability of creating a quasi-particle at site l at time 0, and detecting it at site k at time t. We will use this quantity to interpret the quench dynamics of the magnetization and the entanglement entropy. If the dynamics conserve the particle number, $\mathcal{G}(k,l,t)$ equals the wave packet, starting from site l at $t=0$. To see the previous statement we first observe that any particle number conserving Hamiltonian destroys the vacuum, and consequently the dynamics conserves the vacuum state:

$$\exp(-itH)|0\rangle = \left[1 + iHt + (iHt)^2/2 + \dots\right]|0\rangle = |0\rangle \tag{B.14}$$

Adding a constant factor to the Hamiltonian causes a time dependent phase factor to the vacuum, which is unimportant.

$$\begin{aligned}\mathcal{G}(k,l,t) = \langle 0|c_k(t)c_l^\dagger(0)|0\rangle = \langle 0|\exp(iHt)c_k(0)\exp(-iHt)c_l^\dagger(0)|0\rangle =\\ = \langle 0|c_k(0)\exp(-iHt)c_l^\dagger(0)|0\rangle\end{aligned} \tag{B.15}$$

Here $c_l^\dagger(0)|0\rangle$ is a localized state at site l, $\exp(-iHt)c_l^\dagger(0)|0\rangle$ is the wave packet, in time t which started from site l at $t=0$. The $\langle 0|c_k(0)$ vector is the (bra) basis vector, localized at site k. In consequence $\mathcal{G}(k,l,t)$ is the wave packet starting form site l at $t=0$, in time t, in the space representation.
We will refer to the $\mathcal{G}(k,l,t)$ propagator simply as "wave packet", even if the considered Hamiltonian is not particle number conserving.

B.3 Entanglement entropy

Quantum entanglement is one of the most interesting aspects of quantum mechanics, it was first written down by Schrödinger [190]. Entanglement was an actively studied field already in the early times of the quantum theory both in theory [191] [192] and in experiments citehidden-test-1, [194], [195], [197], [198], [199]. Today investigations about entanglement are motivated partially by applications such DMRG [206] [207] and quantum-information theory [201] [202] [203] [205], and partially by the need of better understood of basics concepts [208] [209]
In Section B.3.1 I introduce the Schmidt decomposition. In Section B.3.2 I present a detailed definition of entanglement entropy using the Schmidt decomposition. In Section B.3.3 some properties of the entanglement entropy are listed. In Section **??** the calculation method presented.

B.3.1 Schmidt decomposition

With the singular value decomposition the $[B]_{i,j} = b_{i,j}$ matrix can be written as the product of two unitary matrices (U and V) and a positive semi-definite matrix (Σ):

$$B = U\Sigma V^T \tag{B.16}$$

Where the Σ matrix is semidiagonal, it has non-zero elements only in its main diagonal, but Σ can be a non-square matrix.
With components:

$$b_{i,j} = \sum_k u_{i,k}\sigma_k v_{j,k} \tag{B.17}$$

A general vector $v = \sum_{i,j} b_{i,j}|i\rangle_A \otimes |j\rangle_B$ of the tensor product space can be written in the following form with the singular value decomposition of the $b_{i,j}$ matrix:

$$v = \sum_{i,j}\sum_k u_{i,k}\sigma_k v_{j,k}|i\rangle_A \otimes |j\rangle_B \tag{B.18}$$

Defining the vectors:

$$\begin{aligned} u_k &= \sum_i u_{i,k}|i\rangle_A \\ v_k &= \sum_j v_{jk}|j\rangle_B \end{aligned} \tag{B.19}$$

one gets:

$$v = \sum_k \sigma_k u_k \otimes v_k$$

which is the Schmidt decomposition of the v vector. Note, that the u_k vectors and the v_k vectors are orthogonal sets:

$$\begin{aligned} \langle u_k|u_q\rangle &= \delta_{k,q} \\ \langle v_k|v_q\rangle &= \delta_{k,q} \end{aligned} \tag{B.20}$$

B.3.2 Definition of entanglement entropy

The investigated system is in a pure state, denoted by $|\Psi\rangle$. One can equivalently use the density matrix $\rho = |\Psi\rangle\langle\Psi|$ to describe the system. We divide the system to two parts denoted by A and B.

The reduced density matrices for A and B:

$$\begin{aligned} \rho_A &= \mathrm{Tr}_B \rho \\ \rho_B &= \mathrm{Tr}_A \rho \end{aligned} \tag{B.21}$$

The entanglement (von Naumann) entropy is defined as:

$$\begin{aligned} S_A &= \mathrm{Tr}_A \rho_A \log \rho_A \\ S_B &= \mathrm{Tr}_B \rho_B \log \rho_B \\ S_A &= S_B \end{aligned} \tag{B.22}$$

The last equation is non-trivial. To see it we recall the Schmidt decomposition of quantum states. We will see that not only the two definitions of the entanglement entropy (S_A and S_B) equal, but the two reduced density matrix (ρ_A and ρ_B) has the same structure. (They are defined on different Hilbert spaces (H_A and H_B), usually with different dimensions. The non-zero eigenvalues of ρ_A, and ρ_B are the same.) A general vector in the $H_A \otimes H_B$ Hilbert space is:

$$v = \sum_{i,j} b_{i,j} |i\rangle_A \otimes |j\rangle_B \tag{B.23}$$

With the Schmidt decomposition it can written in the next form:

$$v = \sum_k \sigma_k u_k \otimes v_k \tag{B.24}$$

$$\begin{aligned} \rho_A &= \mathrm{Tr}_B |v\rangle\langle v| = \sum_{n_B} \sum_k \sigma_k |v_k\rangle\langle n_B|u_k\rangle_B \sum_q \sigma_q^* \langle u_q|n_B\rangle\langle v_q| = \\ &= \sum_{k,q} \sigma_k \sigma_q^* \delta_{k,q} |v_k\rangle\langle v_q| = \\ &= \sum_k |\sigma_k|^2 |v_k\rangle\langle v_k| \end{aligned} \tag{B.25}$$

With similar calculation one gets:

$$\rho_B = \sum_k |\sigma_k|^2 |u_k\rangle\langle u_k| \tag{B.26}$$

If we restrict ρ_A and ρ_B to their non-zero subspaces, we get the same operator, in consequently $S_A = S_B$.

B.3.3 Properties of entanglement entropy

In this short section I summarize the basic properties of entanglement entropy, and its connection with other entanglement measures, and the correlation functions. First I recapitulate the basic results about the connection with the operational entanglement measures. Than I recapitulate that the entanglement entropy can be considered as a bound for any normalized correlation function in a bipartite system.

The basic idea about comparing operationally entanglement in bipartite systems is that LOCC operations cannot create quantum correlations [189]. If it is possible (with probability one) to convert a ρ_1 state to an other one (ρ_2) using only LOCC operations, ρ_1 is more entangled then ρ_2. There is a maximally entangled state, in a finite d dimensional system it is:

$$|\psi_d^+\rangle = \frac{|0,0\rangle + |1,1\rangle + \cdots + |d-1,d-1\rangle}{\sqrt{d}} \,. \tag{B.27}$$

Maximally entangled here means, that $|\psi_d^+\rangle$ can be converted to any other state using LOCC operations. Let's denote the density matrix corresponding to $|\psi_d^+\rangle$ with $\Phi(K)$ where K is the dimension of the Hilbert space.

One can investigate how difficult is it to convert the maximally entangled state $\Phi(K)$ to the investigated state ρ using LOCC operations. It turned out that no meaningful definition is possible if one requires exact conversion of $\Phi(K)$ to ρ. One has to consider copies of the maximally entangled state and also the investigated state, and requires only asymptotically exact transformation. This measure is called entanglement cost and defined as [189] [210]:

$$E_C(\rho) = \lim_{\epsilon\to 0} \sup_{n\to\infty} \left\{ \frac{m}{n} : \frac{m}{n} \in C_\epsilon \right\} \tag{B.28}$$

where

$$C_\epsilon = \left\{ \frac{m}{n} : \text{there exists an LOCC } \Lambda \text{ such that } ||\rho^{\otimes n} - \Lambda([\Phi(dim(\rho))]^{\otimes m})|| < \epsilon \right\} \,. \tag{B.29}$$

Another operational measure can be the distillable entanglement which characterize how many copies of the maximally entangled state can be extracted from many copies of the investigated state ρ. Formally the distillable entanglement is defined as:

$$E_d(\rho) = \lim_{\epsilon\to 0} \sup_{n\to\infty} \left\{ \frac{m}{n} : \frac{m}{n} \in D_\epsilon \right\} \tag{B.30}$$

where

$$D_\epsilon = \left\{ \frac{m}{n} : \text{there exists an LOCC } \Lambda \text{ such that } ||\Lambda(\rho^{\otimes n}) - [\Phi(dim(\rho))]^{\otimes m}|| < \epsilon \right\} \quad \text{(B.31)}$$

It can be shown that if ρ is a reduced density matrix of a bipartite pure state, then $E_d(\rho) = E_c(\rho) = S(\rho)$. So either the distillable entanglement or the entanglement cost can be considered as an operational definition of the entanglement entropy.
Let us consider the mutual information $I(A:B)$ of a bipartite system:

$$I(A:B) = S(\rho_A) + S(\rho_B) - S(\rho) \ . \quad \text{(B.32)}$$

Here ρ is the density matrix of the system, ρ_A and ρ_B are the reduced density matrices. Let O_A (O_A) be a hermitian operator acting on subsystem A (B). The correlation function is usually defined as: $C(A,B) = \langle O_A O_B \rangle - \langle O_A \rangle \langle O_B \rangle$. It can be proven [109] that the normalized correlation function can be overestimated by the mutual information:

$$I(A:B) \geq \frac{1}{2} \frac{C(A,B)}{\| O_A \|_\infty^2 \| O_B \|_\infty^2} \ . \quad \text{(B.33)}$$

If ρ is a pure state, as it is everywhere in this dissertation, then $S(\rho) = 0$ an $I(A:B) = 2S_A = 2S_B = 2S_{\text{entanglement}}$. Hence in a closed system any correlations can be overestimated by the entanglement entropy:

$$S_{\text{entanglement}} \geq \frac{1}{4} \frac{C(A,B)}{\| O_A \|_\infty^2 \| O_B \|_\infty^2} \ . \quad \text{(B.34)}$$

For example: The entanglement entropy remains small, $O(1)$ after a quench which ends in the localised phase of the Harper model (See Chapte 6.2.) than all normalized correlation functions has to be $O(1)$.

In the axiomatic definition of the measures of the bipartite entanglement one of the axioms states, that any measure should give the entanglement entropy on pure states [189] [212] [213].

B.3.4 Calculation of entanglement entropy in spin chains

In this work we consider a simple geometry, where the subsystem A is the continuous block of the first l spin, and the subsystem B is the continuous block of the other $L - l$ spins. We follow [122] and [211] in the main ideas.
Since the simple time evolution eq. (A.37) Wick's theorem holds for the corrections in any time. For example the expectation value of the four operator product $\langle c_n^\dagger(t) c_m^\dagger(t) c_k(t) c_l(t) \rangle$ can be evaluated as:

$$\begin{aligned} \langle c_n^\dagger(t) c_m^\dagger(t) c_k(t) c_l(t) \rangle = & \langle c_n^\dagger(t) c_l(t) \rangle \langle c_m^\dagger(t) c_k(t) \rangle \\ & - \langle c_n^\dagger(t) c_k(t) \rangle \langle c_m^\dagger(t) c_l(t) \rangle \\ & + \langle c_n(t) c_m(t) \rangle \langle c_k^\dagger(t) c_l^\dagger(t) \rangle \ , \end{aligned} \quad \text{(B.35)}$$

and in a similar way, the expectation value of any string of creation/annihilation operators equals the sum of the non-zero parings. Since Wick theorem holds for the correlations, the reduced density matrix ρ_A is the exponential of an appropriate Hermitian operator $\mathcal{H}$, and $\mathcal{H}$ is quadratic in the annihilation and creation operators. (In other words, ρ_A is a fermionic Gaussian state.)

$$\rho_A = \frac{\exp(\mathcal{H})}{\mathrm{Trexp}(\mathcal{H})} \tag{B.36}$$

$$\mathcal{H} = \sum_{i,j=1}^{l} \tilde{A}_{ij} c_i^\dagger c_j + \frac{1}{2} \sum_{i,j=1}^{l} \tilde{B}_{ij} (c_i^\dagger c_j^\dagger - \mathrm{h.c.}) \; . \tag{B.37}$$

Now we recall how to compute the von Neumann entropy of a fermionic Gaussian state. We diagonalize this Hamiltonian $\mathcal{H}$ by means of a Bogoliubov transformation

$$\xi_k = \sum_{i=1}^{l} \left(\frac{1}{2}(\phi_k(i) + \psi_k(i)) c_i + \frac{1}{2}(\phi_k(i) - \psi_k(i) c_i^\dagger) \right) \; . \tag{B.38}$$

Then, the Hamiltonian reads

$$\mathcal{H} = \sum_{k=1}^{l} \epsilon_k \xi_k^\dagger \xi_k \; , \tag{B.39}$$

where $\xi_k^\dagger$ and ξ_k are creation and annihilation operators of some fermionic modes. The density matrix ρ_A can simply be expressed as

$$\rho_A = \prod_{k=1}^{l} \tilde{\rho}_k = \prod_{k=1}^{l} \frac{e^{\epsilon_k \xi_k^\dagger \xi_k}}{1 + e^{-\epsilon_k}} \quad \text{where} \quad \tilde{\rho}_k = \frac{e^{\epsilon_k \xi_k^\dagger \xi_k}}{1 + e^{-\epsilon_k}} \; . \tag{B.40}$$

$$\tilde{\rho}_k = \frac{1}{1 + e^{-\epsilon_k}} \begin{pmatrix} e^{-\epsilon_k} & 0 \\ 0 & 1 \end{pmatrix} = \begin{pmatrix} \frac{1+\nu_k}{2} & 0 \\ 0 & \frac{1-\nu_k}{2} \end{pmatrix} \; , \tag{B.41}$$

where $\nu_k = -\tanh(\epsilon_k/2)$. Thus, the entanglement entropy of the density matrix ρ_L is merely the sum of binary entropies

$$S(l) = \sum_{k=1}^{l} S(\tilde{\rho}_k) = \sum_{k=1}^{l} H\left(\frac{1+\nu_k}{2} \right) \; . \tag{B.42}$$

where $H(p) \equiv -p \log p - (1-p) \log(1-p)$ is the binary Shannon entropy.

In order to determine the parameters of the reduced density matrix (the spectra ν_k and the vectors $\tilde{\Phi}_k(i)$, $\tilde{\Psi}_k(i)$)), let us consider the dynamical correlation matrix,

$$C_{m,n}(t) = \langle \Psi | \check{a}_m(t) \check{a}_n(t) | \Psi \rangle \; . \tag{B.43}$$

Notice that matrix C can be computed using the initial correlations and the $P_{m,l}(t)$ coefficients as:

$$C_{m,n}(t) = \sum_{k_1,k_2} P_{m,k_1}(t) P_{m,k_2}(t) \langle \check{a}_{k_1}(t=0) \check{a}_{k_2}(t=0) \rangle \tag{B.44}$$

Let us define $T \equiv C(1:2l, 1:2l)$ as the $2l \times 2l$ upper-left sub-matrix of the correlation matrix C. If we transform the $\check{a}$ Majorana operators accordingly to (B.38):

$$\check{b}_{2n-1} = \sum_{m=1}^{l} \tilde{\phi}_m(n)\check{a}_{2m-1} = \xi_n^\dagger + \xi_n \tag{B.45}$$

$$\check{b}_{2n} = \sum_{m=1}^{l} \tilde{\psi}_m(n)\check{a}_{2m} = -i(\xi_n^\dagger - \xi_n) \; . \tag{B.46}$$

The $B_{mn} = \langle \check{b}_m \check{b}_n \rangle$ correlation matrix is:

$$B = \begin{bmatrix} 1 & -i\nu_1 & & & & & & \\ i\nu_1 & 1 & & & & & & \\ & & 1 & -i\nu_2 & & & & \\ & & i\nu_2 & 1 & & & & \\ & & & & \ddots & & & \\ & & & & & & 1 & -i\nu_l \\ & & & & & & i\nu_l & 1 \end{bmatrix} \tag{B.47}$$

The B matrix is connected to the C matrix by an unitary basis transformation, so they have the same spectra. As a consequence, the spectra of the $C - \mathbb{1}$ matrix is built up from the ν_k and the $-\nu_k$ numbers ($k = 1 \dots l$).
Numerical recipe to calculate the entanglement entropy: To calculate the entanglement entropy one has to calculate the C correlation matrix, then solve the eigenvalue problem of $C - \mathbb{1}$. (Here $\mathbb{1}$ stands for the $2l$x$2l$ unit matrix.) The eigenvalues of $C - \mathbb{1}$ are $\pm\nu_l$. One gets the entanglement from equation (B.42) entropy as

$$S = \sum_{r=1}^{l} \left[\frac{1+\nu_l}{2} \log\left(\frac{1+\nu_l}{2}\right) + \frac{1-\nu_l}{2} \log\left(\frac{1-\nu_l}{2}\right) \right] \; . \tag{B.48}$$

Renyi entropies

The Renyi entropies are generalizations of the entanglement entropy, and defined as:

$$S^{(\alpha)} = \frac{1}{1-\alpha} \log \mathrm{Tr}\rho^\alpha \; . \tag{B.49}$$

One gets the entanglement entropy in the $\alpha \to 1$ limit. The Renyi entropies can be calculated with the methods described above only equation (B.42) has to be replaced with:

$$S_A^{(\alpha)} = \frac{1}{1-\alpha} \sum_{j=1}^{l} \ln \left[\left(\frac{1+\nu_j}{2}\right)^p + \left(\frac{1-\nu_j}{2}\right)^p \right] \; . \tag{B.50}$$

Bibliography

[1] M. Greiner, O. Mandel, T. W. Hänsch, I. Bloch Nature **419** 51 (2002)

[2] B. Paredes *et al.* Nature **429**, 277 (2004)

[3] T. Kinoshita, T. Wenger and D. S. Weiss Science **305** 1125 (2004)

[4] T. Kinoshita, T. Wenger, D.S. Weiss Nature **440** 900 (2006)

[5] A. Lamacraft Phys. Rev. Lett. **98** 160404 (2006)

[6] L.E. Sadler, J. M. Higbie, S.R. Leslie, M. Vengalattore, D.M. Stamper-Kurn Nature **443** 312 (2006)

[7] S. Hofferberth, I. Lesanovsky, B. Fischer, T. Schumm, and J. Schmiedmayer Nature **449** 324 (2007)

[8] I. Bloch, J. Dalibard and W. Zwerger *Rev. Mod. Phys.***80** 885 (2008)

[9] S. Trotzky, Y.-A. Chen, A. Flesch, I.P. McCulloch, U. Schollwöck, J. Eisert, and I. Bloch Nature Phys. **8** 325 (2012)

[10] M. Cheneau, P. Barmettler, D. Poletti, M. Endres, P. Schauss, T. Fukuhara, C. Gross, I. Bloch, C. Kollath, and S. Kuhr Nature **481**, 484 (2012)

[11] M. Gring, M. Kuhnert, T. Langen, T. Kitagawa, B. Rauer, M. Schreitl, I. Mazets, D.A. Smith, E. Demler and J. Schmiedmayer Science **337** 1318 (2012)

[12] A. Polkovnikov, K. Sengupta, A. Silva and M. Vengalattore *Rev. Mod. Phys.***83** 863 (2011)

[13] E. Barouch, B. McCoy and M. Dresden Phys. Rev. A **2** 1075 (1970)
E. Barouch, B. McCoy Phys. Rev. A **3** 786 (1971)
E. Barouch B. McCoy Phys. Rev. A **3** 2137 (1971)

[14] Iglói F and Rieger H, 2000 *Phys. Rev. Lett.***85** 3233

[15] K. Sengupta, S. Powell, S. Sachdev Phys. Rev. A **69** 053616 (2004)

[16] M. Rigol, V. Dunjko, V. Yurovsky and M. Olshanii, *Phys. Rev. Lett.***98** 50405 (2007)
M. Rigol, V. Dunjko and M. Olshanii, *Nature* **452** 854 (2008)

[17] M.A. Cazalilla, *Phys. Rev. Lett.***97** 156403 (2006)
A. Iucci and M.A. Cazalilla , *Phys. Rev. A* **80** 063619 (2009)
A. Iucci and M.A: Cazalilla , *New J. Phys.* **12** 055019 (2010)

[18] S.R. Manmana, S. Wessel, R.M. Noack and A. Muramatsu *Phys. Rev. Lett.***98** 210405 (2007)

[19] M. Cramer, C. M. Dawson, J. Eisert and T. J. Osborne *Phys. Rev. Lett.***100** 030602 (2008)
M. Cramer and J. Eisert, 2010 *New J. Phys.* **12** 055020
M. Cramer, A. Flesch, I. P. McCulloch, U. Schollwöck and J. Eisert *Phys. Rev. Lett.***101** 063001 (2008)
A. Flesch, M. Cramer, I.P. McCulloch, U. Schollwöck and J. Eisert *Phys. Rev. A* **78** 033608 (2008)

[20] T. Barthel and U. Schollwöck *Phys. Rev. Lett.***100** 100601 (2008)

[21] M. Kollar and M. Eckstein *Phys. Rev. A* **78** 013626 (2008)

[22] S. Sotiriadis, P. Calabrese and J. Cardy *Europhys. Lett.* **87** 20002 (2009)

[23] G. Roux *Phys. Rev. A* **79** 021608 (2009)
G. Roux *Phys. Rev. A* **81** 053604 (2010)

[24] S. Sotiriadis, D. Fioretto and G. Mussardo *J. Stat. Mech.* P02017 (2012)
D. Fioretto and G. Mussardo *New J. Phys.* **12** 055015 (2010)
G. P. Brandino, A. De Luca, R. M. Konik and G. Mussardo *Phys. Rev. B* **85** 214435 (2012)

[25] C. Kollath, A. Läuchli and E. Altman *Phys. Rev. Lett.***98** 180601 (2007)
G. Biroli, C. Kollath and A. Läuchli *Phys. Rev. Lett.***105** 250401 (2010)

[26] M.C. Banuls, J.I. Cirac and M.B. Hastings *Phys. Rev. Lett.***106** 050405 (2011)

[27] C. Gogolin, M.P. Mueller and J. Eisert *Phys. Rev. Lett.***106** 040401 (2011)

[28] M. Rigol and M. Fitzpatrick *Phys. Rev. A* **84** 033640 (2011)

[29] T. Caneva, E. Canovi, D. Rossini, G. E. Santoro and A. Silva *J. Stat. Mech.* P07015 (2011)

[30] M. A. Cazalilla, A. Iucci and M. C. Chung *Phys. Rev. E* **85** 011133 (2012)

[31] M. Rigol and M. Srednicki *Phys. Rev. Lett.***108** 110601 (2012)

[32] P. Grisins and I.E. Mazets *Phys. Rev. A* **84** 053635 (2011)

[33] E. Canovi, D. Rossini, R. Fazio, G. E. Santoro and A. Silva *Phys. Rev. B* **83** 094431 (2011)

[34] A. Silva *Phys. Rev. Lett.***101** 120603 (2008)
A. Gambassi and A. Silva arXiv:1106.2671 (2011)

[35] D. Rossini, A. Silva, G. Mussardo and G. E. Santoro, 2009 *Phys. Rev. Lett.***102** 127204 (2009)
D. Rossini, S. Suzuki, G. Mussardo, G. E. Santoro and A.Silva *Phys. Rev. B* **82** 144302 (2010)

[36] L. Campos Venuti and P. Zanardi *Phys. Rev. A* **81** 022113 (2010)
L. Campos Venuti, N. T. Jacobson, S. Santra and P. Zanardi *Phys. Rev. Lett.***107** 010403 (2011)

[37] F. Iglói and H. Rieger *Phys. Rev. Lett.***106** 035701 (2011)

[38] H. Rieger and F. Iglói *Phys. Rev. B* **84** 165117 (2011)

[39] L. Foini, L. F. Cugliandolo and A. Gambassi *Phys. Rev. B* **84** 212404 (2011)
L. Foini, L. F. Cugliandolo and A. Gambassi *J. Stat. Mech.* P09011 (2012)

[40] P. Calabrese, F.H.L. Essler and M. Fagotti *Phys. Rev. Lett.***106** 227203 (2011)

[41] D. Schuricht, F.H.L. Essler *J. Stat. Mech.* P04017 (2012)

[42] P. Calabrese, F.H.L. Essler and M. Fagotti *J. Stat. Mech.* P07016 (2012)
P. Calabrese, F.H.L. Essler and M. Fagotti *J. Stat. Mech.* P07022 (2012)

[43] B. Blaß , H. Rieger and F. Iglói *Europhys. Lett.* **99** 30004 (2012)

[44] F.H.L. Essler, S. Evangelisti, M. Fagotti *Phys. Rev. Lett.***109** 247206 (2012)

[45] S. Evangelisti *J. Stat. Mech.* P04003 (2013)

[46] M. Fagotti *Phys. Rev. B* **87** 165106 (2013)

[47] B. Pozsgay *J. Stat. Mech.* P07003 (2013)
B. Pozsgay *J. Stat. Mech.* P10028 (2013)

[48] M. Fagotti, F.H.L. Essler *J. Stat. Mech.* P07012 (2013)

[49] M. Collura, S. Sotiriadis and P. Calabrese *J. Stat. Mech.* P09025 (2013)

[50] P. Calabrese and J. Cardy *Phys. Rev. Lett.***96** 136801 (2006)

[51] P. Calabrese and J. Cardy *J. Stat. Mech.* P06008 (2007)

[52] L. Bucciantini, M. Kormos, P. Calabrese, J. Phys. A: Math. Theor. **47** 175002 (2014).

[53] M. Fagotti, M. Collura, F. H.L. Essler, P. Calabrese, Phys. Rev. B **89**, 125101 (2014).

[54] J. Cardy Phys. Rev. Lett. **112**, 220401 (2014)

[55] L.F. Santos, A. Polkovnikov and M. Rigol *Phys. Rev. Lett.***107** 040601 (2011)

[56] P. Calabrese and J. Cardy *J. Stat. Mech.* P04010 (2005)

[57] M. Fagotti and P. Calabrese *Phys. Rev. A* **78** 010306 (2008)

[58] T. W. B. Kibble, J. Phys. A **9**, 1387 (1976), and Phys. Rep. **67**, 183 (1980);
W. H. Zurek, Nature (London) **317**, 505 (1985), and Phys. Rep. **276**, 177 (1996).

[59] W. H. Zurek, U. Dorner, and P. Zoller, Phys. Rev. Lett. **95**, 105701 (2005)
J. Dziarmaga, Phys. Rev. Lett. **95**, 245701 (2005)
B. Damski, Phys. Rev. Lett. **95**, 035701 (2005)

[60] A. Polkovnikov, Phys. Rev. B **72**, 161201(R) (2005)
A. Polkovnikov and V. Gritsev, Nature Phys. **4**, 477 (2008)

[61] T. Caneva, R. Fazio and G. E. Santoro, Phys. Rev. B **76**, 144427 (2007)

[62] R. W. Cherng and L. S. Levitov, Phys. Rev. A **73**, 043614 (2006)

[63] V. Mukherjee, U. Divakaran, A. Dutta, and D. Sen, Phys. Rev. B **76**, 174303 (2007)
U. Divakaran, A. Dutta, and D. Sen, Phys. Rev. B **78**, 144301 (2008)
S. Deng, G. Ortiz, and L. Viola, EPL **84**, 67008 (2008)
U. Divakaran, V. Mukherjee, A. Dutta, and D. Sen, J. Stat. Mech: Theory Exp. P02007 (2009)
V. Mukherjee and A. Dutta, EPL **92**, 37004 (2010)

[64] A. Dutta, R. R. P. Singh, and U. Divakaran, EPL **89**, 67001 (2010)
T. Hikichi, S. Suzuki, and K. Sengupta, Phys. Rev. B **82**, 174305 (2010)

[65] K. Sengupta, D. Sen, and S. Mondal, Phys. Rev. Lett. **100**, 077204 (2008)
S. Mondal, D. Sen, and K. Sengupta, Phys. Rev. B **78**, 045101 (2008)

[66] D. Sen, K. Sengupta, and S. Mondal, Phys. Rev. Lett. **101**, 016806 (2008)
S. Mondal, K. Sengupta, and D. Sen, Phys. Rev. B **79**, 045128 (2009)

[67] R. Barankov and A. Polkovnikov, Phys. Rev. Lett. **101**, 076801 (2008)
C. De Grandi, V. Gritsev, and A. Polkovnikov, Phys. Rev. B **81**, 012303 (2010)

[68] D. Patanè, A. Silva, L. Amico, R. Fazio, and G. E. Santoro, **101**, 175701 (2008)

[69] C. de Grandi, R. Barankov, and A. Polkovnikov, Phys. Rev. Lett. **101**, 230402 (2008)

[70] A. Bermudez, D. Patanè, L. Amico, and M. A. Martin-Delgado, Phys. Rev. Lett. **102**, 135702 (2009)

[71] D. Sen and S. Vishveshwara, EPL **91**, 66009 (2010)

[72] F. Pollmann, S. Mukerjee, A. M. Turner, and J. E. Moore, Phys. Rev. E **81**, 020101(R) (2010)

[73] J. Dziarmaga, Advances in Physics **59**, 1063 (2010)
A. Dutta, U. Divakaran, D. Sen, B. K Chakrabarti, T. F. Rosenbaum, and G. Aeppli, arXiv:1012.0653.

[74] M. Thakurathi, W. DeGottardi, D. Sen, S. Vishveshwara, Phys. Rev. B **85**, 165425 (2012)

[75] P. Bordia *et al.* Nature Physics doi:10.1038/nphys4020 (2017)

[76] L. D'Alessio, M. Rigol Phys. Rev. X **4** , 041048

[77] G. Roósz, R. Juhász, F. Iglói Phys. Rev. B **93**, 134305 (2016)

[78] G. De Chiara, S. Montangero, P. Calabrese, R. Fazio J. Stat. Mech., L03001 (2006)

[79] F. Iglói, Zs. Szatmári and Y.-C. Lin *Phys. Rev. B* **85** 094417 (2012)

[80] G.C. Levine, M.J. Bantegui and J.A. Burg *Phys. Rev. B* **86** 174202 (2012)

[81] J. H. Bardarson, F. Pollmann, and J. E. Moore Phys. Rev. Lett. **109**, 017202 (2012)

[82] R. Vosk and E. Altman *Phys. Rev. Lett.***110** 067204 (2013)

[83] D. Shechtman, I. Blech, D. Gratias and J.W.Cahn Phys. Rev. Lett. **53** 1951 (1984)

[84] J.-M. Dubois *Useful Quasicrystals* (World Scientific, Singapore London) (2005)

[85] R. Penrose Bull. Inst. Math. Appl. **10** 266 (1974)

[86] Z. M. Stadnik *Physical Properties of Quasicrystals* (Springer, Berlin Heidelberg New York) (1999)

[87] S. Roche, T. de Laissardiére G and Mayou D J. Math. Phys. **38** 1794 (1997)
D. Mayou, C. Berger, F. Cyrot-Lackmann, T. Klein and P. Lanco Phys. Rev. Lett. **70** 3915 (1993)

[88] P. G. Harper, Proc. Phys. Soc. A **68**, 874 (1955)

[89] S. Aubry and G. André, Ann. Israel Phys. Soc. **3** 133 (1980)

[90] G. Roati,C. D'Errico,L. Fallani,M. Fattori,C. Fort,M. Zaccanti,G. Modugno, M. Modugno and M. Inguscio Nature **453** 895 (2008)

[91] B. Deissler, E. Lucioni, M. Modugno, G. Roati, L. Tanzi, M. Zaccanti, M. Inguscio and G. Modugno New J. Phys. **13** 023020 (2011)

[92] M. Modugno New J. Phys. **11** 033023 (2009)

[93] Ch. Gramsch, M. Rigol, Phys. Rev. A **86**, 053615 (2012)

[94] U. Divakaran, F. Iglói and H. Rieger *J. Stat. Mech.* P10027 (2011)

[95] F. Iglói J. Phys. A **21** L911 (1988)
M.M. Doria, I.I. Satija Phys. Rev. Lett. **60** 444 (1988)
H. A. Ceccatto Phys. Rev. Lett. **62** 203 (1989)
H. A. Ceccatto Z. Phys. B **75** 253 (1989)
G. V. Benza Europhys. Lett. **8** 321 (1989)
M. Henkel, A. Patkós J. Phys. A **25** 5223 (1992)

[96] L. Turban, F. Iglói, B. Berche Phys. Rev. B **49** 12695 (1994)

[97] F. Iglói, L. Turban Phys. Rev. Lett. **77** 1206 (1996)

[98] F. Iglói, L. Turban, D. Karevski, F. Szalma Phys. Rev. B, **56** 11031 (1997)

[99] J. Hermisson, U. Grimm, M. Baake J. Phys. A: Math. Gen. **30** 7315 (1997)

[100] J. Hermisson J. Phys. A: Math. Gen. **33** 57 (2000)

[101] F. Iglói, R. Juhász, Z. Zimborás Europhys. Lett. **79** 37001 (2007)

[102] M. Wilkinson and J. Austin, Phys. Rev. B **50**, 1420 (1994)

[103] F. Iglói and C. Monthus *Physics Reports* **412** 277 (2005)

[104] P. Jordan and E. Wigner *Z. Phys.* **47** 631 (1928)

[105] E. Lieb, T. Schultz, D. Mattis Ann. Phys. (N.Y.) **16** 407 (1961)

[106] P. Pfeuty *Ann. Phys. (N.Y.)* **57** 79 (1970)

[107] J.B. Kogut *Rev. Mod. Phys.***51** 659 (1979)

[108] S. Suzuki, I. J. Chakrabarti, K. Bikas: Quantum Ising Phases and Transitions in Transverse Ising Models Springer (2013)

[109] M. M. Wolf, F. Verstraete, M. B. Hastings, J. I. Chirac *Phys. Rev. Lett.***100** 070502 (2008)

[110] J. Cardy, P. Calabrese J. Stat. Mech. P06002 (2004)

[111] P. Pfeuty Phys. Lett. **72A** 245 (1979)

[112] F. Iglói, R. Juhász, Z. Zimborás J. Stat. Mech. P04004 (2007)

[113] A. Sütő, Beyond Quasicrystals, ed F. Axel and D. Gratias (Springer-Verlag & Les Editions de Physique) p. 481 (1995)

[114] M. Kohmoto, Phys. Rev. Lett. **51**, 1198 (1983)
D. J. Thouless, 1983 Phys. Rev. B **28**, 4272 (1983)
G.-L. Ingold, A. Wobst, C. Aulbach and P. Hänggi, Eur. Phys. J. B **30**, 175 (2002)

[115] D. S. Fisher Phys. Rev. B **51** 6411 (1995)

[116] F. Igloi Phys. Rev. B **65**, 064416 (2002)

[117] F. Iglói and H. Rieger Phys. Rev. B **57** 4238 (1998)

[118] I. Peschel and K.D. Schotte *Z. Phys. B* **54** 305 (1984)

[119] R. B. Griffiths, Phys. Rev. Lett. **23**, 17 (1969)

[120] F. Deylon, H. Kunz, B. Souillard *Journal of Physics A***16** 25-42 (1983)

[121] L. Kroon, E. Lennholm, R. Riklund *Phys. Rev. B* **66**, 094204 (2002)

[122] F. Iglói, Zs. Szatmári and Y.-C. Lin *Phys. Rev. B* **80** 024405 (2009)

[123] A. Sachdev, A. P. Young Phys. Rev. Lett. **78** 2220 (1997)

[124] D. Damanik J. Math. Anal. App., **249** 393 (2000)
D. Damanik and Gorodetski A Comm. Math. Phys. **205** 221 (2011)

[125] W. N. Yessen arXiv:1203.2221 (2012)

[126] M. Fagotti, P. Calabrese Phys. Rev. A **78** 010306(R) (2008)

[127] V. Eisler, F. Iglói, I. Peschel J. Stat. Mech. P02011 (2009)

[128] D. J. Thouless Phys. Rev. Lett. **39** 1167 (1977) F. Piéchon Phys. Rev. Lett. **76** 4372 (1996)

[129] C. Cohen-Tanoudji Advances in Atomic Physics. World Scientific. p. 791. doi:10.1142/6631. ISBN 978-981-277-496-5. (2011)

[130] W. Ketterle, N. J. Van Druten Advances in atomic, molecular, and optical physics. **37**: 181–236. (1996)

[131] T. M. Brzozowski, M. Maczynska, M. Zawada, J. Zachorowski, W. Gawlik: *Journal of Optics B*: Quantum and Semiclassical Optics, **4**, 1 (2002)

[132] B. DeMarco, D. S. Jin *Science* **285**, 5434, pp. 1703-1706 (1999)

[133] C. Chin, R. Grimm, P. Julienne, E. Tiesinga *Rev. Mod. Phys.***82**, 1225 (2010)

[134] I. Bloch Nature Physics. **1** (1): 23–30. (2005)

[135] D. Jakscha, P. Zoller *Annals of Physics* **315** 52–79 (2005)

[136] Waseem S. Bakr, Jonathon I. Gillen, Amy Peng, S. Fölling, M. Greiner *Nature* **462**, 74-77 (2009)

[137] M. Lewenstein, A. Sanpera, V. Ahufinger "Ultracold Atoms in Optical Lattices: Simulating quantum many-body systems" ISBN-13: 9780199573127 (2012)

[138] J. Struck [et al.] Nature Physics **9**, 738–743 (2013)

[139] D. Jaksch, P. Zoller New Journal of Physics, **5**, (2003)

[140] C. N. Weiler, T. W. Neely, D. R. Sherer, A. S. Bradley, M. J. Davis, and B. P. Anderson Nature (London) **455**, 948 (2008)

[141] G. D. Mahan *Many-Particle Physics* (New-York: Plenum) (1990)

[142] P. Calabrese and J. Cardy *J. Stat. Mech.* P10004 (2007)

[143] J.-M. Stéphan and J. Dubail *J. Stat. Mech.* P08019 (2011)

[144] V. Eisler and I. Peschel *J. Stat. Mech.* P06005 (2007)

[145] V. Eisler, D. Karevski, T. Platini and I. Peschel *J. Stat. Mech.* P01023 (2008)

[146] A. Bayat, S. Bose and P. Sodano *Phys. Rev. Lett.***105** 187204 (2010)
P. Sodano, A. Bayat and S. Bose *Phys. Rev. B* **81** 100412 (2010)

[147] A. Zamora, J. Rodriguez-Laguna, M. Lewenstein and L. Tagliacozzo, *arXiv:1401.7916*
V. Alba and F. Heidrich-Meisner, *arXiv:1402.2299*

[148] R.Z. Bariev *Soviet Phys. JETP* **50** 613 (1979)

[149] B.M. McCoy and J.H.H. Perk *Phys. Rev. Lett.***44** 840 (1980)

[150] L.P. Kadanoff *Phys. Rev. B* **24** 5382 (1981)

[151] A.C. Brown *Phys. Rev. B* **25** 331 (1982)

[152] F. Iglói, I. Peschel and L. Turban *Adv. Phys.* **42** 683 (1993)

[153] G. Delfino, G. Mussardo and P. Simonetti *Nucl. Phys. B* **432** 518 (1994)

[154] L. Turban *Journal of Physics A***18** L325 (1985)

[155] L.G. Guimarães and J. R. Drugowich de Felicio *Journal of Physics A***19** L341 (1986)

[156] M. Henkel and A. Patkós *Journal of Physics A***20** 2199 (1987)

[157] M. Henkel and A. Patkós *Nucl. Phys. B* **285** 29 (1987)

[158] M. Henkel and A. Patkós *Journal of Physics A***21** L231 (1988)

[159] M. Henkel, A. Patkós and M. Schlottmann *Nucl. Phys. B* **314** 609 (1989)

[160] M. Oshikawa and I. Affleck *Phys. Rev. Lett.***77** 2604 (1996)

[161] M. Oshikawa and I. Affleck *Nucl. Phys. B* **495** 533 (1997)

[162] A. LeClair and A.W.W. Ludwig *Nucl. Phys. B* **549** 546 (1999)

[163] I. Peschel *Journal of Physics A***36** L205 (2003)

[164] V. Eisler and I. Peschel *Ann. Phys. (Berlin)* **522** 679 (2010)

[165] I. Peschel and V. Eisler *J. Phys. A: Math. Theor.* **45** 155301 (2012)

[166] V. Eisler and I. Peschel *Europhys. Lett.* **99** 20001 (2012)

[167] C.N. Yang *Phys. Rev.***85** 808 (1952)

[168] J.L. Cardy *Journal of Physics A***17** L385 (1984)

[169] E. Fradkin and L. Susskind *Phys. Rev. D* **17** 2637 (1978)

[170] T.D. Schultz, D.C. Mattis and E.H. Lieb *Rev. Mod. Phys.***36** 856 (1964)

[171] J. L. Cardy *Nucl. Phys. B* **240** 514 (1984)

[172] M.N. Barber, I. Peschel and P.A. Pearce *J. Stat. Phys.* **37** 497 (1984)

[173] F. Iglói, H. Rieger and L. Turban Phys. Rev. E **59** 1465 (1999)

[174] S. J. Poon Adv. Phys. **41** 303 (1992)
H. Q. Yuan, U. Grimm, P. Repetowicz and M. Schreiber Phys. Rev. B **62** 15569 (2000)
H. Schulz-Baldes, J. Bellissard Rev. Math. Phys. **10** 1 (1998)
B. Huckestein, L. Schweitzer Phys. Rev. Lett. **72** 713 (1994)
S. Thiem, M. Schreiber Phys. Rev. B **85** 224205 (2012)

[175] H. L. Cycon, R. G. Froese, W. Kirsch and B. Simon, Schrödinger Operators (Berlin: Springer) (1987)

[176] F. Iglói, G. Roósz, Y.-C. Lin, New J. Phys. **15**, 023036 (2013)

[177] D. Karevski and L. Turban, J. Phys. A**29**, 3461 (1996)

[178] E. C. G. Stückelberg, Helv. Phys. Acta **5**, 369 (1932)

[179] S. N. Shevchenko, S. Ashhab and F. Nori, Phys. Rep. **492**, 1 (2010)

[180] Y. Zhao, F. Andraschko and J. Sirker Phys. Rev. B **93** 205146 (2016)

[181] D. Pekker, G. Refael, E. Altman, E. Demler and V. Oganesyan Phys. Rev. X **4** 011052 (2014)

[182] R. Vosk and E. Altman Phys. Rev. Lett. **110** 067204 (2013)

[183] R. Vosk and E. Altman Phys. Rev. Lett. **112** 217204 (2014)

[184] It can be seen in Ref. [117], by solving the eigenvalue problem in Eq. (2.2) with $J_i = 0$, $i = 1, 2, \ldots, L$.

[185] I. Peschel Phys. Rev. B **30** 6783 (1984)

[186] C. Monthus Phys. Rev. B **69** 054431 (2004)

[187] I. Peschel and J. Zhao J. Stat. Mech. P11002 (2005)

[188] F. Iglói, G. Roósz, L. Turban J. Stat. Mech. P03023 (2014)

[189] B. P. Martin, S. Virmani, Quant.Inf.Comput.7:1-51, (2007)

[190] E. Schrödinger "Discussion of probability relations between separated systems". Mathematical Proceedings of the Cambridge Philosophical Society **31** (4): 555-563. (1935)

[191] A. Einstein, B. Podolsky, N. Rosen Physical Review. **47** (10): 777–780.

[192] J.S. Bell Reviews of Physics, **1**: 195–200. (1964)
J.S. Bell Reviews of Modern Physics, **38**: 447–452. (1966)

[193] Stuart J. Freedman and John F. Clauser Phys. Rev. Lett. **28**, 938 (1972)

[194] A. Aspect, P. Grangier, G. Roger Phys. Rev. Lett. **47**, 460 (1981)

[195] W. Tittel, J. Brendel, H. Zbinden, N. Gisin Phys.Rev.Lett. **81** 3563-3566 (1998)

[196] N. N. Bogoliubov, Nuovo Cimento 7, 794 (1958)

[197] G. Weihs; T. Jennewein; C. Simon; H. Weinfurter; A. Zeilinger Phys. Rev. Lett., **81**: 5039–5043 (1998)

[198] B.G. Christensen, K. T. McCusker, J. Altepeter, B. Calkins, T. Gerrits, A. Lita, A. Miller, L. K. Shalm, Y. Zhang, S. W. Nam, N. Brunner, C. C. W. Lim, N. Gisin, P. G. Kwiat Physical Review Letters. **111** (7448) (2013)

[199] M. Giustina, et al. arXiv:1511.03190 (2015)

[200] W. K. Wootters Roy Soc of London Phil Tr A, **356**, 1743, p.1717 (1998)

[201] P. W. Shor, Algorithms for quantum computation: Discrete logarithms and factoring, Proc. 35nd Annual Symposium on Foundations of Computer Science (Shafi Goldwasser, ed.), IEEE Computer Society Press 124-134. (1994)

[202] A. Barenco, C. H. Bennett, R. Cleve, D. P. DiVincenzo, N. Margolus, P. Shor, T. Sleator, J. Smolin, and H. Weinfurter, Elementary gates for quantum computation, Phys. Rev. A, **52**, pp. 3457-3467 (1995)
I. L. Chuang, R. Laflamme, P. W. Shor and W. H. Zurek, Quantum computers, factoring and decoherence, Science, **270**, pp. 1635-1637 (1995)

[203] W. Wootters and W. Zurek, Phys. Today, vol. **62**, no. 2, pp. 76-77, (2009)

[204] A. B. Harris J. Phys. C **7**, 1671 (1974)
J. M. Luck, Europhys. Lett. **24**, 359 (1993)

[205] N. Gisin, G. Ribordy, W. Tittel, and H. Zbinden Rev. Mod. Phys. **74**, 145 (2002)

[206] U. Schollwoeck Annals of Physics **326**, 96 (2011)

[207] M. B. Hastings, J. Stat. Mech. , P08024. (2007)
I. Peschel, J. Stat. Mech. , P12005 (2004)
N. Schuch, M. M. Wolf, F. Verstraete, and J. I. Cirac, Phys. Rev. Lett. **100**, 030504. (2008)
F. Verstraete, and J. I. Cirac, Phys. Rev. B **73**, 09442 (2006)

[208] Sz. Szalay Phys. Rev. A **92**, 042329 (2015)

[209] A. Miyake Phys. Rev. A **67**, 012108 (2003)

[210] N. Lie, S. Luo *Phys. Rev. A* **76**, 032327 (2007)

[211] G. Vitagliano, A. Riera and J. I. LatorreNew Journal of Physics 12 113049 (16pp) (2010)

[212] V. Vedral and M.B. Plenio, Phys. Rev. A **57**, 1619 (1998)

[213] M.J. Donald, M. Horodecki, and O. Rudolph, J. Math. Phys. **43**, 4252 (2002)